공학박사 학위논문

Preparation and Characterization of Graphene Oxide Modified Membranes for Water Treatment

수처리용 그래핀 옥사이드 복합 분리막의

제조 및 특성 평가

2015년 2월

서울대학교 대학원

화학생물공학부

이 재 우

Abstract

Preparation and Characterization of Graphene Oxide Modified Membranes for Water Treatment

Lee Jaewoo

School of Chemical and Biological Engineering

The Graduate School

Seoul National University

Today a third of the global population lives in water shortage country, one of the pressing needs of people throughout the world is adequate supply of drinking water. To satisfy the demand for an enormous amount of water required by expanding global population, there have been much erudite discussions and practical attempts covering a wide scope including wastewater reuse as well as desalination. Among several technologies, in particular, membrane bioreactor (MBR) and reverse osmosis (RO) process have attracted much attention in the field of wastewater treatment and desalination, respectively, due to various strengths such as high quality of treated water and a small footprint. However, MBR have membrane fouling which is the major obstacle in maximizing their efficiency leading to short membrane lifetime and high operating costs. Also, for the RO process, low energy efficiency still remains unanswered as a serious challenge in RO process over the past few decades. In this study, it is demonstrated that the

application of graphene oxide (GO) to membrane fabrication can be a novel strategy to overcome the aforementioned residual problems with each membrane process. In detail, GO was applied to fabrication of polysulfone (PSf) ultrafiltration (UF) membrane for the improvement of hydrophilicity and electrostatic repulsion characteristics, and the anti-biofouling capability of GO nanocomposite membrane was proved to be effective in MBR. Furthermore, addition of GO enhanced mechanical strength of GO nanocomposite membrane due to its high modulus and aspect ratio, which enabled the GO nanocomposite UF membrane to have mechanical strength comparable to existing support layer for commercial RO membrane and highly porous structure simultaneously. It is worth noting that RO membrane consisting of the PSf/GO nanocomposite support layer outperformed others including commercial membranes as well as the previously reported membranes in open literature. Also noteworthy is increasing the porosity of support layer could lead to improving the efficiency of RO membrane. To clarify the reason why porous structure of support layer induces higher water permeability of RO membrane, a non-intrusive experimental method was devised for representing the characteristics of the support layer as related to water flux.

Keywords

Ultrafiltration (UF) membrane, Thin-film composite (TFC) reverse osmosis (RO) membrane, Graphene oxide (GO), Anti-biofouling property, Mechanical property, Support layer impact

Student Number: 2009-21016

Table of Contents

List of Figures

List of Tables

Chapter I

I. Introduction

I.1. Backgrounds

The world is gradually running short of water which is directly related to human survival and the quality of life. To make matters worse, water scarcity problem is accelerated by climate change and increasing demographic pressure. Over the past few decades, various attempts have been made to solve the water shortage problem. One of the efforts is recycling of used water, which is realized by advanced wastewater treatment such as membrane bioreactors (MBRs). MBR combines conventional activated sludge process and membrane filtration making it very effective and popular water purification technology as its installment in various municipalities around the world is increasing (Shannon, Bohn et al. 2008). This growing worldwide employment of MBR is due to its advanced features which include: high quality of processed water, reduction in excess sludge, controllability of solids and hydraulic retention time, and minimization possible in required footprint (Judd 2008, Kraume and Drews 2010, Le-Clech 2010). Another approach to the production of clean water is desalination of sea water which is the most abundant resources on earth (Oki and Kanae 2006, Piao, Ciais et al. 2010, Green, Taniguchi et al. 2011). Reverse osmosis (RO) technology among several technologies for desalination has been actively sought to alleviate the problems caused by water deficiency because it consumes relatively low energy compared with any other desalination technologies such as thermal desalination (Elimelech and Phillip 2011).

However, aforementioned processes have inherent weaknesses in the processes themselves. For instance, on the one hand microorganisms remove organic pollutants and materials in wastewater, while they cause membrane fouling

that the bioreactor suffers from. Intricate interactions between membrane material and numerous components of activated sludge mixed liquor lead to biofouling of the membrane, which makes the MBRs for wastewater treatment costly. In the case of RO membrane, semipermeable selective layer which can reject salts such as sodium chloride enables RO membrane to produce fresh water from sea water due to much smaller-sized pores than salt, but it requires high hydraulic pressure that exceeds the osmotic pressure of feed solution (Sourirajan 1970).

To make the treated water by MBRs readily available to people economically, it is highly desirable to have a membrane with antifouling capability, or anti-biofouling membrane. Meanwhile, high water permeability is desired in RO membrane to achieve high water flux under low operating pressure while retaining high salt rejection to reduce energy consumption in RO process.

I.2. Objectives

The objective of this study was to develop a novel UF with anti-biofouling characteristics and RO membranes with high permeability by applying graphene oxide (GO) to membrane fabrication, and investigate the inhibition of membrane fouling in MBR and high permeability and mechanical strength in RO membrane consisting of support layer with both tensile strength comparable to existing support layer and highly porous by exceptional characteristics of GO. It was quite a surprise to discover that inclusion of only about 1 wt% of graphene oxide in the fabrication of membrane could spring up a new generation of membrane with anti-fouling capability and high permeability for MBRs and RO, respectively. The specific objectives of this study are as follows:

(1) Preparation and application of graphene oxide nanoplatelets composite membrane with hydrophilic and antifouling properties for wastewater treatment.

Polysulfone (PSf) ultrafiltration (UF) membranes including graphene oxide (GO) nanoplatelets were prepared for MBRs for wastewater treatment. Compositional and structural changes of GO nanocomposite membranes were investigated to clarify the impacts of added GO on the changes in characteristics and performances of PSf/GO nanocomposite membranes according to GO contents. Lastly, optimum GO content to improve membrane performance was derived from several characterizations, and the PSf/GO nanocomposite membrane including GO of the amount corresponding to the optimum content was applied to MBR in order to estimate the feasibility of PSf/GO nanocomposite membrane in the continuous operation of MBR.

(2) Investigation for effect of support layer on reverse osmosis membrane performance.

Unlike active layer of reverse osmosis (RO) membrane, little work has been done on the support layer of RO membrane because it has been regarded as merely peripheral factor of RO membrane. In this study, it was demonstrated that the support layer is not necessarily negligible although the pressure drop in the support layer is not a substantial portion. In detail, support layers with five different structures were prepared to fabricate RO membranes with different structure of support layers, and both water flux and salt rejection of all the RO membranes were tested in cross-flow system. To elucidate reason why RO membrane performance changed depending on the pore structure of support layer, a non-intrusive experimental method was devised to characterize the support layer's water flux performance as aforementioned in abstract. Lastly, it was theoretically confirmed that significant difference in hydraulic resistance can lie in the support layer depending on the pore structure of the support layer during RO operation by using Ergun equation.

(3) Development of high performance RO membrane with both mechanical property comparable to existing support layer and highly porous structures.

Prior to applying thin-film composite (TFC) RO membrane comprised of highly porous support layer to RO process under high hydraulic pressure, mechanical strength of the TFC RO membrane with the porous support layer should be ensured for its feasibility. In an effort to secure availability of RO membrane consisting of porous support layer, GO was utilized to enhance tensile

property of porous support layer. In order to maximize the effect of GO addition on improving mechanical strength of porous support layer, the size of GO was controlled by adjusting mechanical energy input per volume of graphite oxide (GtO) solution for exfoliation of GtO. The size effect of GO on mechanical property of support layer was examined by various characterizations such as Raman D/G-band peak intensity ratio, degree of oxygenation, zeta potential, and thickness of GO platelets according to their size. The most adequate size of GO platelets determined by the above-mentioned characterizations were used to fabricate PSf/GO nanocomposite support layer, and water flux, salt rejection, and feasibility of RO membrane consisting of the PSf/GO nanocomposite support layer were tested and compared to others including commercial RO membranes as well as the previous reported RO membranes in open literature.

Chapter II

II. Literature Review

II.1. Phase inversion in polymer system

II.1.1. Introduction

Since microfiltration (MF) porous membranes comprised of cellulosic materials were devised by Goetz in the 1960s, many ways to prepare polymeric membranes including electro-spinning, interfacial polymerization, stretching, track-etching, and phase inversion have been developed to fabricate membranes to carry out manifold purposes. Among the above-mentioned methods, the majority of membranes used for industrial such as MF, ultrafiltration (UF), membrane distillation (MD), nanofiltration (NF), reverse osmosis (RO), and forward osmosis (FO) membranes are prepared from a homogeneous polymer solution by a technique referred to as phase inversion due to its industrial and economic feasibility (Baker 2000), which is well revealed in **Table II-1**. In detail, phase inversion features the conversion of liquid homogeneous polymer solutions consisting of two or more components into a two-phase system with a solid and a liquid (Strathmann and Kock 1977, Strathmann 1985). Also, it is worth noting that the phase separation in polymeric systems is determined by thermodynamic and kinetic parameters, such as the chemical potentials and diffusivities of the individual components and the Gibb's free energy of mixing of the entire system (Strathmann and Kock 1977, Strathmann 1985). After phase separation is completed, the solid corresponding to polymer-rich phase and liquid corresponding to polymer-poor phase form the rigid membrane structure and the membrane pores, respectively (Strathmann and Kock 1977, Strathmann 1985). Phase inversion can be achieved by several techniques such as solvent evaporation, nonsolvent or vapor precipitation and thermal gelation (Mulder 1996).

Table II-1.Summary of typically used polymers and fabrication methods to prepare polymeric membranes for water and wastewater treatment (Lalia, Kochkodan et al. 2013).

Water treatment process	Polymers used for membrane fabrication	Fabrication techniques
MF	- Polyvinylidene fluoride (PVDF) - Poly(tetrafluorethylene) (PTFE) - Polypropylene (PP) - Polyethylene (PE) - Polyethersulfone (PES) - Polyetheretherketone (PEEK)	- Phase inversion - Stretching - Track-etching
UF	- Polyacrylonitrile (PAN) - PES - Polysulfone (PSf) - Poly(phthazine ether sulfone ketone) (PPESK) - Poly(vinyl butyral) - PVDF	- Phase inversion - Solution wet-spinning
MD	-PTFE -PVDF	- Phase inversion - Stretching - Electrospinning
NF	- Polyamides - PSf - Polyols - Polyphenols	- Interfacial polymerization - Layer-by-layer deposition - Phase inversion
RO	- Cellulose acetate/triacetate - Aromatic polyamide - Polypiperzine -Polybenzimidazole	-Phase inversion -Solution casting

A brief description of each technique is as follows:

- Nonsolvent induced phase separation (NIPs): According to this method, homogeneous polymer solution is precipitated due to change in composition by the addition of nonsolvent.

- Thermally induced phase separation (TIPs): This method is to precipitate a homogeneous solution consisting of polymer and solvent by cooling below a specific temperature appearing a miscibility gap based on the phenomenon that the solvation ability of solvent generally decreases with decreasing temperature (Lalia, Kochkodan et al. 2013).

- Vapor induced phase separation (VIPs): VIPs and NIPs are similar to both driven by nonsolvent, but they differ in the phase of nonsolvent inducing the precipitation of polymer solution. VIPs is caused by gas type of nonsolvent unlike NIPs induced by liquid type of nonsolvent.

- Evaporation induced phase separation (EIPs): This is one of the earliest methods used in fabrication of microporous membranes (Strathmann and Kock 1977, Strathmann 1985). According to this method, a three-compound mixture comprised of polymer, solvent, and nonsolvent undergoes the precipitation due to evaporation of more volatile solvent than nonsolvent.

Although the above-mentioned four different phase separation methods are induced by different factors, all phase inversion processes are based on the same thermodynamic principles regardless of type inducing phase separation since the starting point in all cases is a thermodynamically stable solution which is subjected to demixing (Mulder 1996).

II.1.2. Nonsolvent induced phase separation method

Among the aforementioned four methods, NIPs has been the most commonly used to fabricate commercial membrane, because it is adequate to prepare membrane easily at low cost. Thus, NIPs, namely the immersion precipitation process will be addressed in detail with special attention. Although commercial phase inversion membranes are mostly prepared from mixtures consisting of several components, only three components system comprised of a polymer, a solvent and a nonsolvent will be considered in order to help us to understand the basic principles.

A brief description for membrane fabrication procedure by NIPs is as follows:

1) After a polyester non-woven fabric is wetted with solvent, the polymer solution is drawn down on the fabric using casting knife as shown in **Figure II-1 (a)**.
2) Casted polymer solution is immersed into a nonsolvent coagulant bath to induce NIPs.
3) As shown in **Figure II-1 (b)**, an exchange between solvent and nonsolvent, namely liquid-liquid (L-L) demixing occurs in coagulant bath due to the activity and concentration gradient of all components. A polymer solution exposed to nonsolvent becomes thermodynamically unstable, and L-L demixing continues until equilibrium is achieved (Lee, Chae et al. 2013).
4) After L-L demixing is completed, solidified porous polymeric membrane is formed.

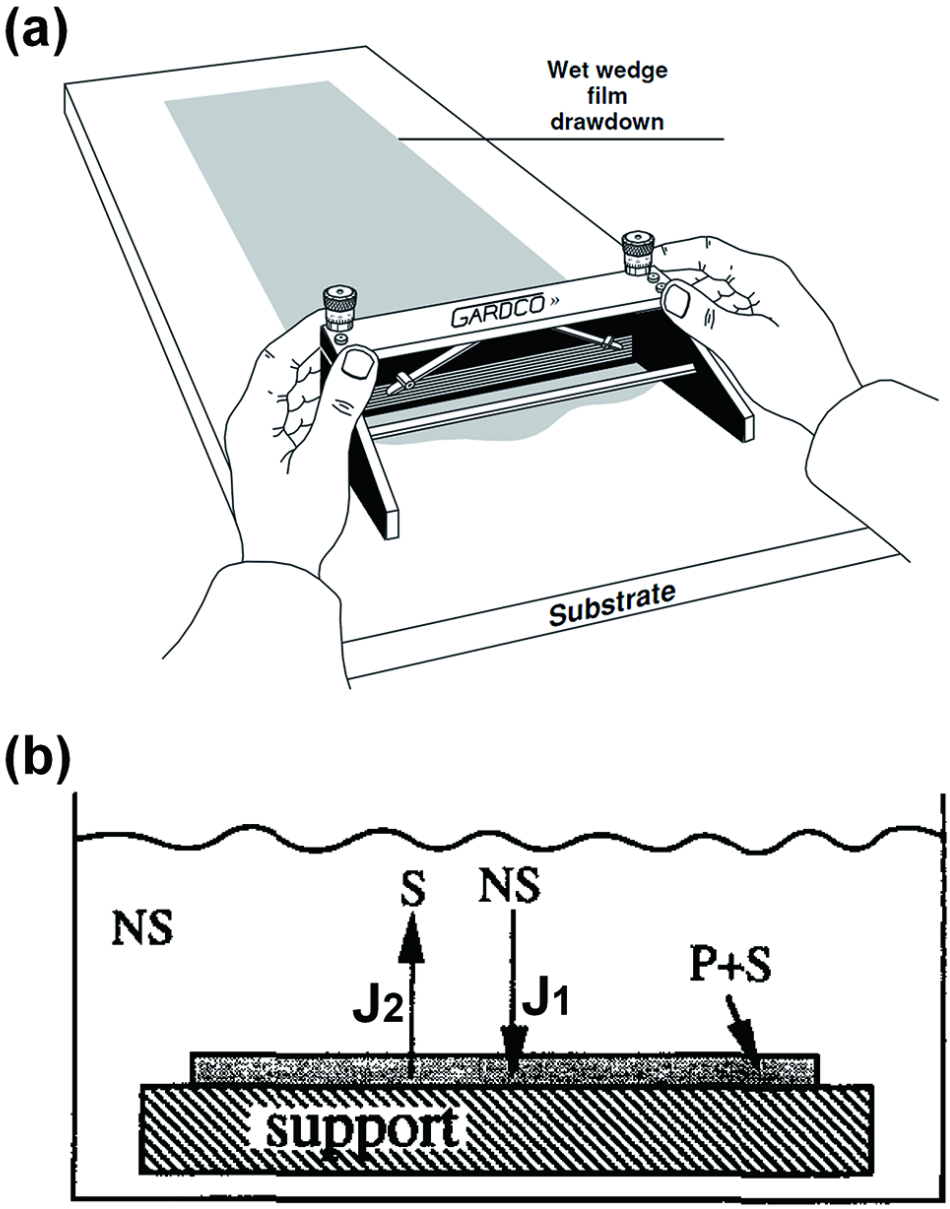

Figure II-1. (a) A typical casting knife and spreading an even film of a polymer solution across a substrate using it (Baker 2000), and (b) schematic depiction of the nonsolvent induced phase separation: P, polymer; S, solvent; NS, nonsolvent (Van de Witte, Dijkstra et al. 1996).

It is interesting to note that the ratio of diffusion velocity between outflow of solvent into the coagulation bath (at a flux = J2) and inflow of nonsolvent into the casting solution layer (at a flux = J1) can lead to different pore size (Lalia, Kochkodan et al. 2013). In detail, UF membranes with pore size of 1-30 nm are formed at J2 >> J1, whereas MF membranes with pore size of 0.2-0.5 μm are obtained at J2 = J1 (Lalia, Kochkodan et al. 2013).

For a deeper understanding of phenomena, it is also helpful to think of the precipitation pathway of the polymer solution occurring upon immersion of polymer solution into coagulant bath during membrane formation. **Figure II-2** shows the phase diagram of the three-component mixture revealing a miscibility gap over a wide variety of constituents, when a homogeneous polymer solution comprised of 25 wt% of polymer and 75 wt% of solvent is immersed and exposed to a nonsolvent capable of being miscible with solvent (Strathmann 1985). As aforementioned, counter diffusion between nonsolvent and solvent occurs, once polymer solution is exposed to nonsolvent. If an influx of nonsolvent into polymer solution occurs at similar rate to an outflow of solvent from polymer solution, the composition of polymer solution will change from the point A on the polymer-solvent line to the point B on the polymer-nonsolvent line by way of C and D sequentially (Strathmann 1985). When the composition of polymer solution reaches the point C, one-phase system begins to separate into a polymer-rich phase and a polymer-poor phase (Strathmann 1985, Baker 2000). As precipitation proceeds along the path, polymer solution including polymer-rich phase becomes viscous enough to be regarded as a solid by a lasting L-L demixing (Baker 2000). Solidified porous membrane is formed by further exchange of solvent and nonsolvent, and its structure such as porosity is roughly determined by point B

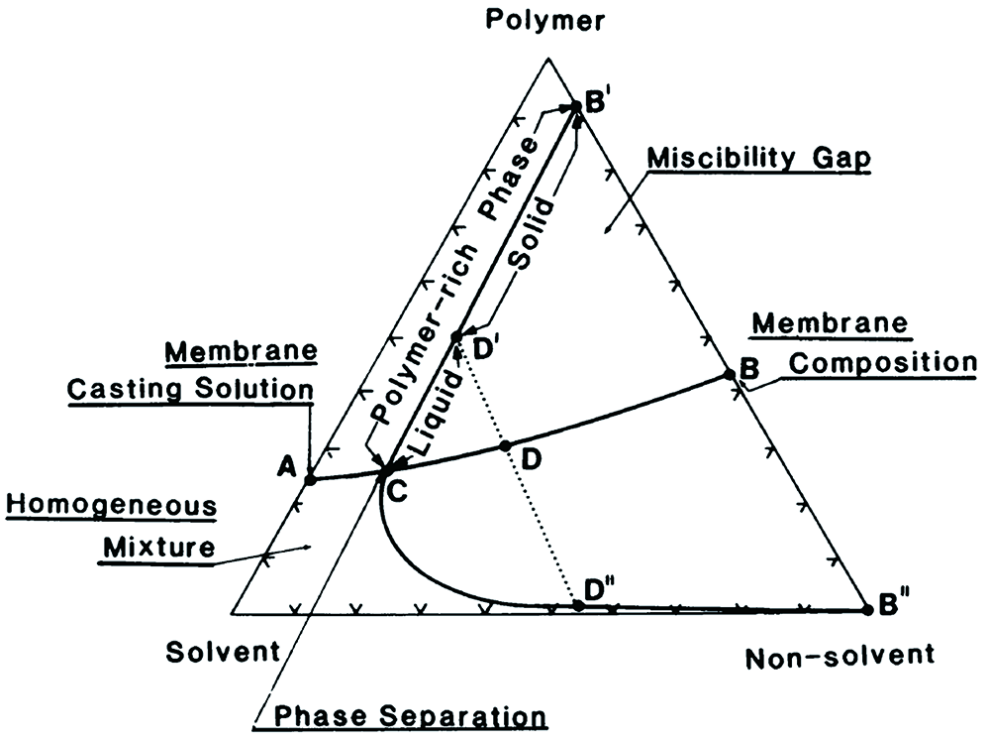

Figure II-2. The phase diagram of the three-component mixture showing the phase separation of a homogeneous polymer solution induced by a nonsolvent (Strathmann 1985).

(Strathmann 1985, Baker 2000). However, equilibrium thermodynamics does not provide any information about the pore sizes which are determined by the spatial distribution of the two phases or structural variations within the membrane cross-section such as whether the membrane has a symmetric or asymmetric structure (Strathmann 1985). The parameters are dictated by kinetic effects which depend on system properties such as the diffusivities of the diverse components in the polymer solution, the viscosity of the polymer solution, and the chemical potential gradients causing diffusion of the several components in the polymer solution (Strathmann 1985). Thus, the phase separation process is considered along with thermodynamic and kinetic relations.

II.1.3. Membrane structures prepared by nonsolvent induced phase separation: “finger”- and “sponge”-like structure

Depending on kinetic characteristics of polymer solution system, membrane structures are differently formed and divided into two types of structure, finger- and sponge-like structures. The formation of finger-like structure begins with rapid solidification of polymer solution at the interface between polymer solution and nonsolvent due to the steep activity and concentration gradient of all components on a macroscopic scale (Lee, Chae et al. 2013). As a result of the rapid solidification, the condensed solid polymer skin layer is formed with randomly distributed fractured points generated by immitigable stresses due to the shrinkage occurring during continuous desolvation as shown in **Figure II-3 (a)** (Lee, Chae et al. 2013). Once inflow of nonsolvent is initiated through the fractured points playing the role of pores, the propagation of fingers is simultaneously progressed with the growth of the fingers accompanying a perpendicular movement of the precipitated polymer to the side of the finger from the bottom of the finger since shrinkage of the polymer causes the freshly precipitated polymer to be tugged to upper region of the finger as shown in **Figure II-3 (b)** (Strathmann 1985). Much faster demixing rate within the finger than underneath the defect-free skin enables the precipitation front to advance rapidly within the finger, and these phenomena appear prominently when the precipitation front propagation is further facilitated by the faster influx of nonsolvent than an outflux of solvent due to solvent with high affinity for PSf such as N-methyl-2-pyrrolidone (NMP) (Strathmann 1985, Hansen 2007, Tiraferri, Yip et al. 2011). **Figure II-4 (a)** shows finger-like structured membrane prepared by the above-mentioned formation process.

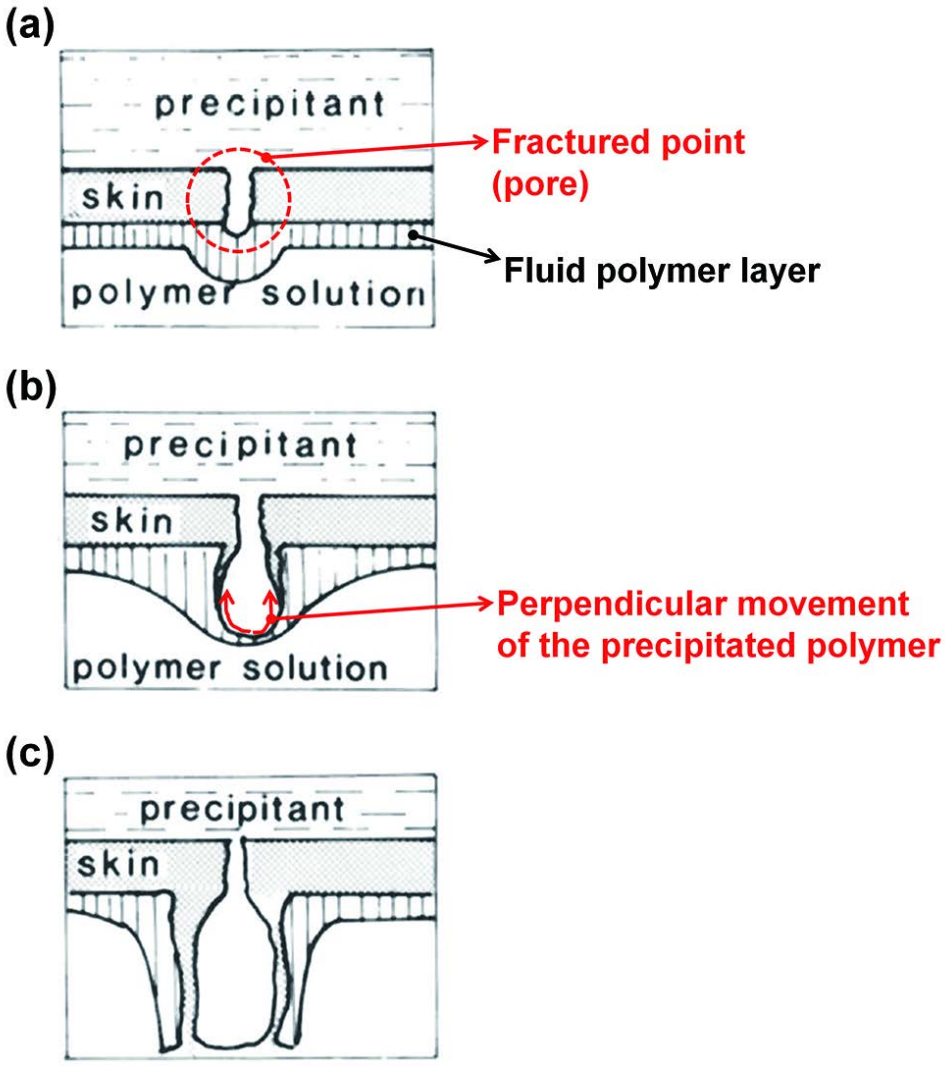

Figure II-3. Schematic diagram showing the formation process of finger-like structure at various times during phase separation (Strathmann 1985).

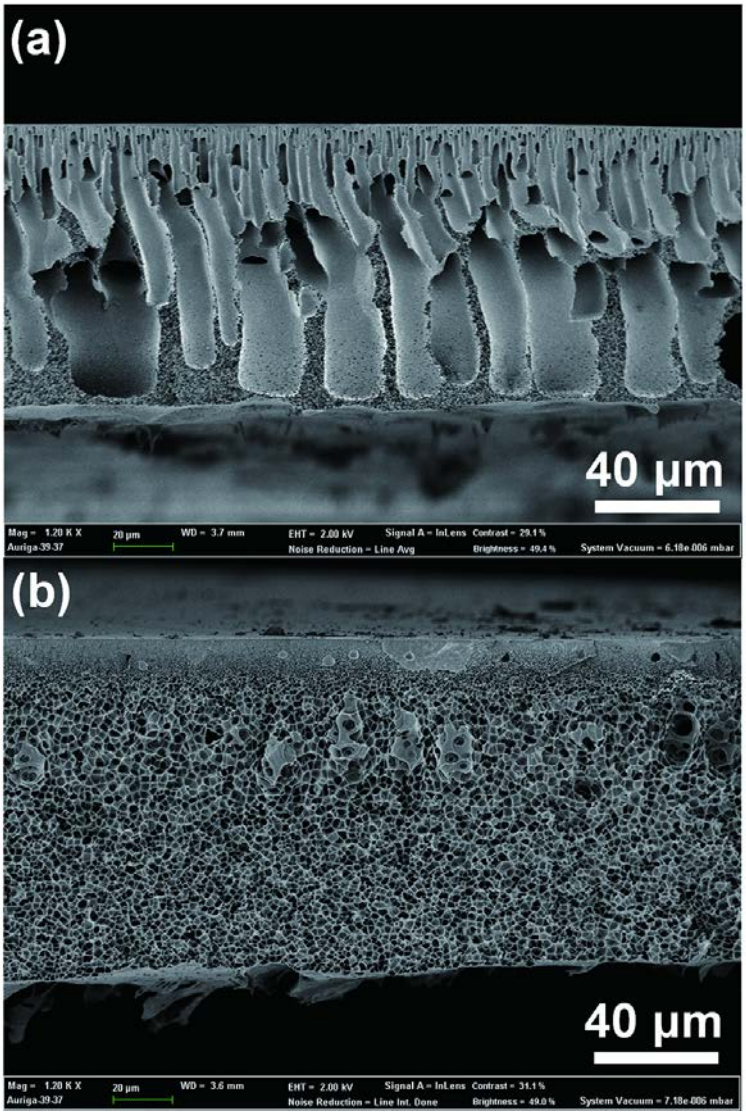

Figure II-4. Cross-sectional images of porous membrane with (a) finger- and (b) sponge-like structure.

Meanwhile, the rate of precipitation decreases with the increasing viscosity of polymer solution, which leads to a change from a finger-like structure to a sponge-like structure (Mulder 1996, Han and Nam 2002). The skin layer of porous membrane with sponge-like structure is identically formed with that of the finger-like structured membrane. However, the initiation of finger growth in the very viscous polymer solution is inhibited by the decrease of mutual diffusivities between solvent and nonsolvent due to rheological hindrance, so that precipitation in fluidic polymer layer under the solidified surface processes similarly to that in the polymer solution between the fingers in the finger-like structure (Strathmann 1985). In this case, the concentration profiles are flatter than those of the polymer solution having low viscosity because polymer concentration gradient is caused only by thermal molecular motions on a microscopic scale (Strathmann 1985). For this reason, the precipitation of polymer solution proceeds with few macroscopic gradients of the polymer concentration or chemical potential over the entire membrane cross section, so that a more or less homogeneous structure such as sponge-like structure is formed due to randomly distributed nuclei for precipitation (Strathmann 1985). **Figure II-4 (b)** presents cross-sectional image of porous membrane with sponge-like structure.

II.1.4. Factors affecting pore structure of membrane prepared by nonsolvent induced phase separation

As is discussed in the above two sections, final structure of porous membrane prepared by NIPs can vary depending on kinetic effects. For this reason, several researches have studied on how to control the pore structure of porous membrane by adjusting several significant parameters determining the membrane structure such as the precipitation and temperature, polymer concentration in the casting solution and the multi components system consisting of polymer, solvent, nonsolvents, and additives. (Strathmann and Kock 1977, Strathmann 1985, Smolders, Reuvers et al. 1992, Kim, Tyagi et al. 1996, Kim, Yoon et al. 2002, Ulbricht 2006, Zheng, Wang et al. 2006, Amirilargani, Saljoughi et al. 2010, Lalia, Kochkodan et al. 2013).

II.1.4.1. The selection of the polymer/solvent/nonsolvent system

Although solvent and nonsolvent used in membrane fabrication are determinant factor of the activity coefficient of the polymer in the three components system comprised of a polymer, a solvent and a nonsolvent, a quantitative approach to the membrane fabrication process is virtually impossible since it is very difficult to identify the activity coefficient of all the components and the relationship with these activity coefficients and the composition (Strathmann 1985). Fortunately, the interaction between polymer and solvent can be roughly estimated using the difference in the solubility parameter between them (Strathmann 1985). For example, the smaller difference in the solubility parameter, namely the better compatibility between polymer and solvent causes delayed demixing rate, which leads to the formation of sponge-like structured membrane,

all other conditions being equal (Strathmann 1985). The reciprocal action between polymer and nonsolvent can also be predicted using the difference in the solubility parameter between polymer and nonsolvent. The greater difference in the solubility parameter, namely less compatibility between polymer and nonsolvent induces larger activity coefficient of the polymer in the mixture of solvent and nonsolvent, so that finger-like structured membrane is formed due to the faster precipitation (Strathmann 1985). Lastly, the interaction between solvent and nonsolvent can be evaluated by measuring the heat of mixing of a solvent and nonsolvent (Strathmann 1985). Generally, finger-like structured membrane is formed by the three components system with a greater heat of mixing due to faster demixing rate (Strathmann and Kock 1977, Strathmann 1985).

For the reasons previously stated in the above paragraph, aprotic solvents without hydrogen atoms capable of participating hydrogen bonding such as dimethylacetamide (DMA), dimethylformamide (DMF), dimethyl sulfoxide (DMSO), and NMP lead to instantaneous demixing, so that they are widely used to fabricate highly porous membrane (Pinnau and Freeman 2000, Lalia, Kochkodan et al. 2013). Meanwhile, it is worth noting that variable structures can be formed by subtle difference in the compatibilities between polymer and solvent although aprotic solvents inducing instantaneous demixing are equally used to prepare membrane. For instance, NMP slowly diffuses out of casting solution during phase separation compared to DMF due to higher affinity for PSf than DMF (Hansen 2007, Tiraferri, Yip et al. 2011), which allows faster influx of nonsolvent into the casting solution layer than outflow of solvent unlike DMF (Tiraferri, Yip et al. 2011). As a result, the propagation of precipitation front appears exclusively in the casting solution layer consisting of NMP and PSf (Tiraferri, Yip et al. 2011).

Consequently, this disparity in affinity for PSf between NMP and DMF results in structural difference of membrane, in other words NMP and DMF induce finger- and sponge-like structure, respectively.

II.1.4.2. The effect of polymer concentration of polymer solution on the membrane structure

Polymer concentration in polymer solution is an important determinant of the structure of porous membrane prepared by NIPs. Generally, it is well known that a low and high polymer concentration in polymer solution cause to form finger- and sponge-like structure, respectively (Strathmann 1985). The influence of polymer concentration on the formation of membrane structure can be interpreted by the formation of finger-like structure and rheological effect. When polymer solution with a low polymer concentration is used to prepare porous membrane, membrane structure is formed by the initiation and propagation of fingers in sub-surface layer as aforementioned in the previous section. It is why a dilute polymer solution results in the finger-like structured membrane. However, the casting solution with higher polymer concentration forms skin layer with the increasing mechanical strength, which prevents the formation of fractured points on the skin layer and the consequential initiation of finger (Strathmann 1985). In addition, the increase in viscosity of polymer solution due to higher polymer concentration causes variation within the cross-sectional structure of membrane. In other words, the propagation of precipitation front toward bottom surface is inhibited by delayed demixing due to unusual increase in the viscosity of polymer solution, and the rheological hindrance by delayed demixing consequently results in the formation of membrane with a dense sub-layer such as sponge-like structure

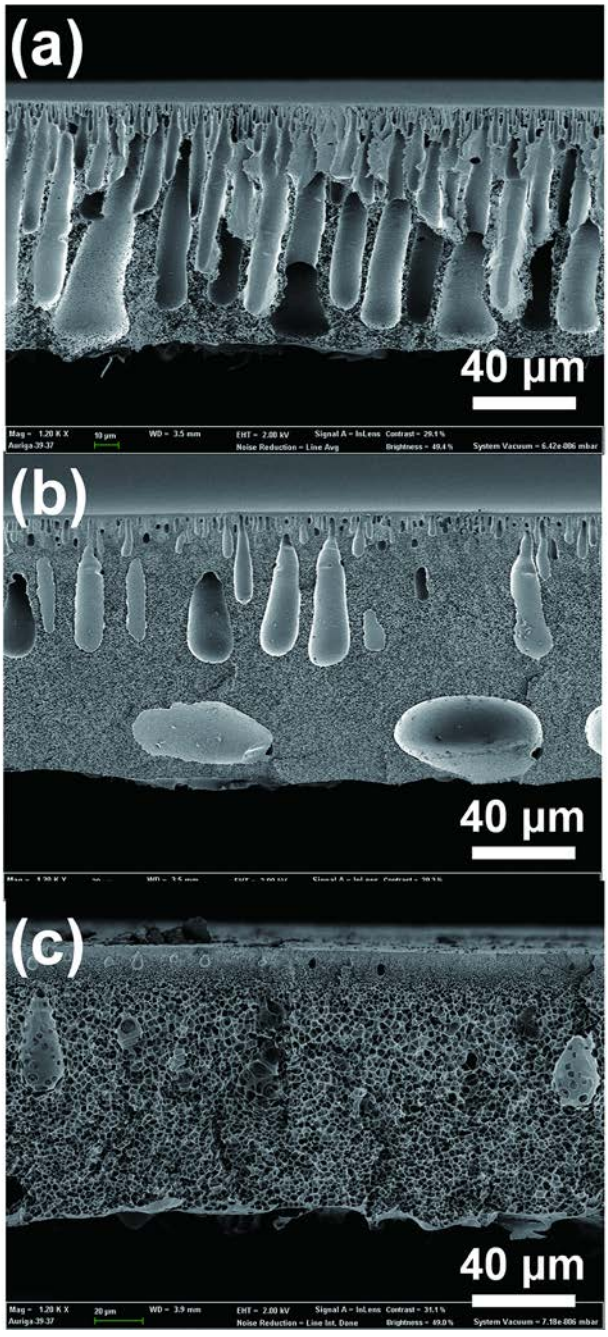

Figure II-5. SEM cross-sectional images displaying the membranes prepared by polymer solutions with different polymer concentration. (a) 20 wt%, (b) 25 wt%, and (c) 30 wt%.

(Lee, Chae et al. 2013). The structural variations of porous membrane according to polymer concentration of polymer solution are shown in **Figure II-**5.

II.1.4.3. The effect of additives on the membrane structure

It is known that several additives can lead to the increase in water permeability, hydrophilicity, pore density, and porosity of membrane (Lee, Won et al. 2002, Marchese, Ponce et al. 2003, Fontananova, Jansen et al. 2006, Arthanareeswaran, Thanikaivelan et al. 2007, Wang, Yu et al. 2009). For these reasons, various organics such as poly(ethylene glycol) (PEG) or polyvinyl pyrrolidone (PVP)) and inorganics such as LiCl additives have been widely used to prepared membrane with favorable morphology or properties for water permeability (Lafreniere, Talbot et al. 1987, Chuang, Young et al. 2000). Also, organics such as CNT or graphene oxide (GO) and inorganics such as Ag or TiO2 nanomaterials have attracted a great deal of attention as additives to improve membrane structure or hydrophilicity (Choi, Jegal et al. 2006, Yang, Zhang et al. 2007, Zodrow, Brunet et al. 2009, Lee, Chae et al. 2013).

The improvement by the aforementioned additives results from the variation of the thermodynamic and kinetic characteristics of polymer solution induced by the additives. Since additives increase the thermodynamic immiscibility of polymer solution with nonsolvent, the additives can enhance the thermodynamic instability concomitant with the change in the composition of polymer solution (Han and Nam 2002). The enhancement in thermodynamic instability or immiscibility by additives facilitates instantaneous demixing, so that porous structure such as finger-like structure is formed in sub-surface layer (Shi, Wang et al. 2008). However, excess additives causes delayed kinetic hindrance and the

resultant delayed demixing, which partially offsets the thermodynamic enhancement for phase inversion induced by additives (Lalia, Kochkodan et al. 2013). As a result, the formation of macrovoids is suppressed gradually with the increasing amount of additives, and solidified membrane prepared by polymer solution with excess additives has dense structure in sub-surface layer (Wang, Li et al. 2000, Lee, Won et al. 2002, Shi, Wang et al. 2008, Wang, Yu et al. 2009, Lalia, Kochkodan et al. 2013). This trend is exemplified in **Figure II-6**. Thus, a trade-off relationship between the thermodynamic enhancement and the kinetic hindrance in the phase separation system should be considered to prepare membrane with optimized porous structure for high performance.

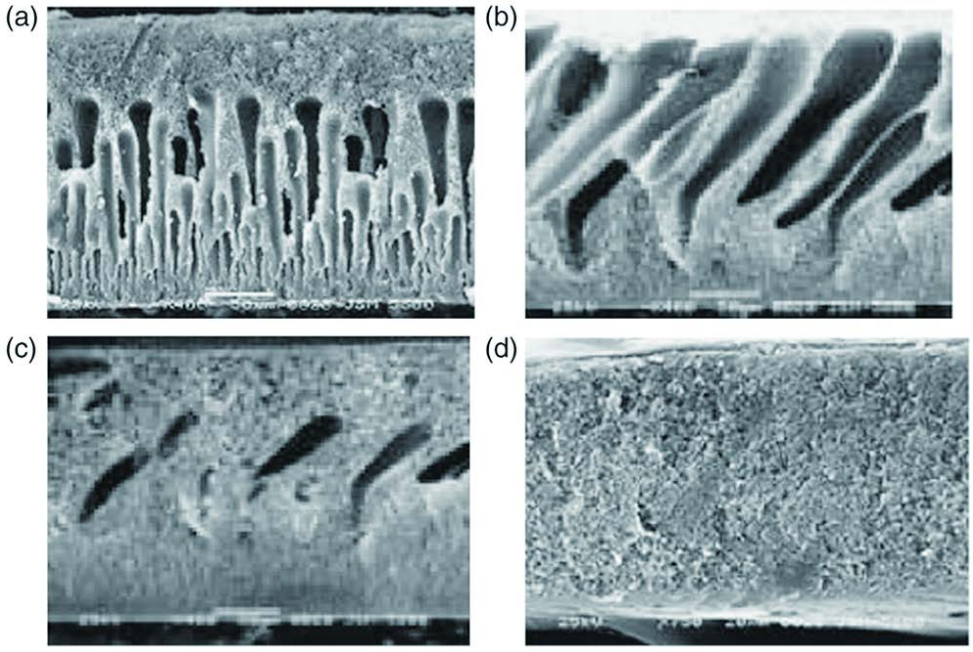

Figure II-6. SEM cross-sectional images displaying the structure of PSf/TiO_2 composite membranes with different contents of TiO_2.
(a) 0 wt% TiO_2, (b) 1 wt% TiO_2, (c) 3 wt% TiO_2, and (d) 5 wt% TiO_2 (Yang, Zhang et al. 2007).

II.2. Interfacial polymerization

II.2.1. History of reverse osmosis membrane

Since research on salt-rejecting membranes was initiated by a report entitled *The Sea as a Source of Fresh Water* in 1949, the research to develop reverse osmosis (RO) membrane with both comparable water permeability and salt rejection has undergone in phases (Lee, Arnot et al. 2011). After symmetric cellulose acetate (CA) membrane exhibiting 98% rejection but lower permeability than 10^{-2} $L \cdot m^{-2} \cdot h^{-1}$ was reported by Reid and Breton in 1959 (Reid and Breton 1959), an asymmetric CA membrane which can be seen as a milestone in addressing the first feasible RO membrane was announced by the Loeb-Sourirajan in 1962 (Loeb and Sourirajan 1962). The molecular compositions of materials used to fabricate the asymmetric RO membrane including the asymmetric CA membrane are presented in **Table II-2**. However, the asymmetric CA membrane has several disadvantages such as inadequate water permeability and salt rejection to meet commercial use, densification occurring under pressure, and a narrow range of choice of soluble polymer available in one-step casting to prepare the asymmetric membrane (Congjie 2003).

For these reasons, two-step casting methods were developed to optimize individual materials used for porous support layer and the dense active layer (Lee, Arnot et al. 2011). The molecular compositions of materials used to fabricate the major TFC RO membrane are presented in **Table II-3**. The first thin-film composite (TFC) membrane was prepared by floating a CA thin film followed by lamination onto a pre-prepared CA porous support and subsequent annealing (Francis 1966). Subsequently, a dip-coating method was suggested as an alternative

Table II-2. The chemical structures displaying segments of the asymmetric RO membranes (Lee, Arnot et al. 2011).

Chemical type & description	Chemical structure
1. Cellulose Acetate – Loeb-Sourirajan CA Flux: 0.35 $m^3 m^{-2} day^{-1}$ Salt rejection: 99% Test: > 100 bar, 4% NaCl solution	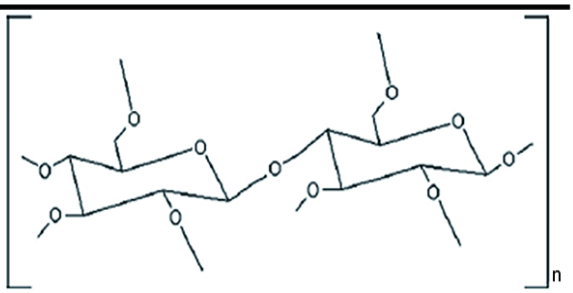
2. Aromatic Polyamide – Polyamide-hydrazide Flux: 0.67 $m^3 m^{-2} day^{-1}$ Salt rejection: 99.5% Test: 30 °C, > 100 bar, 3.5% NaCl solution	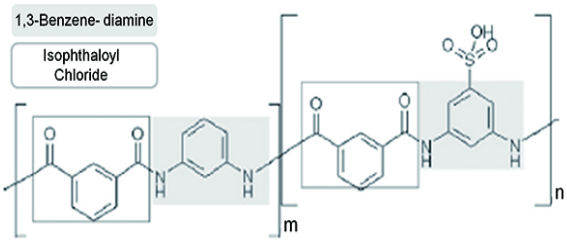
3. Polypiperzine-amide Flux: 0.67 $m^3 m^{-2} day^{-1}$ Salt rejection: 97.2% Test: > 80 bar, 0.36% NaCl solution	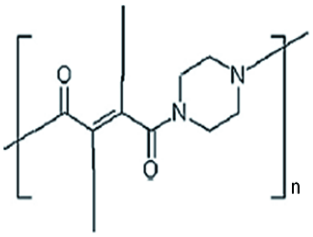
4. Polybenzimidazoline Flux: 0.13 $m^3 m^{-2} day^{-1}$ Salt rejection: 95% Test: > 6 bar, 0.105% NaCl solution	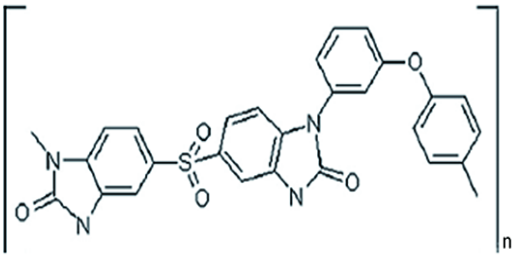
5. Polyoxadiazole Flux: 0.07 $m^3 m^{-2} day^{-1}$ Salt rejection: 92% Test: > 45 bar, 0.5% NaCl solution	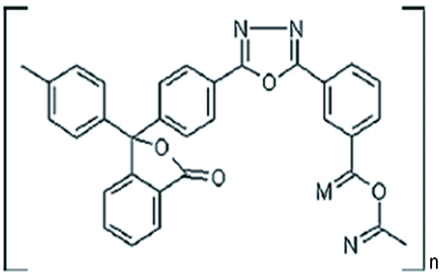

Table II-3. The chemical structures displaying segments of the TFC RO membranes (Lee, Arnot et al. 2011).

Chemical type & description	Chemical structure
1. Polyfurane – Name: NS-200 Flux: 0.8 $m^3 m^{-2} day^{-1}$ Salt rejection: 99.8% Test: > 100 bar, 3.5% NaCl solution	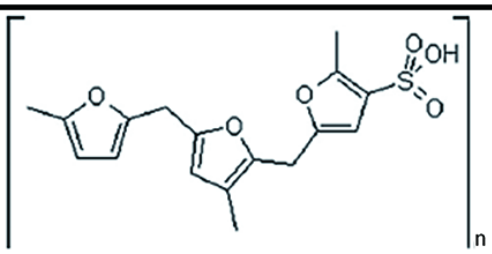
2. Polyether-Polyfurane – Name: PEC-1000 Flux: 0.5 $m^3 m^{-2} day^{-1}$ Salt rejection: 99.9% Test: > 69 bar, 3.5% NaCl solution -Excellent organic rejection	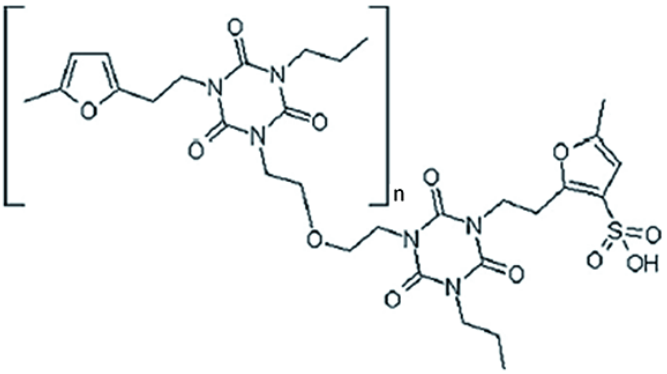
3. Sulfonated Polysulfone – Name: Hi-Flux CP Flux: 0.06 $m^3 m^{-2} day^{-1}$ Salt rejection: 98% Test: > 69 bar, 3.5% NaCl solution -Excellent chlorine resistance	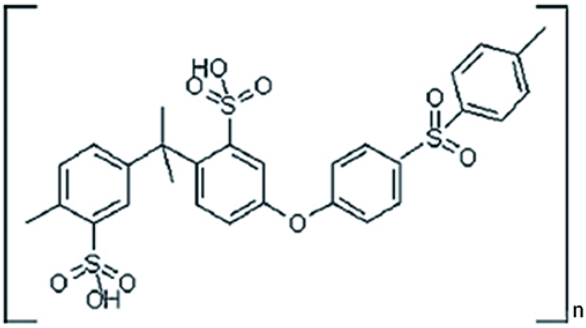
4. Polyamide via polyethylenimine – Name: NS-100 Flux: 0.7 $m^3 m^{-2} day^{-1}$ Salt rejection: 99% Test: > 100 bar, 3.5% NaCl solution	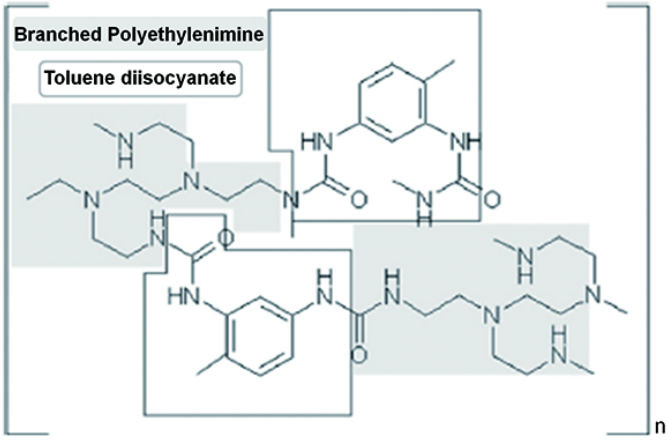

Table II-3 (*Continued*)

Chemical type & description	Chemical structure
5. Polyamide via polyepiamine – Name: PA- 300 or RC-100 Flux: 1.0 $m^3 m^{-2} day^{-1}$ Salt rejection: 99.4% Test: > 69 bar, 3.5% NaCl solution	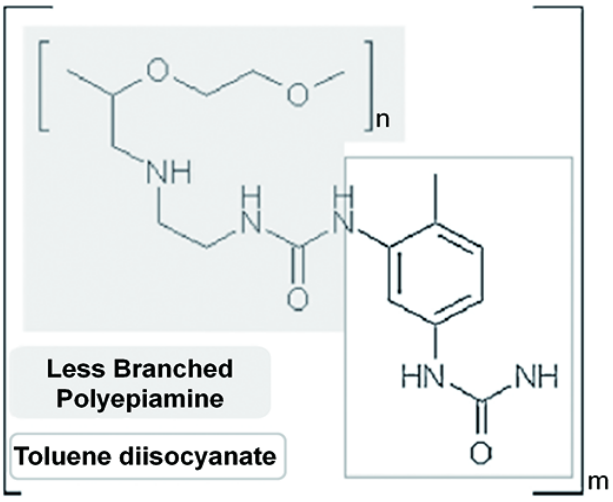
6. Polyvinylamine – Name: WFX-X006 Flux: 2.0 $m^3 m^{-2} day^{-1}$ Salt rejection: 98.7% Test: > 40 bar, Conductivity-5000 μS cm^{-1}	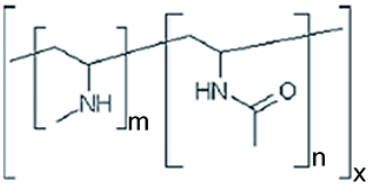
7. Polypyrrolidine Flux: 0.8 $m^3 m^{-2} day^{-1}$ Salt rejection: 99.7% Test: > 40 bar, 0.5% NaCl solution	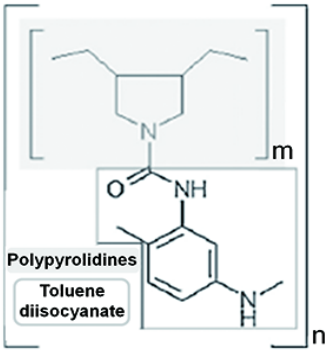
8. Polypiperazine-amide – Name: NS-300 Flux: 3.3 $m^3 m^{-2} day^{-1}$ Salt rejection: 68% Test: > 100 bar, 3.5% NaCl solution	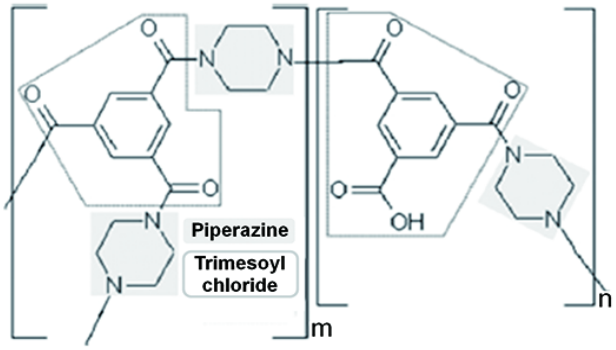

Table II-3 (*Continued*)

Chemical type & description	Chemical structure
9. Cross linked Fully Aromatic Polyamide – 1 -Name: FT-30 Flux: 1.0 $m^3 m^{-2} day^{-1}$ Salt rejection: 99% Test: > 15 bar, 0.2% NaCl solution	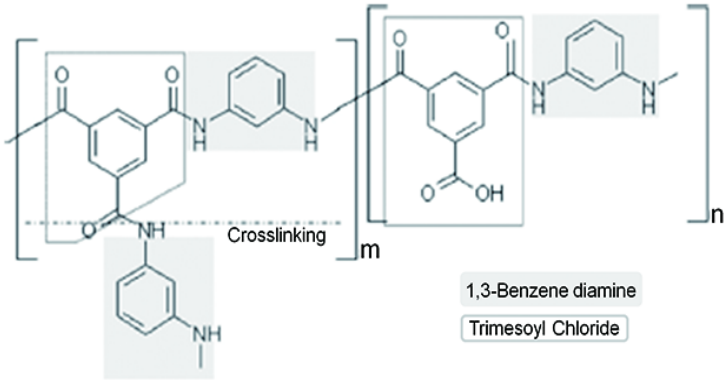
10. Cross linked Fully Aromatic Polyamide – 2 -Name: UTC series Flux: 0.8 $m^3 m^{-2} day^{-1}$ Salt rejection: 98.5% Test: > 15 bar, 0.5% NaCl solution	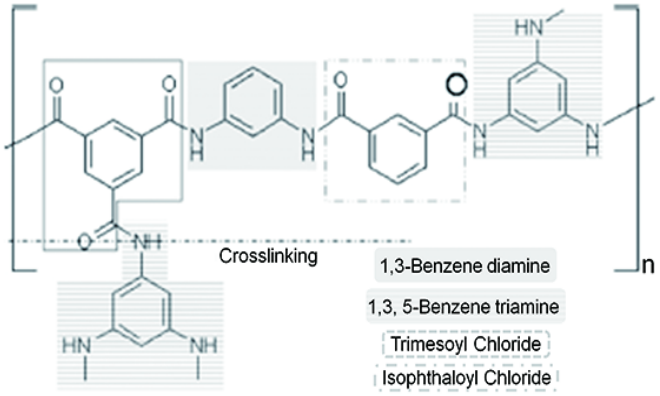
11. Cross linked Aralkyl Polyamide -Name: A-15 Flux: 0.26 $m^3 m^{-2} day^{-1}$ Salt rejection: >98% Test: > 55 bar, 3.2% NaCl solution	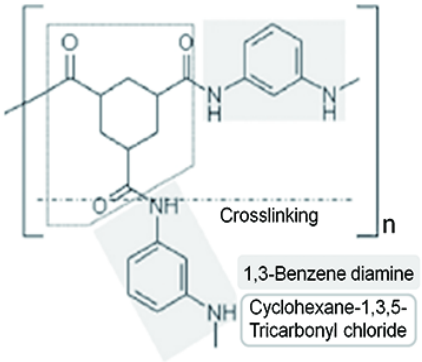
12. Cross linked Fully Aromatic Polyamide - 3 -Name: X-20 Flux: 1 $m^3 m^{-2} day^{-1}$ Salt rejection: 99.3% Test: > 15 bar, 0.2% NaCl solution	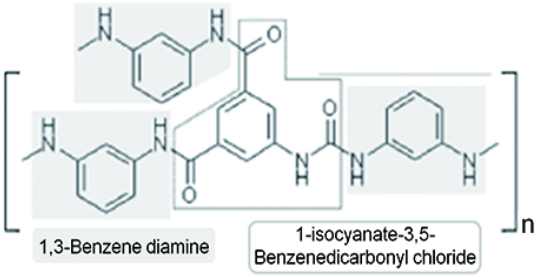

to overcome difficulties inherent in float-casting method respecting mass production (Riley, Lonsdale et al. 1971, Kirsh and Popkov 1988). The reaction of furfural alcohol, sulphuric acid and polyoxyethylene (or 1, 3, 5-tris(hydroxyethyl) isocyannuric acid) was used to realize the dip-coating method including acid polycondensation as shown in **Table II-3** (1975, Kurihara, Kanamaru et al. 1980). The membranes prepared by the dip-coating method revealed excellent salt rejection but were susceptible to irreversible swelling, hydrolysis of the sulphate linkage, or chlorine attack (Lee, Arnot et al. 2011). Plasma or atomic polymerization were also applied onto a PSf support layer to form dense active layer, but they also did not solve problems with regard to poor chemical durability such as low chlorine resistance (Lee, Arnot et al. 2011).

Since PSf is known to have superior properties such as stability in the alkaline environment, the fabrication of TFC membrane using interfacial polymerization (IP) was facilitated because a support layer must be able to withstand the caustic conditions for removing hydrogen halides formed during the IP process (Lee, Arnot et al. 2011). The first non-cellulosic RO membrane was successfully developed by Cadotte through the reaction of polythylenimine with toluene di-isocyanate (**Table II-3**), which demonstrated comparable water permeability and salt rejection as well as thermal and pH stabilities (Cadotte 1977, Bartels 1989, Mysels and Wrasidlo 1991). However, this membrane has limitations such as poor resistance to chlorine and very severe surface brittleness due to a highly cross-linked structure (Lee, Arnot et al. 2011). Subsequently, Cadotte succeeded in developing FT-30 membrane (**Table II-3**) with superior permselectivity corresponding to fluxes of about 1 $m^3 \cdot m^{-2} \cdot day^{-1}$ with salt rejection of 99.2% under operating pressure of 55 bar through the interfacial reaction

between aromatic amines and acyl halides (Cadotte, Petersen et al. 1980, Cadotte 1981, Koo, Petersen et al. 1986). In addition, FT-30 exhibited thermal, chemical, pH stabilities as well as resistibility against compression according to Cadotte. Furthermore, it was not perfect but showed improved tolerance to chlorine (Glater, Zachariah et al. 1983). As a result, products derived from FT-30 have been commercialized by DOW FILMTEC^{TM} (Larson, Cadotte et al. 1981), which led to launching comparable products such as the CPA2 membrane and the UTC-70 produced by Hydranautics and Toray Industries, respectively (Light, Chu et al. 1987, Himeshima, Kurihara et al. 1988, Tomaschke 1990).

II.2.2. Fabrication of thin-film composite reverse osmosis membrane using interfacial polymerization

Interfacial polymerization (IP) is the most widely used method to prepare commercial TFC RO membrane due to the significant strengths in optimizing independently the characteristics of dense active layer and porous support layer (Petersen 1993, Lau, Ismail et al. 2012). Among several IP methods, the combination of monomeric aromatic amines such as 1,3-benzendiamine (m-phenylenediamine, MPD) and aromatic acyl halide with carbonyl halide groups more than three such as trimesoyl chloride (TMC) is regarded as the best option for IP, because both polymerization and cross-linking occurring during IP are rapid in the combination even if acyl lower concentration of halide is used (Cadotte, Petersen et al. 1980, Cadotte 1981, Koo, Petersen et al. 1986, Lee, Arnot et al. 2011). For this reason, surfactants or acid acceptor to neutralize hydrogen halides generated during the IP are not absolutely necessary in the above system (Lee, Arnot et al. 2011). Another reason we have to notice is that the above system leads to unusual surface properties which have been addressed as a ‘ridge and valley’ structure unlike aliphatic amines inducing smooth surface (Petersen and Cadotte 1990). In this section, mechanism for the formation of ridge and valley structure will be addressed based on IP process.

In IP, a porous support membrane is first immersed in an aqueous solution containing amine monomers to impregnate the reactive prepolymer in support membrane. Subsequently, the amine soaked support membrane is immersed in a water-immiscible organic solvent solution of aromatic acyl halide after excess amine solution on the surface of support membrane is removed through rolling or air knife process. While the amine-saturated support membrane is immersed in the

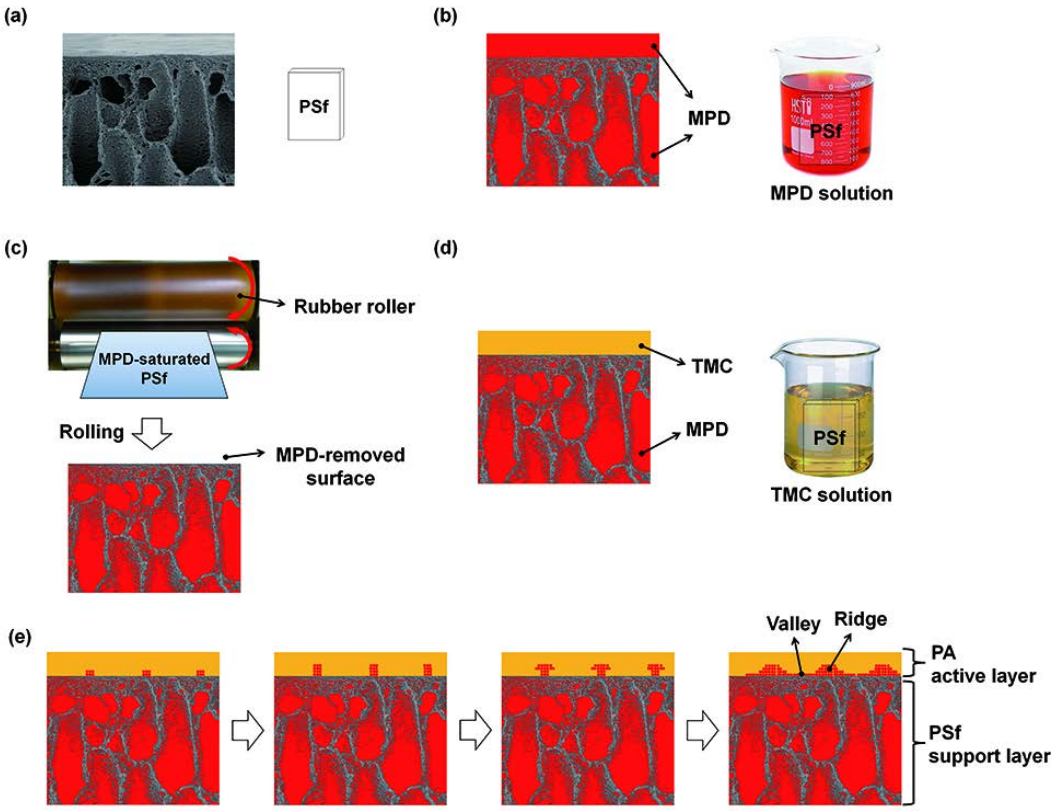

Figure II-7. Schematic illustration of polyamide active layer formation by interfacial polymerization. (a) polysulfone (PSf) support membrane, (b) m-phenylene diamine (MPD) soaked PSf support membrane, (c) the MPD soaked PSf support membrane that excess MPD solution on its surface is removed, (d) immersion of the MPD soaked support membrane in trimesoyl chloride (TMC) solution, and (e) schematic depiction of interfacial polymerization (IP) occuring on the interfacial layer between aqueous phase and organic phase while the MPD-saturated PSf is immersed in the TMC solution.

aromatic acyl halide solution, IP occurs on the interfacial layer between aqueous phase and organic phase to form a thin and densely cross-linked active layer. A series of the aforementioned IP process is depicted in **Figure II-7**.

Incipient polyamide (PA) film formation on the support membrane is initiated by “volcano-like” reaction accompanying the amine monomers eruption from surface pores of the support layer during the IP, because only the amine monomer can diffuse into organic solvent unlike the acyl halide unable to diffuse into water (Freger 2005, Ghosh and Hoek 2009) (**Figure II-7**). After the amine monomers eruption, the amine monomers diffuse laterally, so that a continuous and integral PA film is formed. Consequentially, the initial PA clumps reaching earlier a high molecular weight than the laterally spreading base film develops into ridges, and the lateral film connecting the initial clumps becomes valleys (Ghosh and Hoek 2009). This ridge and valley structure only appears in fully aromatic polyamide membranes prepared by MPD and TMC while TFC membranes made from aliphatic amines or semi-aromatic polyamide membranes prepared by piperazine (PIP) and TMC have smooth surface (Petersen and Cadotte 1990, Tang, Kwon et al. 2009). **Figure II-8** shows structural differences between active layers of semi-aromatic poly(piperazinamide) membrane and MPD/TMC based fully aromatic membrane.

.

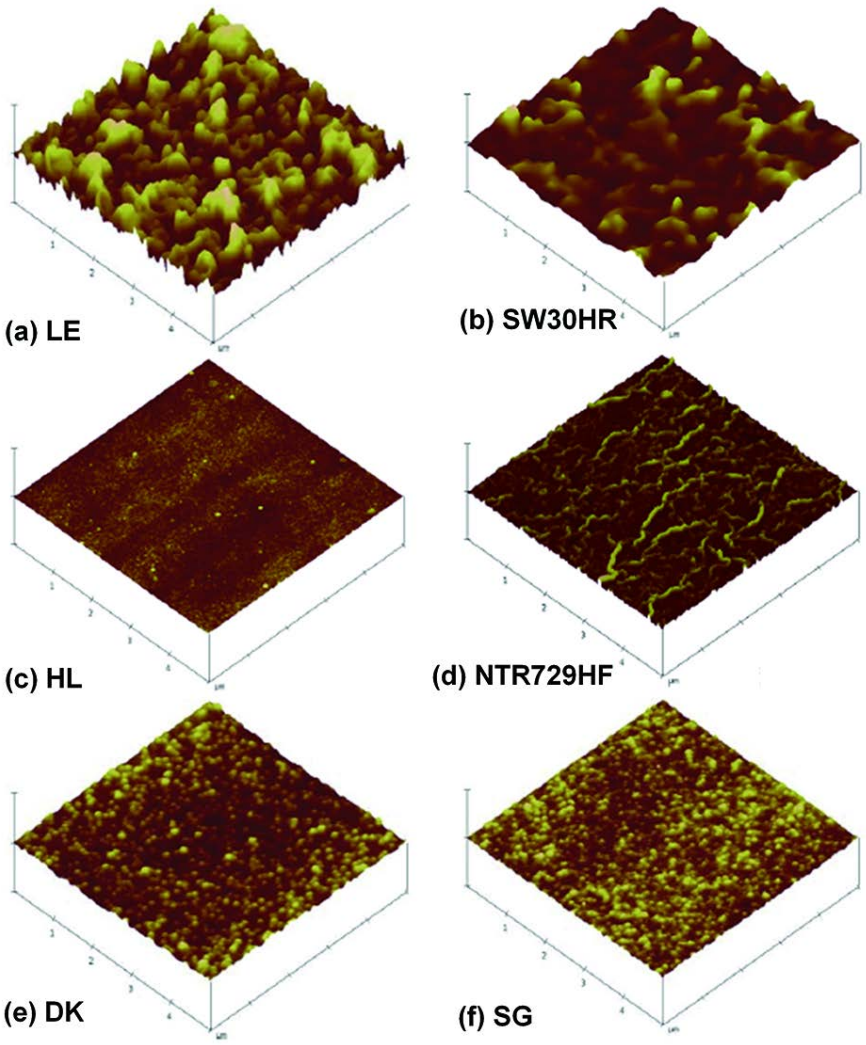

Figure II-8. AFM images showing active layers of commercial RO membranes. (a) LE, (b) SW30HR, (c) HL, (d) NTR729HF, (e) DK and (f) SG. LE and SW30HR were made from MPD and TMC. Others were fabricated using PIP and TMC. SW30HR, HL, and NTR729HF were additionally coated using polyvinyl alcohol (PVA) (Tang, Kwon et al. 2009).

II.2.3. Recent trend of reverse osmosis membrane

Since an asymmetric CA membrane was introduced as the first feasible RO membrane by the Loeb-Sourirajan in 1962 (Loeb and Sourirajan 1962), the fabrication technology of RO membrane has undergone much progress. Mogan first announced TFC membrane fabricated by IP in 1965 (Morgan 1965), and Cadotte successfully developed the first non-cellulosic TFC RO membrane with comparable flux and rejection such as FT-30 by using IP of aromatic amines and acyl halides (Cadotte 1977, Cadotte, Petersen et al. 1980, Cadotte 1981, Koo, Petersen et al. 1986, Bartels 1989, Mysels and Wrasidlo 1991). However, conventional RO membranes have still limitations such as high energy consumption, because it requires hydraulic pressure exceeding the osmotic pressure of feed solution to permeate water molecule through the pores smaller than diameter of hydrated ion (Sourirajan 1970). For this reason, several researches have been conducted to reduce high operational costs associated with high hydraulic pressure in RO process through various approaches from addition of nanomaterials to molecular layer-by-layer (mLbL) assembly.

II.2.3.1. Thin film nanocomposite membranes

Nanomaterials have been used to improve RO membrane performance by combining the benefits of the nanomaterials such as good permselectivity, controllable hydrophilicity, zeta potential, and pore structure along with better physical and chemical stabilities with strengths of conventional TFC RO membranes such as flexibility and high packing density (Jeong, Hoek et al. 2007). There are two strategies for the preparation of TFC nanocomposite membranes. One is to incorporate inorganic materials into TFC membranes, and another is to

add organic materials to TFC membranes.

Zeolite nano-particles are representative inorganic materials that have been used to prepare TFC nanocomposite membranes. Jeong prepared TFC nanocomposite membranes by embedding hydrophilic zeolite nano-particles with negatively charged 0.4 nm pores throughout the polyamide active layer of TFC membranes via IP of MPD and zeolite dispersed TMC solution as shown in **Figure II-9** (Jeong, Hoek et al. 2007). The authors found that hydrophilicity and zeta potential of TFC nanocomposite membranes increases while roughness decreases with increasing amount of zeolite nano-particles. In addition, the TFC nanocomposite membranes including 0.4 wt% of pore-opened zeolites showed the increase in water permeability as much as 80 % with equivalent salt rejection (Jeong, Hoek et al. 2007). This tendency appeared even when pore-filled zeolites were used to fabricate TFC nanocomposite membranes. The authors suggested that these results could result from the enhancement in Donnan exclusion and permeability as well as structural variation of membrane induced by zeolite fillers (Jeong, Hoek et al. 2007, Lind, Ghosh et al. 2009).

Among several organic nanofillers, carbon nano-tubes (CNTs) have attracted much attention in the field of membrane fabrication due to similar water transport properties of CNTs to those of fluid transport channels incorporated in biological cell membranes (Noy, Park et al. 2007). In response to a lot of attention, CNTs composite polymeric membranes and their characteristics regarding water transport have been addressed in many papers and the knowledge respecting CNTs membranes is becoming increasingly common (Qiu, Wu et al. 2009, Wu, Tang et al. 2010, Roy, Ntim et al. 2011, Vatanpour, Madaeni et al. 2011, Chan, Chen et al. 2013, Van der Bruggen 2013, Wu, Tang et al. 2013, Zhao, Qiu et al. 2014).

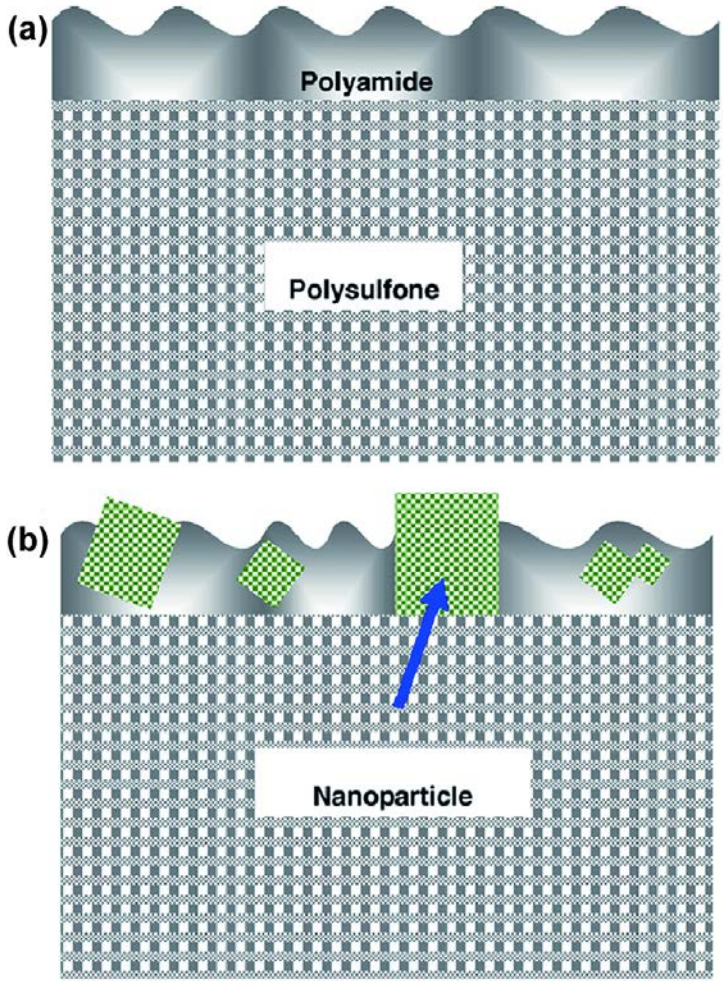

Figure II-9. Conceptual illustration of (a) conventional TFC, and (b) TFC nanocomposite membrane structures (Jeong, Hoek et al. 2007).

According to the previous studies, the fast water transport of a slug flow manner results from repulsion between water molecules bound by a strong hydrogen bond and flat hydrophobic inner wall of CNTs and the resultant vapor layer on interface between them (Hummer, Rasaiah et al. 2001, Kalra, Garde et al. 2003). Another research suggested that a liquid layer of water molecules formed on the inner wall of CNTs leads to the frictionless water transport by shielding the bulk water molecules (Kotsalis, Walther et al. 2004). CNTs with the above-mentioned characteristics can be embedded into active layer of TFC membrane via IP of MPD and CNTs dispersed TMC solution as shown in **Figure II-10**. In this way, untreated CNTs can be effectively incorporated onto the active layer formed on a porous support membrane by conventional IP, and it exhibited superior performance (Ratto, Holt et al. 2011).

II.2.3.2. Molecular layer-by-layer (mLbL) assembled TFC composite membranes

Separation of water from feed solution occurs through active layer of TFC membrane (Elimelech and Phillip 2011). In other words, hydraulic resistance and salt rejection are determined by characteristics of active layer such as thickness, cross-linking degree, roughness, hydrophilicity, and surface charge. Thus, it is important to adjust structural and chemical properties of active layer in the phase of IP. However, it is difficult to control thickness and structure of active layer since the system consisting of aromatic amines and acyl halides fast reaches a gel point due to the rapid reaction between them (Freger 2003). To solve this problem, recent research attempted to prepare active layer with tunable thickness, density and structure via molecular layer-by-layer (mLbL) (Gu, Lee et al. 2013). **Figure II-11**

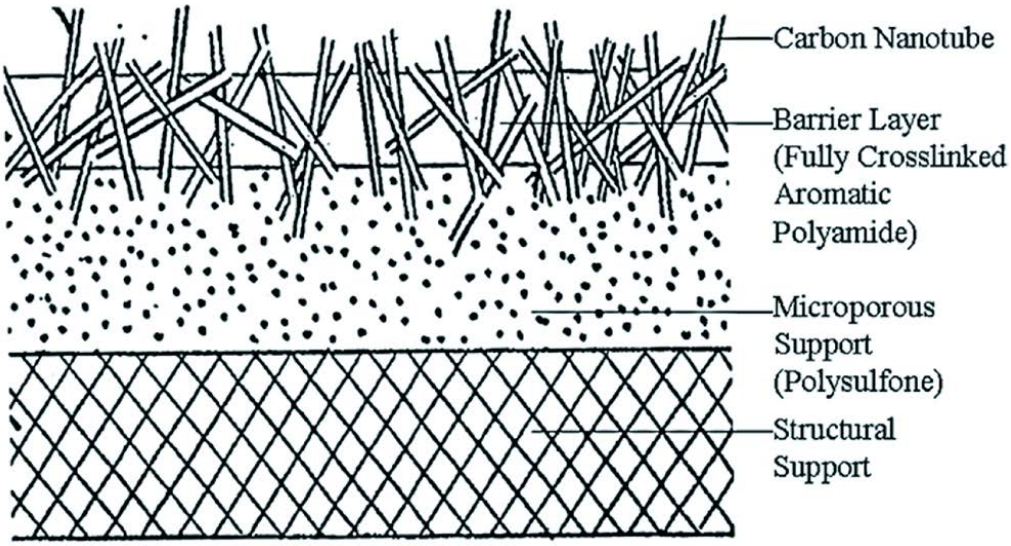

Figure II-10. Schematic illustration of CNTs nanocomposite TFC membrane (Ratto, Holt et al. 2011).

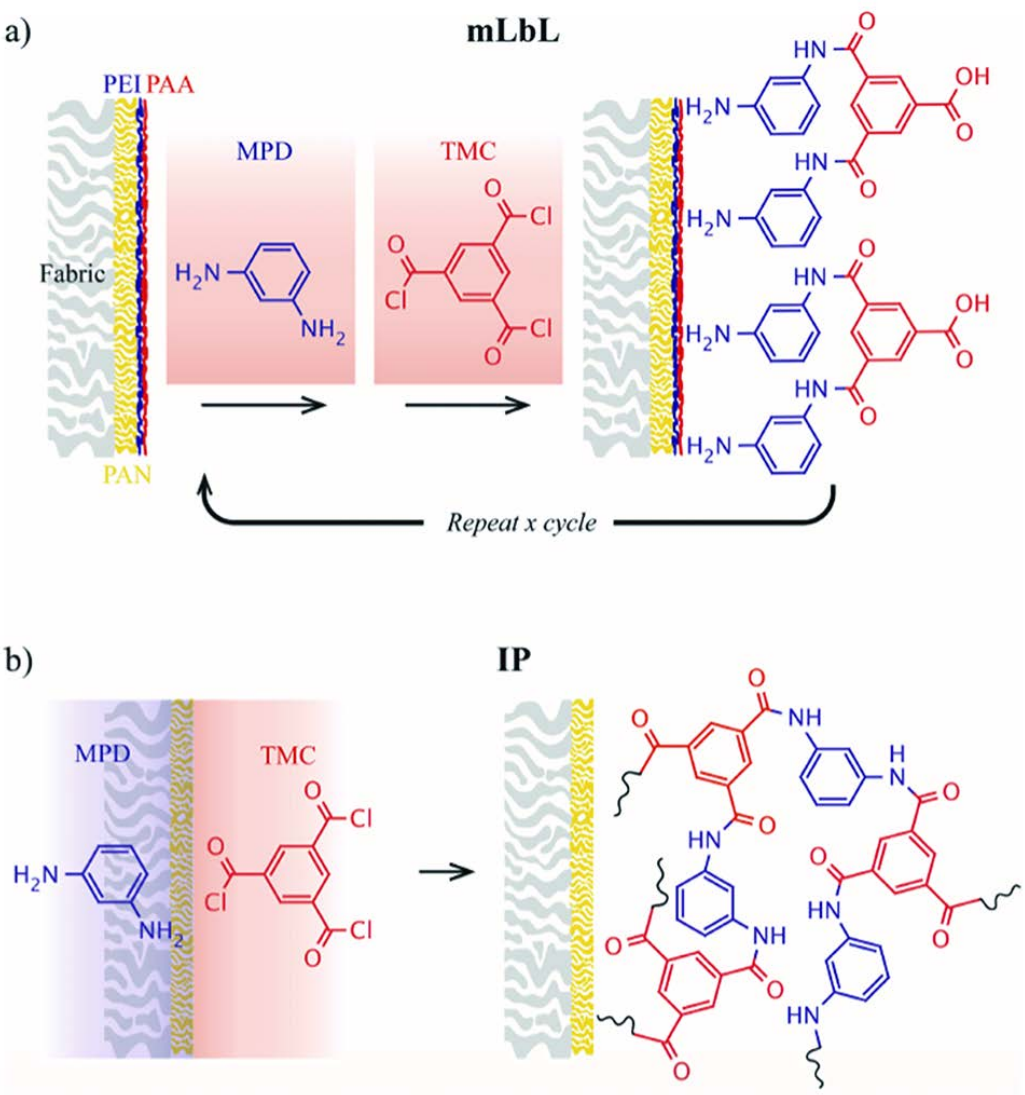

Figure II-11. Conceptual illustration of the preparation of TFC membranes via (a) mLbL deposition and (b) conventional IP (Gu, Lee et al. 2013).

shows conceptual illustration of the preparation of TFC membranes via (a) mLbL deposition and (b) conventional IP. The mLbL permits thickness control at monomer length-scale, minimal surface roughness, and well-defined chemical composition of active layer. As a result, the mLbL assembled membranes exhibited a fivefold decrease in the active layer thickness (mLbL: 20 nm, IP: 110 nm) and the consequential 80% increase in the water permeability when 15 cycles of mLbL assembly were conducted to achieve comparable salt rejection. In addition, roughness of mLbL membrane (mLbL: 3.4 nm, IP: 45.1 nm) was decreased by as much as 13 times in comparison to that of IP membrane, so that flux decline due to fouling caused by bovine serum albumin (BSA) was mitigated from 16% to 10% decline.

II.2.3.3. Bio-inspired RO membranes

Aquaporin with an hourglass-shaped structure are water-selective protein channels capable of controlling water permeation across biological cell membranes (Agre 2005). Agre first showed the aquaporin can exclude ion species revealing fast water diffusion in a single-file line caused by osmotic gradients as shown in **Figure II-12** (Agre, Sasaki et al. 1993, Meinild, Klaerke et al. 1998, Agre 2004). Subsequent molecular dynamics simulations also exhibited that aquaporin have water permeability at close to the transport of 10^8 to 10^9 water molecules/s (Jensen and Mouritsen 2006). The potential of aquaporin as an alternative for desalination membrane led to the development of desalination membranes incorporating aquaporin. Daniel incorporated aquaporin into the wall of self-assembled polymer consisting of tri-block co-polymer, poly(2-methyl-2-oxazoline)-blockpoly(dimethylsiloxane)-block-poly(2-methyl-2-oxazoline), and demonstrated

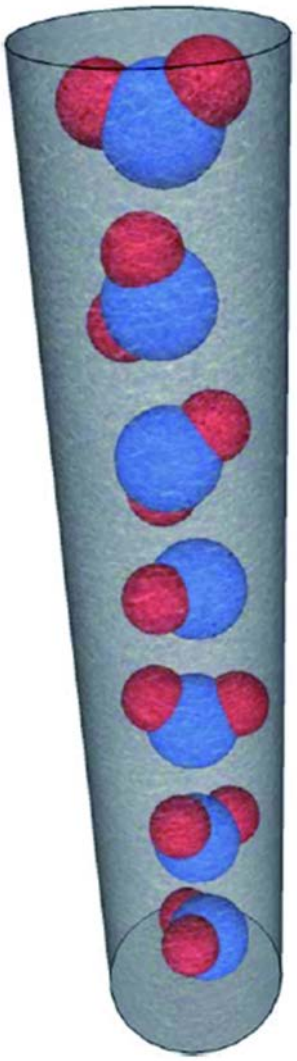

Figure II-12. Water molecules passing through nanoscale channels such as aquaporins and CNTs depicted by molecular dynamics simulations (Hummer, Rasaiah et al. 2001).

exceptional water permeability compared to conventional TFC membranes (Fierro, Buhr et al. 2009). Their results exhibited a ten-fold increase in water permeability relative to commercial TFC RO membranes. Although salt rejection capability of membranes incorporating aquaporin has not been reported yet, the previous studies suggest that it might be possible to develop desalination membranes with fairly enhanced performance via incorporation of aquaporin.

II.3. Graphene oxide

II.3.1. Introduction

Graphene sheets with two-dimensional structure composed of sp^2-bonded carbon have drawn tremendous attention from researchers in various fields due to a range of remarkable characteristics such as electron mobility (2×10^5 $cm^2 \cdot V^{-1} \cdot s^{-1}$) (Bolotin, Sikes et al. 2008), mechanical properties (Young's modulus of 1 TPa, tensile strength of 130 GPa) (Lee, Wei et al. 2008), high surface area (1850-2630 $m^2 \cdot g^{-1}$) (McAllister, Li et al. 2007), and thermal properties (Stankovich, Dikin et al. 2006, Geim and Novoselov 2007, Geim 2009, Zhang, Liang et al. 2009, Pan and Aksay 2011, Lin, Shen et al. 2012). Mass production of graphene sheets must take precedence in order for industrial utilization of them with the above-mentioned exceptional properties. Among the best-known techniques to produce graphene sheets and their derivatives such as chemical vapour deposition (Eizenberg and Blakely 1979, Aizawa, Souda et al. 1990), growth of epitaxial graphene on insulating substrates (Berger, Song et al. 2006), mechanical exfoliation of graphite powder (Novoselov, Geim et al. 2004), and chemical reduction of graphene oxide prepared by modified Hummers method (Stankovich, Piner et al. 2006, Stankovich, Piner et al. 2006), the last chemical method is regarded as one of the most practical approaches to produce the bulk quantity of graphene sheets (Rafiee, Rafiee et al. 2009, Lin, Shen et al. 2012). For this reason, graphene oxide produced by the exfoliation of graphite oxide has recently attracted attention as an alternative for large-scale synthesis of graphene sheets (Stankovich, Dikin et al. 2006, Rafiee, Rafiee et al. 2009, Lin, Shen et al. 2012). Detailed information for the current synthesis methods of graphene and graphene derivatives and the corresponding

features are summarized in **Table II-4**.

Graphene oxide, which is a layered material prepared by the exfoliation of graphite oxide, has myriad functional groups such as hydroxyl and epoxy functional groups on its basal plane as well as carbonyl and carboxyl groups located at its edge as shown in **Figure II-13** (He, Klinowski et al. 1998, Lerf, He et al. 1998, Stankovich, Dikin et al. 2006). These functional groups allow graphene oxide to have very hydrophilic properties (Stankovich, Dikin et al. 2006, Stankovich, Dikin et al. 2007, Nair, Wu et al. 2012). In addition, GO sheets can form stable aqueous colloids due to electrostatic repulsion caused by ionization of the phenolic hydroxyl groups and carboxylic acid as shown in **Figure II-14** (Li, Müller et al. 2008). These characteristics render graphene oxide sheets a good precursors for use of graphene sheets in many applications from polymer composites to biomedical applications by forming stable suspension of quasi-two-dimensional carbon sheets (Stankovich, Dikin et al. 2006, Dreyer, Park et al. 2009). However, graphene oxide sheets should be chemically modified prior to their applications, because they could only be well dispersed in aqueous solution being incompatible with most polymers due to their hydrophilic property (Stankovich, Dikin et al. 2006). Furthermore, their electrically insulating property restricts their feasibility for the fabrication of conductive polymer nanocomposites (Stankovich, Dikin et al. 2006).

Recently, many researches have been reporting on utilization of exceptional characteristics of graphene oxide themselves unlike the approaches to prepare precursors for chemically modified graphene sheets. For instance, several researchers have developed hydrophilic membranes by incorporating graphene oxide as hydrophilic additives in the membranes for water and wastewater

Table II- 4 . Graphene synthesis methods (Kumar and Lee 2013).

Synthesis Method	Brief Description/Remarks
Mechanical Exfoliation	- Using a regular Scotch tape to peel off graphene from HOPG. - Atomic layer of graphene can be seen on ~300 nm SiO2 substrates under an optical microscope. - Pristine graphene with highest quality of electrical properties. - The size, thickness and location are uncontrollable, with limited practical applications.
Solution based exfoliation of graphene oxide (GO)	- Graphite powders are initially oxidized by chemical modification (Hummers' method) to be dispersed in solution. - GO are subsequently reduced to graphene by thermal annealing or chemical reducing agents. - Large scale production for bulk applications, such as supercapacitors, composite materials, etc. - Significant structural defects and leaving oxygen functional groups on the product.
Epitaxial growth using SiC substrates	- A conversion of SiC substrate to graphene via sublimation of silicon atoms on the surface. - Done at high temperature (~1300 °C) and ultrahigh vacuum condition. - Limited accessibility due to high-end equipment.
CVD growth Graphene	- Most promising, inexpensive and feasible method for single layer or multilayers graphene production. - Using transition metal (Ni, Cu, etc.) substrates or thin films as catalyst. - Flowing carbon source (CH_4) and reactant gases (H_2) at high temperature (~1000 °C) for the nucleation of graphene. - Single layer graphene can usually be obtained on Cu. - Can be scaled up for large area graphene production for practical applications, such as transparent electrode applications.

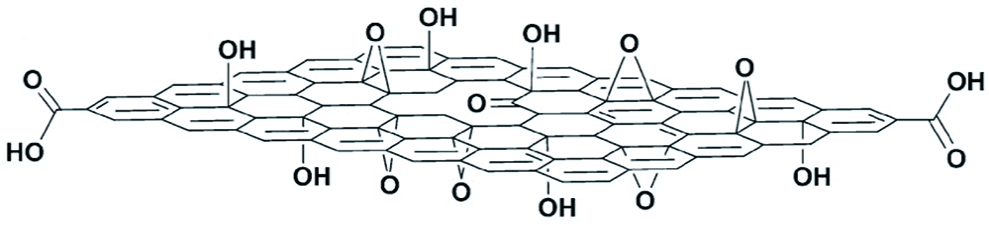

Figure II-13. Schematic model of a graphene oxide sheet (Compton and Nguyen 2010).

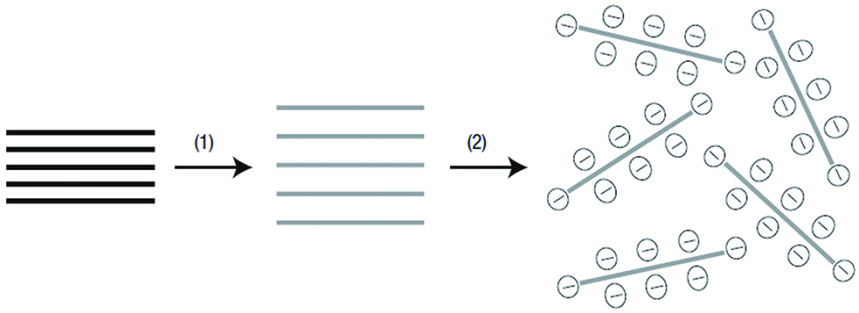

Figure II-14. Schematic illustration of the chemical route to the synthesis of well-dispersed GO colloids (Li, Müller et al. 2008).

treatment (Wang, Yu et al. 2012, Zhang, Xu et al. 2013). In addition, it has been demonstrated that graphene oxide with a great number of functional groups could induce superoxide anion-independent oxidative stress on microorganisms as well as membrane stress by damaging cell membranes of bacteria (Liu, Zeng et al. 2011). Lastly, the functional groups of graphene oxide can be used to remove heavy metal ions due to their high sorption ability for the ions (Zhao, Li et al. 2011).

II.3.2. Synthesis of graphene oxide platelets

Graphite oxide (GtO) is typically prepared by the oxidation of natural graphite power using mixture of strong acids and oxidizing agents, such as $KMnO_4$ and H_2SO_4 (Hummers method) or $KClO_3$ (or NaClO3) and HNO_3 (Staudenmaier or Brodie methods) (Dreyer, Park et al. 2009). These oxidation process leads to reproducible levels of oxidation (C:O≈2:1) (Dreyer, Park et al. 2009) which causes the delocalized electronic structure of graphite to be disturbed and endow its basal plane and edge with a number of oxygen functionalities. Although the exact structure of GtO remains unanswered (Dreyer, Park et al. 2009), it is considered that hydroxyl and epoxy groups are located on the basal plane, with carboxyl groups around the edge of the GtO as shown in **Figure II-15**. Interlayer are spaced out in GtO with an expanded structure compared to graphite which depends on humidity (for example, 0.6 nm under high vacuum (Buchsteiner, Lerf et al. 2006) to approximately 0.8 nm at 45% relative humidity (Dikin, Stankovich et al. 2007)) owing to intercalation of water molecules (Buchsteiner, Lerf et al. 2006). GtO could be exfoliated via various approaches such as sonication, yielding a structurally similar material to that of pristine graphene.

The hydrophilic property and expended structure of GtO facilitate exfoliation into aqueous media by means of mechanical exfoliation such as ultrasonication, ultimately forming graphene oxide (GO) suspensions (Park and Ruoff 2009). **Figure II-15** reveals the structural difference between unexfoliated GtO and exfoliated GO sheets. As appeared by zeta potential measurements, GO suspension are electrostatically stabilized by negative charges due to carboxylate groups that are meant to be located at edge (Park and Ruoff 2009). Colloidal suspensions prepared by mechanical exfoliation of GtO such as sonication are

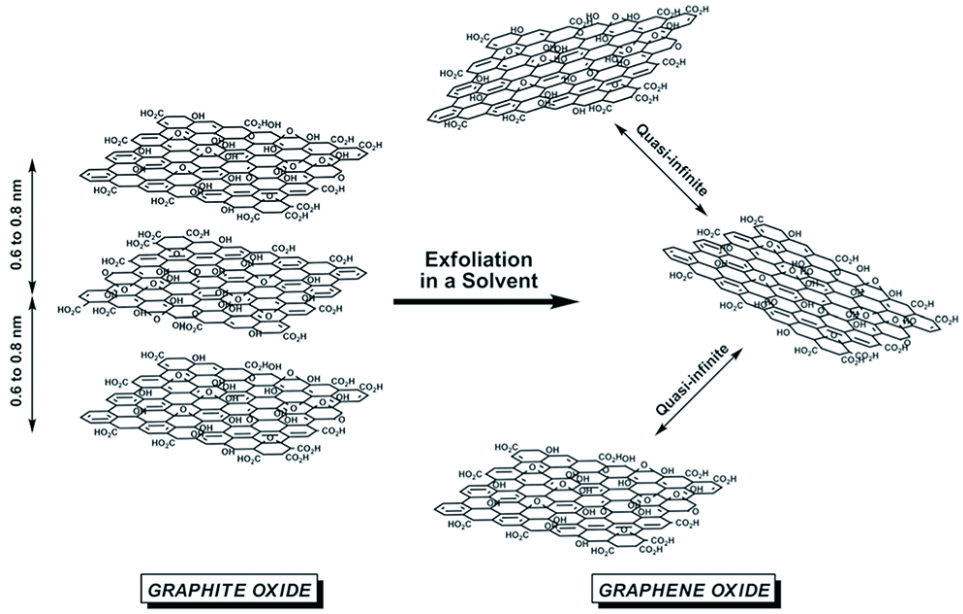

Figure II-15. Schematic showing the chemical structure of graphite oxide (GtO) and the structural difference between GtO and exfoliated graphene oxide platelets (Potts, Dreyer et al. 2011).

comprised primarily of single-layer GO sheets (**Figure II-16**) (Gómez-Navarro, Weitz et al. 2007, Becerril, Mao et al. 2008); however, the sonication causes their lateral dimensions of GO platelets to be reduced by a few hundred nanometers (Dreyer, Park et al. 2009, Li, Zhang et al. 2009). Stirring can be an alternative to fabricate single-layer GO sheets with larger lateral dimensions than those of GO platelets prepared by sonication. However, it has been known that exfoliation of GtO by magnetic stirring is very slow, so that causes low yield (Dreyer, Park et al. 2009). Alternatively, polar organic solvents such as NMP, DMF, and PC can be used to exfoliate GtO to GO platelets with similar lateral dimension to that of the platelets exfoliated in aqueous media via sonication (Paredes, Villar-Rodil et al. 2008, Zhu, Stoller et al. 2010).

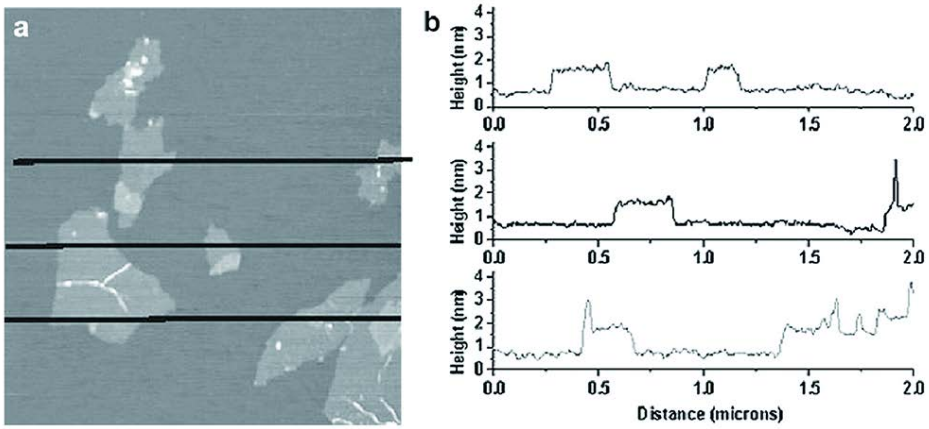

Figure II-16. AFM images of graphene oxide exfoliated in aqueous solution through sonication (Stankovich, Dikin et al. 2007).

II.3.3. Preparation of graphene-based polymer nanocomposite:

Non-covalent dispersion methods

In general, solution-based methods to prepare graphene-based polymer nanocomposite include the mixing of suspensions of graphene derivatives such as GO with the desired polymer by dissolving the polymer in the colloidal suspension of graphene derivatives via stirring. Then, the resultant polymer solution can be solidified using a non-solvent, causing the polymer chains to surround and entangle the nanofiller upon solidification. Lastly, the entirely solidified polymer nanocomposites could be extracted, dried, and followed by post treatment for their application. Alternatively, the suspension consisting of polymer solution including graphene derivatives could be cast into a mold without the precipitation by non-solvent and followed by the solvent evaporation. However, the latter technique can cause the nanofillers to agglomerate in the polymer nanocomposite, which could ultimately aggravate mechanical properties of the polymer nanocomposite (Moniruzzaman and Winey 2006).

II.3.4. Mechanical properties of graphene-based polymer nanocomposite

GO-derived nanofillers could reinforce mechanical properties of polymer nanocomposites due to their higher intrinsic stiffness. Besides their inherent modulus, there are several factors affecting reinforcing capability of the nanofillers. First, there is close correlation between the enhancing mechanical properties of graphene-based polymer nanocomposite and improved dispersibility of nanofiller (Alexandre and Dubois 2000). For example, if nanofillers (including CNTs and organoclays) revealing well-dispersed on short length scales are actually aggregated into micron-scale fractal-like structures (Klüppel 2003, Schaefer and Justice 2007, Vaia and Maguire 2007), such aggregates could cause the decrease in the effective aspect ratio of the nanofiller followed by the decrease in the reinforcing effect (Schaefer and Justice 2007). On the other hand, a few researchers have reported that large-scale aggregates of nanofillers contribute to the improving mechanical properties of polymer nanocomposites (Akcora, Kumar et al. 2009, Akcora, Liu et al. 2009).

Next, the exfoliation degree of nanofillers is also a significant element in the improving tensile properties of polymer nanocomposites when the same amount of the nanofillers is used. It is generally known that the more exfoliated GtO-derived fillers evidently lead to superior mechanical properties of polymer nanocomposites at equivalent loadings due to the relatively smaller platelet thicknesses of nanofillers. Since the nanofillers with smaller platelet thicknesses result in a higher aspect ratio and effective platelet modulus, their reinforcing effect can increase. These characteristics are well revealed in comparisons with graphite nanoplatelets (GNP)-filled composites (Kalaitzidou, Fukushima et al. 2007,

Kalaitzidou, Fukushima et al. 2007, Ramanathan, Stankovich et al. 2007, Kim and Drzal 2009, Kim, Do et al. 2010).

Meanwhile, mechanical performances of polymer nanocomposites can be altered according to the orientation of nanofillers. Some modeling researches have showed that randomly oriented graphene platelets could also be favorable in the increase of nanocomposites' stiffness and strength compared to randomly oriented nanotubes at equivalent loading, although calculations exhibited that aligned CNTs may be more desirable to better reinforcement than aligned platelets (Liu and Brinson 2008).

Also, an expended structural hierarchy of nanocomposite may ultimately be beneficial for maximizing the reinforcement potential of nanofillers such as graphene platelets, and polymer-grafted graphene platelets could be used to tailor the spatial distribution of the nanofillers in composite materials (Akcora, Kumar et al. 2009, Akcora, Liu et al. 2009).

Chapter III

III. Graphene Oxide Nanoplatelets Composite Membrane with Hydrophilic and Antifouling Properties for Wastewater Treatment

(This chapter includes the contents published in *Journal of Membrane Science* Vol.448 (2013) pp.223-230.)

III.1. Introduction

Recycling of used water, which is realized by advanced wastewater treatment, is an area where technological advancements are demanded and deserved to have clean water available to any person anywhere. A recently advanced technology of membrane bioreactors (MBRs) is being actively pursued including installations of the system in various municipalities around the world (Shannon, Bohn et al. 2008) because of many favorable features it offers: high quality of processed water, reduction in excess sludge, controllability of solids and hydraulic retention time, and minimization possible in required footprint (Judd 2008, Kraume and Drews 2010, Le-Clech 2010). A critical issue in MBRs that awaits a technological advancement is membrane fouling that the bioreactor suffers from. Intricate interactions between membrane material and numerous components of activated sludge mixed liquor lead to biofouling of the membrane, which makes the MBRs for wastewater treatment costly. To make the treated water by MBRs readily available to people economically, therefore, it is highly desirable to have a membrane with antifouling capability, or anti-biofouling membrane.

A membrane material among synthetic polymers that has widely been used in membrane processes is polysulfone (PSf). It is often preferred because of its desirable thermal and mechanical properties, and its chemical stability (Wu 1982). However, it is not immune from the biofouling problem. In fact, it suffers more than other membrane materials due to hydrophobic and charge interactions between membrane surface and diverse foulants (Chang, Le Clech et al. 2002). To help relieve the biofouling problem, various approaches have been taken. These include application of plasma treatment, amphiphilic graft copolymer, and

chemical reaction of hydrophilic components to modify membrane surface (Higuchi and Nakagawa 1990, Kim, Lee et al. 2002, Park, Acar et al. 2006). Recently, incorporation of hybrid materials such as mesoporous silica, TiO2, ZnO, and oxidized multi-walled carbon nanotubes have been tried for other membrane forming materials to attain high permeability selectivity, and antifouling property in membrane applications (Choi, Jegal et al. 2006, Yang, Zhang et al. 2007, Celik, Park et al. 2011, Liang, Xiao et al. 2011, Huang, Zhang et al. 2012). While these approaches have led to improvements, the improvements are not as significant as the large amount of additive needed would indicate, the amount ranging from around 10 to 30 weight percentage relative to the polymer weight. In the case of oxidized multi-walled carbon nanotubes, small quantities are needed. However, their O/C ratio is too low to impart superior functionality to membrane surface (Kuznetsova, Popova et al. 2001).

Our motivation in utilizing graphene oxide (GO) in preparing the membrane for MBRs stems from the unique properties that GO possesses owing to its functional groups such as carboxyl, epoxy, and hydroxyl groups on its basal planes and edges (Dikin, Stankovich et al. 2007, Dreyer, Park et al. 2009). The presence of GO in membrane material would induce hydrophilicity, which would ensure high water permeation and impede biofouling owing to the low interfacial energy between a surface and water (Le-Clech, Chen et al. 2006, Krishnan, Weinman et al. 2008). In addition, its functional groups would ensure a large negative zeta potential, which should also impede biofouling process of attachment of bio-foulants and their accumulation on the membrane surface (Kang, Subramani et al. 2004, Liu, Zhang et al. 2010). It is noted in this regard that the functional groups in GO enabled exploitation of unusual properties such as hydrophilicity or

antibacterial activity as exemplified by several studies in recent years (Stankovich, Dikin et al. 2006, Hu, Peng et al. 2010, Mejías Carpio, Santos et al. 2012, Nair, Wu et al. 2012). We were also encouraged by a recent study based on an ultrafiltration cup experiment (Wang, Yu et al. 2012, Zhang, Xu et al. 2013) that addition of GO to polyvinylidene fluoride (PVDF) membrane resulted in an increase in water flux and also an improvement in mechanical properties.

III.2. Experimental section

III.2.1. Materials

Polysulfone (PSf, Udel® P 3500 BM7, Solvay Korea, Seoul) was used as the membrane material. N-Methyl-2-pyrrolidinone (NMP) was purchased from Sigma-Aldrich and used as a solvent to prepare cast solution. Graphite (Aldrich) was used to manufacture graphene oxide for modification of a PSf membrane. Nitric (HNO_3, DC chemical Co. Ltd.), sulfuric acid (H_2SO_4, DC chemical Co. Ltd.), potassium permanganate ($KMnO_4$, Sigma-Aldrich) and hydrogen peroxide (H_2O_2, Junsei) were used to oxidize graphite to graphene oxide for exfoliation.

III.2.2. Preparation of graphene oxide and reduced graphene oxide solution

Graphene oxide was prepared from natural graphite (Aldrich) using following chemicals according to modified Hummers method (Hummers Jr and Offeman 1958). Nitric (HNO_3, DC chemical Co. Ltd.), sulfuric acid (H_2SO_4, DC chemical Co. Ltd.), potassium permanganate ($KMnO_4$, Sigma-Aldrich) and hydrogen peroxide (H_2O_2, Junsei) were used to oxidize graphite to graphene oxide. Graphite flakes (0.12 g) were added to a mixture of concentrated H_2SO_4/HNO_3 (6 mL : 0.132 mL), and $KMnO_4$ (0.72 g) were gradually added to this mixture with stirring at 35-45 °C for 2 h. The mixture was then heated to 100 °C and stirred for 30 min after water (42 mL) and H_2O_2 (1.2 mL) were added. On being cooled to room temperature, the mixture was centrifuged (Hanil Science Industrial Co., Ltd., Mega 17R) at 13000 rpm for 15 min to remove acidic supernatant from the mixture. Subsequently, the acidic supernatant was removed after centrifugation finished, and deionized water (DI water) was then added to dilute acidic remnant from graphite oxide. The mixture of graphite oxide pellet and DI water was vortex-stirred for 1 min to redisperse the pellet. This process which centrifugation and vortex alternatively were conducted was repeated until nearly neutral aqueous solution was obtained. The pellet, graphite oxide, was then added in NMP. Exfoliation of graphite oxide to GO was achieved by ultrasonication using a tip sonicator (Sonic VCX-750, Sonics & Materials, Inc.) in ice water bath for 1 h.

Reduced graphene oxide (rGO) solution was prepared by reducing dispersed GO in the resultant homogeneous GO solution obtained from aforementioned procedure for chemical conversion of graphite oxide to graphene oxide using hydrazine (N_2H_4, Sigma-Aldrich) as reported in another research (Li,

Müller et al. 2008). The hydrazine was added in the ratio of 0.7 mg per mg of GO. The mixture was then heated to 80 °C, and stirred for 10 h.

III.2.3. Preparation of the membranes

GO was exfoliated by sonication in N-methyl pyrrolidone (NMP). The nanoplatelets of GO thus obtained was dispersed in NMP solution of PSf (15 wt% PSf and 85 wt% of NMP) to attain various GO concentrations (0.02, 0.05, 0.14, 0.20, and 0.39 wt%). After stirring for 12 h at 60 ºC, the solutions were kept overnight at room temperature without stirring until no bubbles appear in the solution after sonication for 1 h. The polymer solution was casted on a polyester non-woven fabric using a micrometric film applicator (Elcometer 3570, Elcometer). The nascent membranes were then immersed in a water bath for 24 h for the purpose of entire liquid-liquid demixing. The PSf/GO membranes thus prepared had the following contents of GO with respect to PSf: 0.16, 0.32, 0.92, 1.30, and 2.60 wt%.

III.2.4. Characterization

2.4.1. Polymer solution viscosity measurement

The viscosity of the polymer solution was measured by an Advanced Rheometric Expansion System (ARES) (Rheometric Scientific ARES, Rheometric Scientific, USA). The relationship of viscosity and shear rate for each casting solution was obtained at a shear rate ranging from 0-10 s^{-1} at 25 ◦C.

III.2.4.2. Pore size distribution measurement

The pore size distribution of the membranes was measured by gas flow/liquid displacement method using the capillary flow porometer (CFP-1500AEL, PMI, USA). All membrane samples were prepared in diameter of 25 mm, and then analyzed by the “wet up-dry down” method. In detail, the gas flow was measured as a function of the transmembrane pressure through a wet membrane by 1,1,2,3,3,3-hexafluoropropene (“Galwick”, PMI; surface tension 16 dyn cm^{-1}) and then a dry membrane. The pore size distribution was estimated by the PMI software.

III.2.4.3. Mean Contact angle measurement

Dynamic contact angle measurements on the flat sheet membranes were conducted using a single fiber tensiometer (K100SF, KRUSS, Germany) to investigate the surface wetting characteristics of membrane as a function of GO contents in the nanocomposite membrane. The results from the measurements represent the hydrophilicity of each membrane. The measurements were carried out using deionized water as the probe liquid in all measurements in room temperature, and seven measurements were averaged to obtain contact angle for each sample to

minimize the experimental error.

III.2.4.4. Zeta potential measurement

The surface zeta potential of membrane is determined by measuring the particle mobility induced only by the surface charge of membrane. The surface charge of each membrane was measured by electrophoretic light scattering spectrometer (ELS-Z2, Ostuka Electronic, Tokyo, Japan) equipped with a plated sample cell. PSf/GO nanocomposite membrane and PSf membrane without GO were prepared in 2 cm × 4 cm size plates, and the measurements of their zeta potential were carried out at room temperature in 10 mM NaCl solution with polystyrene latex monitor particles of which surface charge is defined as 0.

The surface charge of flocs in sludge was assessed by zeta potential measurement using the Malvern zetasizer Nano ZS90 (Malvern Instruments, UK) and by applying a field strength of 25 V/cm. The zeta potential of particles depends on the dispersion medium, therefore the surface charge had been measured without washing or diluting to evaluate the surface charge of flocs in the original condition.

III.2.4.5. Field emission scanning electron microscopy and energy dispersive X-ray spectrometer

To study membrane morphology and its chemical composition, each dried specimen was mounted on an aluminum stub and sputter-coated with platinum using a sputter coater (SCD 005, BAL-TEC, Germany) to make the samples appear electric conductivity. The specimens were observed under a Field Emission Scanning Electron Microscope (FESEM, AURIGA, Carl Zeiss, Germany) in standard high-vacuum conditions at 5 kV and photographed to obtain the cross-

sectional images of each membrane. The specimens were also analyzed by an energy dispersive spectrometry amounted in FESEM (EDS, SUPRA 55VP, Carl Zeiss, Germany) to identify elements of the PSf/GO nanocomposite membrane at 15 kV. To analyze the elements of membrane sub-surface layer, each membrane was immersed in liquid nitrogen to prevent intrinsic membrane structures from destroying during fracturing, and then broken in intact state.

III.2.4.6. Raman spectroscopy

Raman spectra were obtained using a micro-Raman system (JY-Horiba, LabRam 300) which combined a x50 objective lens (Olympus, NA 0.75) with a 633 nm CW He-Ne laser. For Raman analysis of the PSf/GO nanocomposite membranes, the membranes were mounted on a glass substrate, and then the laser beam was focused on the center of membrane surface.

III.2.4.7. Mechanical strength measurement

The mechanical strength of each membrane was confirmed by measuring tensile modulus of membrane using Universal testing machine (Instron, USA). All the specimens were about 7.2 cm long and 2.4 cm wide, with a thickness of 60 μm. The samples were measured at a rate of 3 mm/min using 50 N load cells, and the initial distance between the clamps was of 30 mm.

III.2.5. Pure water flux measurement

The pure water flux (PWF) of PSf/GO membranes was measured at different transmembrane pressure (20-100 kPa). Before measuring the flux, all membranes were compacted with deionized water at 400 kPa for 2 h to prevent the compaction effect of the membrane during this measurement.

III.2.6. Microorganism attachment test

The effect of GO on the hindrance for microorganism attachment on membrane surface was verified by following experiment. Pseudomonas aeruginosa (PAO1) with green fluorescent protein (GFP) tag cultured in 1/10 Tryptic Soy Broth (TSB) for 18 h was inoculated to cocurrent downflow contactor reactor (CDC reactor) filled with 300 mL of 1/100 TSB after the medium was diluted until OD value reached 0.14. Each membrane was mounted in CDC reactor by equally spaced point supports after attached on the supports. PAO1 was cultured for 24 h at 25ºC in CDC reactor with the membranes under batch condition with stirring at 100 rpm. After PAO1 was cultured for 24 h under batch condition, 1/300 TSB as nutrient to culture under a continuous flow stirred tank reactor (CFSTR) condition was continuously pumped into and flow out of the reactor at a flow rate of 1.4 mL/min for 24 h.

III.2.7. Membrane bioreactor operation

The ultimate test for a membrane is how durable and stable it is under the continuous membrane bioreactor (MBR) operation (**Figure III-1**). The PSf/GO membranes with GO contents of 0.0, 0.32, and 1.30 wt% were tested to ascertain the ability of GO to mitigate membrane biofouling and maintain stable operational state. In particular, the transmembrane pressure (TMP) rise-up with time in a continuous MBR was obtained for all the membranes. To verify that graphene oxide with the functional groups, and not graphene, is responsible for the remarkable performance, TMP experiments were also carried out with reduced graphene oxide (rGO). Details for the composition of the synthetic wastewater and operational conditions are given in **Table III-1 and III-2**.

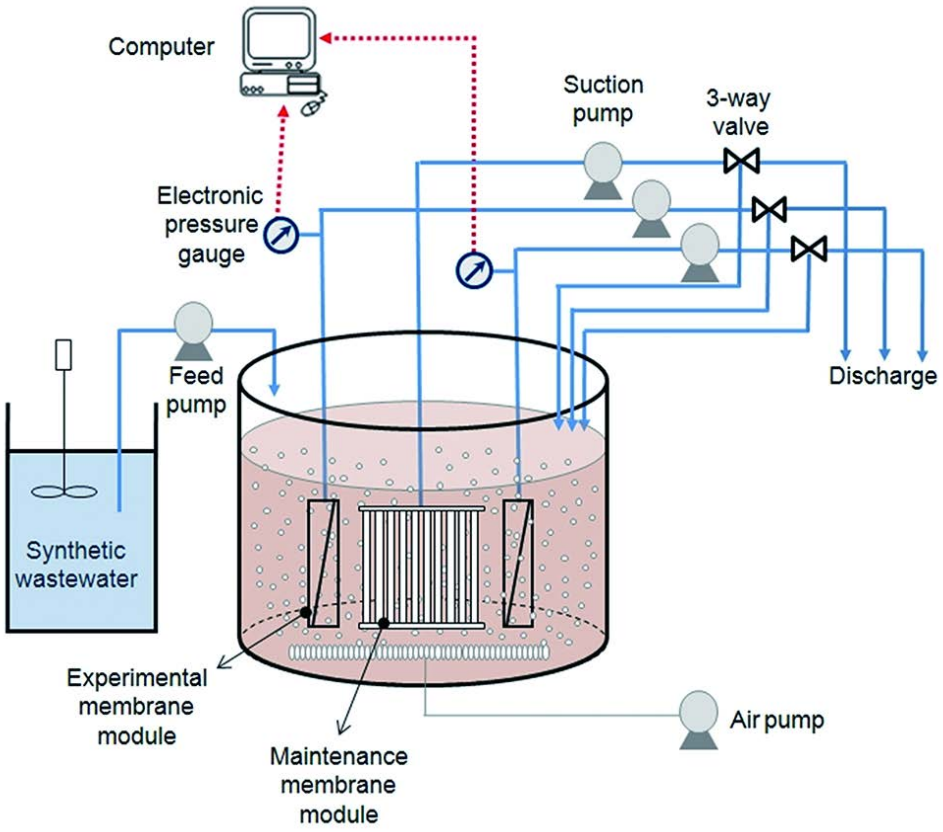

Figure III-1. Schematic diagram of the continuous MBR system.

Table III-1. Composition of the synthetic wastewater.

Composition	Concentration(mg/L)
Glucose	400.00
Yeast extract	14.00
Bactopeptone	115.00
$(NH_4)_2SO_4$	104.75
KH_2PO_4	21.75
$MgSO_4 + 7H_2O$	32.00
$FeCl_3 + 6H_2O$	0.13
$CaCl_2 + 2H_2O$	3.25
$MnSO_4 + 5H_2O$	2.88
$NaHCO_3$	255.50

Table III-2. Operating conditions of the continuous MBR.

Operating condition	
Working volume (L)	6
Hydraulic retention time (hrs)	12
Solid retention time (days)	30
Mixed liquor suspended solid (mg/L)	9860 (±514)
Feed concentration (mg COD/L)	530
F/M ratio	0.11
COD removal rate (%)	96.8
pH	6.5~7
Constant flux ($L/m^2/h$)	16
Membrane module	Plate & Frame
Membrane area (cm^2)	80
Aeration rate (L/min)	1.5 or 4
Sludge source	Sihwa plant

III.3. Results and discussion

III.3.1. Conformation of graphene oxide in polysulfone/graphene oxide membrane

Presence of GO in the PSf/GO membrane can be recognized by the naked eye (**Figure III-2**). As shown in the image, the membrane with GO nanoplatelets looks brownish unlike the membrane without GO. Its presence in the prepared PSf/GO membrane in sub-surface layer was indirectly verified by energy dispersive spectroscopy (EDS) (**Figure III-3**). The presence of GO in the nanocomposite membrane was also confirmed by Raman spectroscopy. The Raman spectrum of PSf/GO membrane (red curve in **Figure III-4**) displays two prominent peaks. One is D-band at 1350 cm^{-1} and another is relatively broad G-band for the G-band of PSf membrane at 1588 (or 1610) cm^{-1} (Gómez-Navarro, Weitz et al. 2007, Graf, Molitor et al. 2007, Yang, Velamakanni et al. 2009). The prominent D peak is from the structural imperfections generated by epoxide and hydroxyl groups on the carbon basal plane, and this fact assures the presence of GO in the nanocomposite membrane (Gómez-Navarro, Weitz et al. 2007, Graf, Molitor et al. 2007, Yang, Velamakanni et al. 2009). In contrast, the PSf membrane without GO shows negligible D peak intensity (black curve in **Figure III-4**).

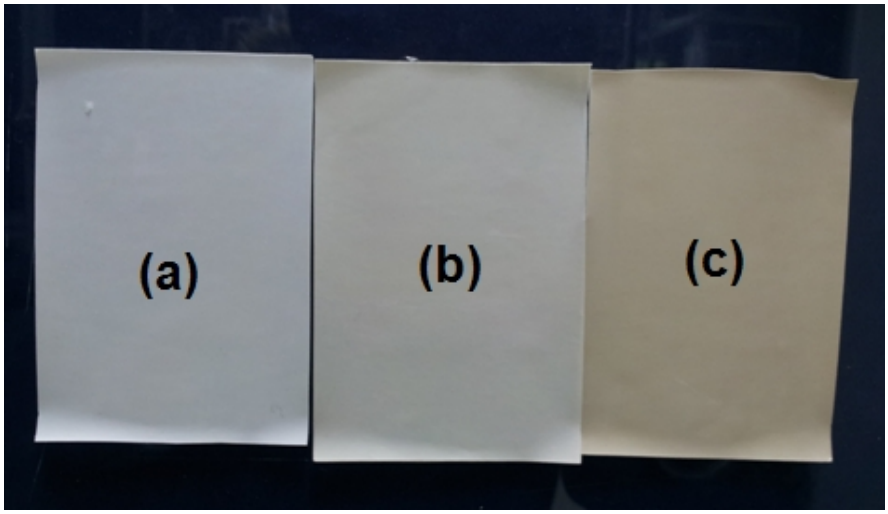

Figure III-2. Presence of GO in the PSf/GO membrane recognizable by the naked eye. (a) PSf membrane without GO, (b) PSf membrane with 0.32 wt% GO, and (c) PSf membrane with 1.30 wt% GO.

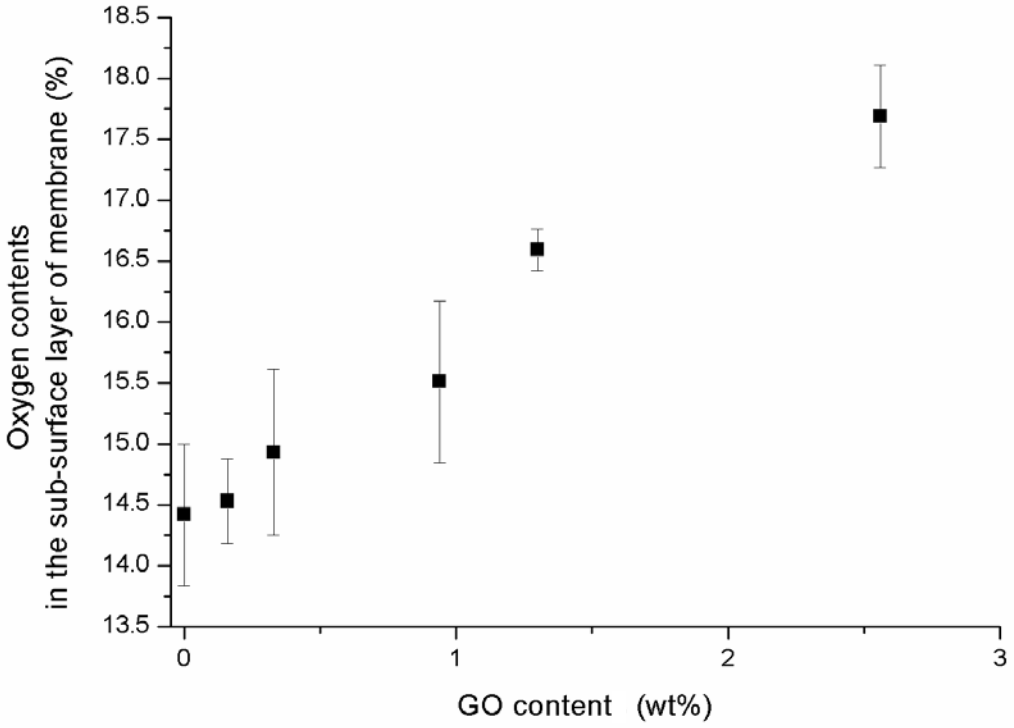

Figure III-3. GO content change in the sub-surface layer of each membrane as given by oxygen content determined by EDS. (error bar: standard deviation, n=5)

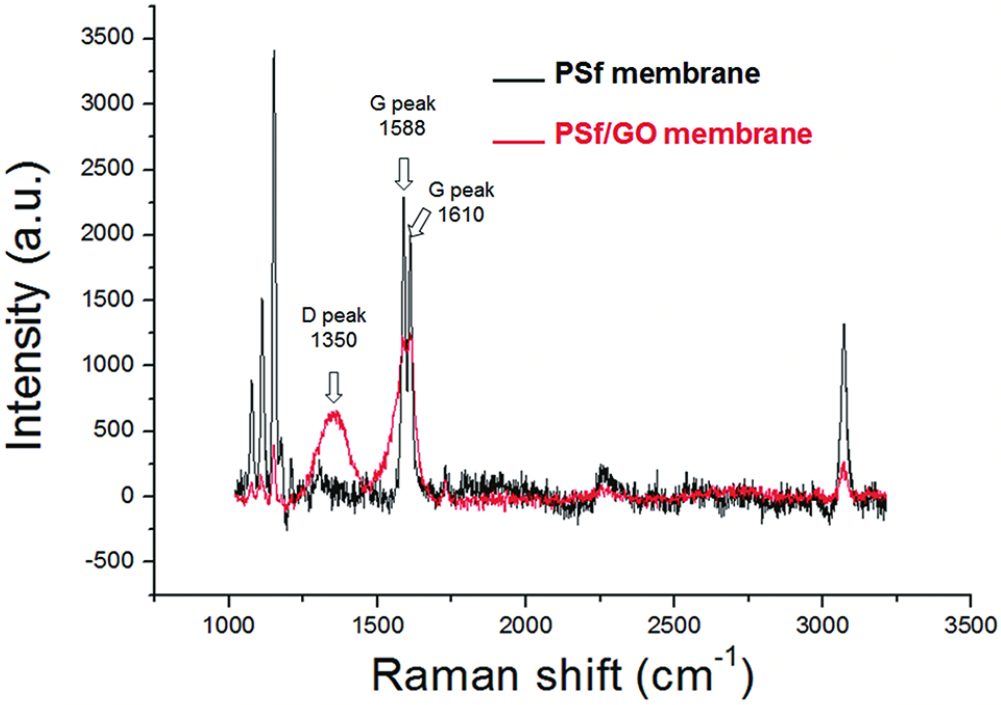

Figure III-4. Raman spectra of PSf/GO nanocomposite membrane and PSf membrane without GO.

III.3.2. Anti-biofouling activity of polysulfone/graphene oxide membrane

The ability of GO imbedded in the membrane to mitigate biofouling, or antifouling capability, is clearly revealed in the images given in **Figure III-5** that were obtained by confocal laser scanning microscopy (CLSM) with a microorganism (Pseudomonas aeruginosa, PAO1) tagged with green fluorescent protein. It is evident from the images that the thickness of biofilm that is formed by the microorganism decreases with increasing GO content in PSf membrane (**Figure III-6**). Even more significant than the film thickness is the sparsity of the microorganism attached on the surface of the membrane for those cases where the GO content exceeds 1 wt% (1.30 and 2.60 wt% relative to PSf weight in **Figure III-5**). For an understanding of the behavior, it is helpful to recognize that most microorganisms (**Table III-3**) in MBR as well as most microbial products in aquatic system such as extracellular polymeric substance, a major fouling component, have negatively charged surface or characteristics (Van Loosdrecht, Lyklema et al. 1987, Van Loosdrecht, Norde et al. 1990, Lee, Kang et al. 2003, Liu and Fang 2003). These microbial products are well known to accelerate deposition of microorganism on membrane surface in the initial stage of MBR operation (Drewsa, Leeb et al. 2006, Jarusutthirak and Amy 2006). A measure of negative surface charge is surface zeta potential. Shown in **Figure III-7** is the surface zeta potential of the PSf/GO membrane for various GO contents. The negative zeta potential is seen to increase with increasing GO content, reaching a value of –20mV as the content becomes larger than 1.30 wt%, which compares with the value of almost zero potential for the sample with no GO. This large negative zeta potential should induce electrostatic repulsion between the microorganism and the

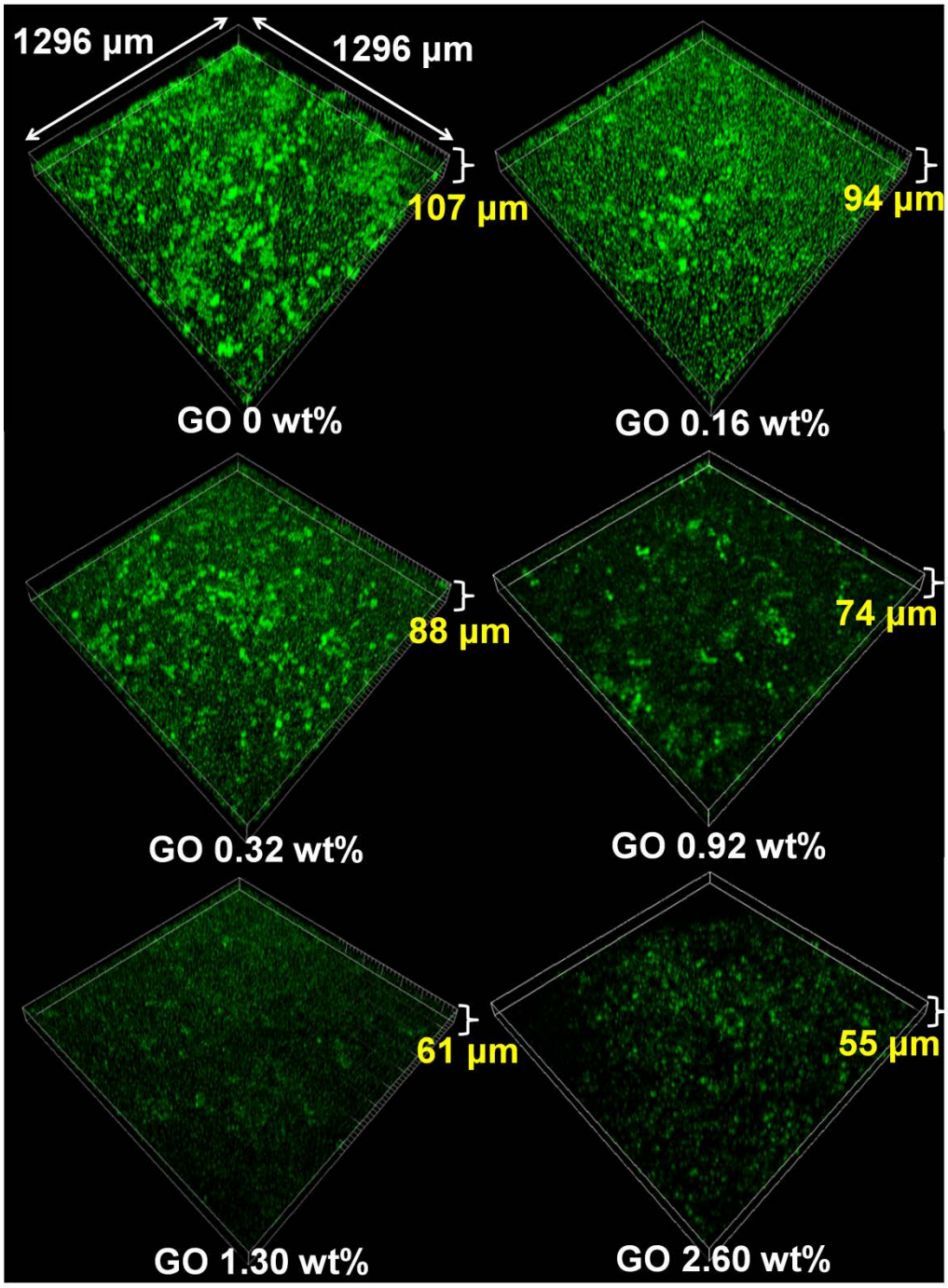

Figure III-5. CLSM images of biofilm formed by attached microorganism on surface of membrane containing various GO contents. Magnification: 100X. Image size: 1296 µm X 1296 µm.

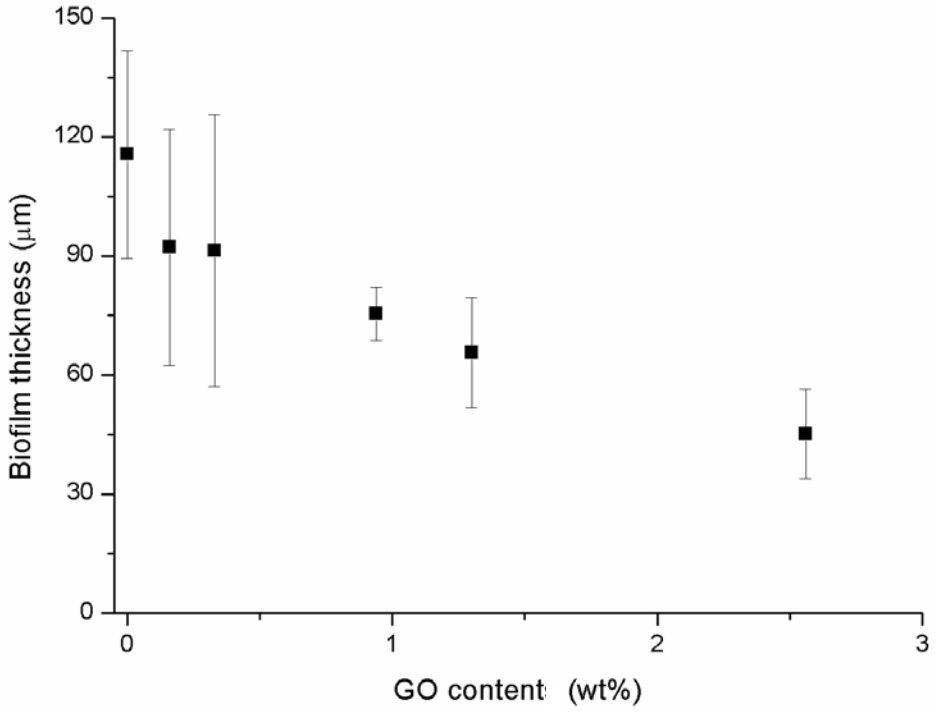

Figure III-6. Biofilm thickness formed by microorganism attachment on PSf/GO nanocomposite membrane as a function of GO content. (error bar: standard deviation, n=5)

Table III- 3. Zeta potential of activated sludge taken from a wastewater treatment plant (Siwha and Tancheon in Korea) and *Pseudomonas aeruginosa*. (The numbers in parenthesis: standard deviation, n=3)

Samples	Zeta potential (mV)
Sludge* of the real MBR plant in Siwha (Korea)	-19.2 (±1.0)
Sludge of the real MBR plant in Tancheon (Korea)	-14.3 (±4.0)
Pseudomonas aeruginosa	-35.2 (±0.5)

*Sludge: a mixture of microorganisms in the broth

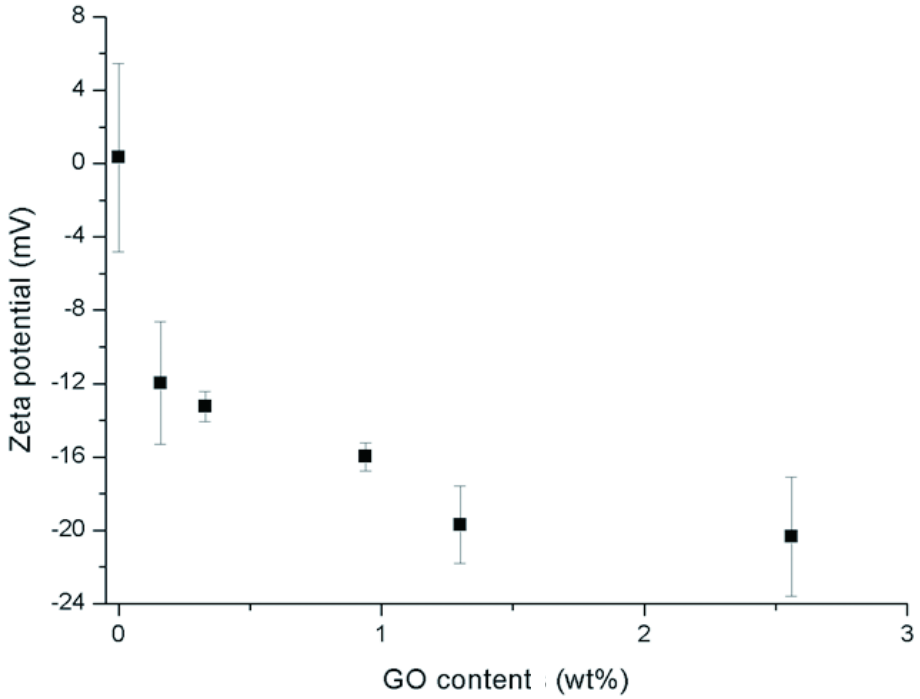

Figure III-7. Zeta potential of the PSf/GO nanocomposite membrane for various GO contents. (error bar: standard deviation, n=6)

membrane surface, thereby impeding the surface attachment of the microorganism. It is expected, therefore, that the GO-containing membrane can also effectively deter membrane fouling due to the biocake formation accelerated by surface attachment of microbial products.

III.3.3. Hydrophilicity of polysulfone/graphene oxide membrane

According to other studies, it is known that water molecules could be easily drawn to the inside of membrane with hydrophilic surface, hence the flux of a membrane can be increased by enhancing hydrophilicity of the membrane (Yang, Wang et al. 2006, Zhang, Xu et al. 2013). The presence of GO in the prepared membrane should make the membrane more hydrophilic than the membrane without GO because of the functional groups, which would result in a higher water flux. In fact, it turns out that the pure water flux through membrane increases with increasing GO content up to 1.30 wt%, as shown in **Figure III-8**, with the exception of the membrane with 2.60 wt% GO. This trend as affected by GO content is almost in accord with the contact angle given in **Figure III-9**, where the angle consistently decreases with increasing GO content, showing more hydrophilic nature of the membrane with increasing GO content.

The hydrophilicity also helps mitigate adhesion of microorganism and microbial products having hydrophobic characteristics (Van Loosdrecht, Lyklema et al. 1987, Van Loosdrecht, Norde et al. 1990). While biomolecules such as proteins easily adsorb on a hydrophobic surface to minimize the interfacial energy, a hydrophilic surface with low surface-water interfacial energy resists protein adsorption and cell adhesion. Hydrophilic surfaces do not offer any significant thermodynamic advantage because of already low interfacial energy (Krishnan, Weinman et al. 2008). Therefore, the inhibition of biofouling shown in **Figure III-5** was affected not only by zeta potential but also by the hydrophilicity of GO membrane.

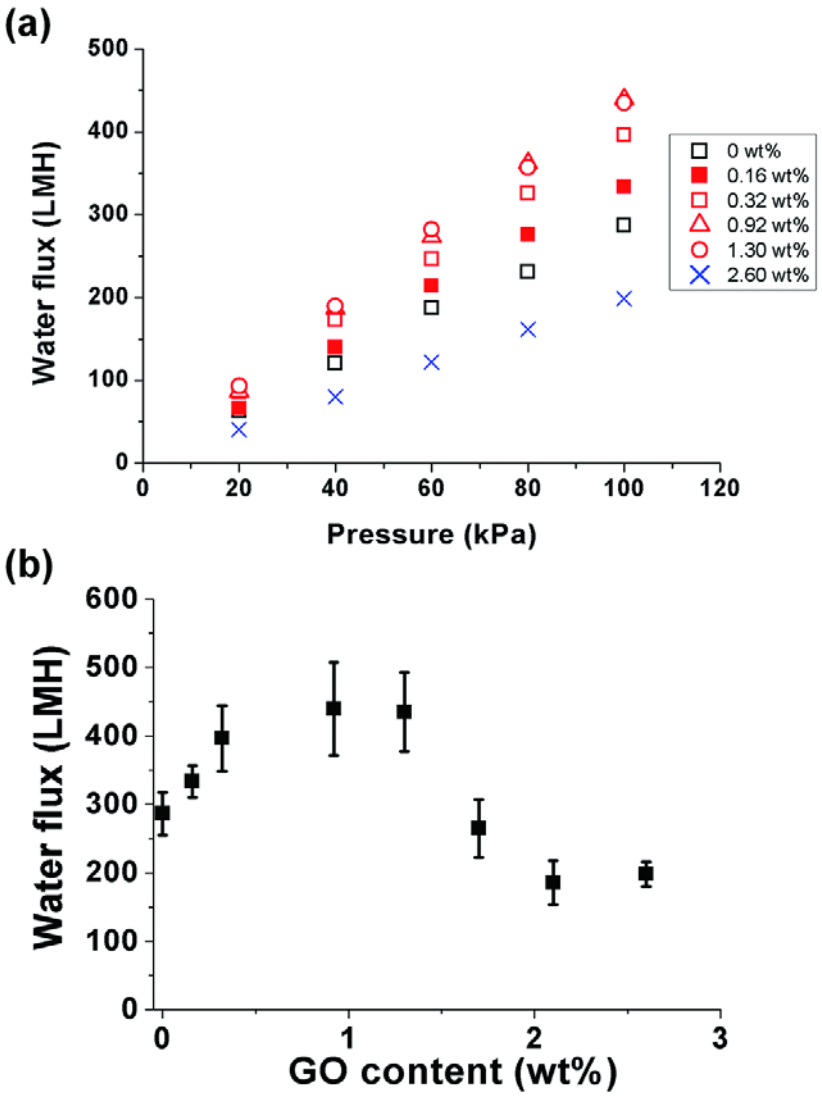

Figure III-8. Pure water flux of PSf/GO nanocomposite membrane (a) as a function of transmembrane pressure (TMP) for various GO contents, and (b) as a function of GO content at the constant TMP of 100 kPa. (error bar: standard deviation, n=5.)

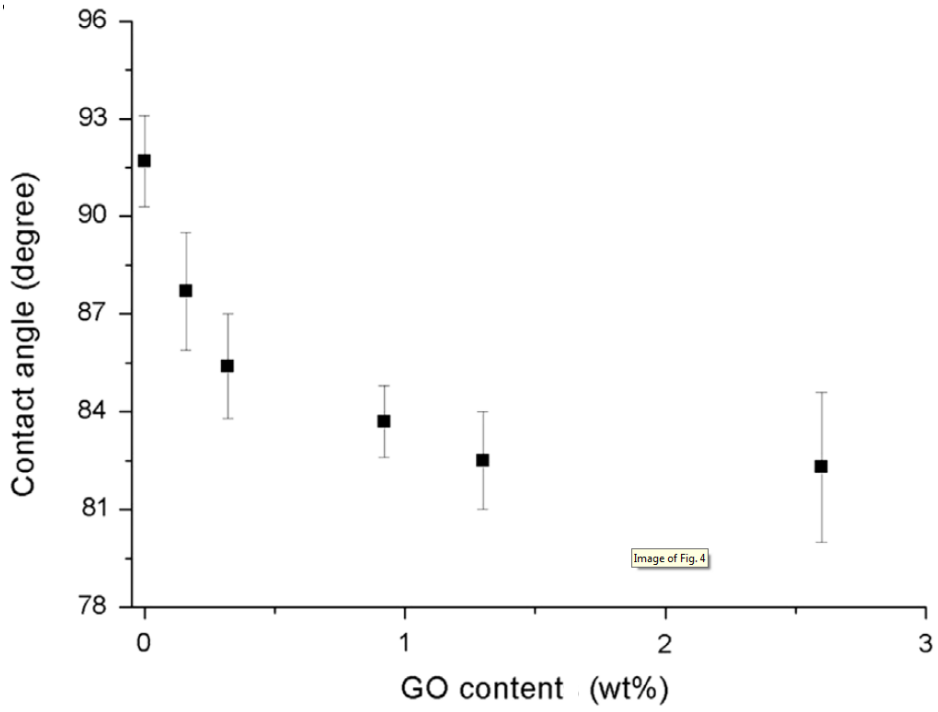

Figure III-9. Contact angle of the PSf/GO nanocomposite membrane as a function of GO content. (error bar: standard deviation, n=5.)

III.3.4. Membrane pore size distribution and pore cross-sectional structure

To explain the decrease in pure water flux of the membrane with 2.60 wt% GO in **Figure III-8**, one has to examine the pore structure resulting from membrane formation process involving phase inversion, which is in turn affected by GO content in the membrane preparation solution. **Figure III-10** shows the change of pore size distribution at different GO contents. While the pore size distribution shifts toward larger pore size with increasing GO content up to 1.30 wt% GO, the distribution shifts back to smaller pore size for the membrane with 2.60 wt% GO. This trend can be explained by the effects that GO can have as a hydrophilic additive on the rate of exchange between solvent and nonsolvent (demixing) during phase separation.

During the separation, polymer solution is rapidly solidified at the interface between polymer solution and nonsolvent due to the steep activity and concentration gradient of all components. Weak points in the solidified polymer surface leads to formation of fractured points due to immitigable stresses produced by the shrinkage or syneresis during continuous desolvation. The fractured points eventually become pores after phase inversion is completed (Strathmann and Kock 1977). The addition of hydrophilic GO to polymer solution could increase the demixing rate by enhancing the thermodynamic instability. As a result, the pores formed by the fractured points could become larger because of more rapid solidification of the polymer solution that induces more stresses in the solid polymer surface. The larger pores lead to a larger pure water flux under the same pressure drop, dynamic viscosity, and membrane thickness according to Hagen-Poiseuille relationship (Cheryan 1998). Thus, the increase in pure water flux can

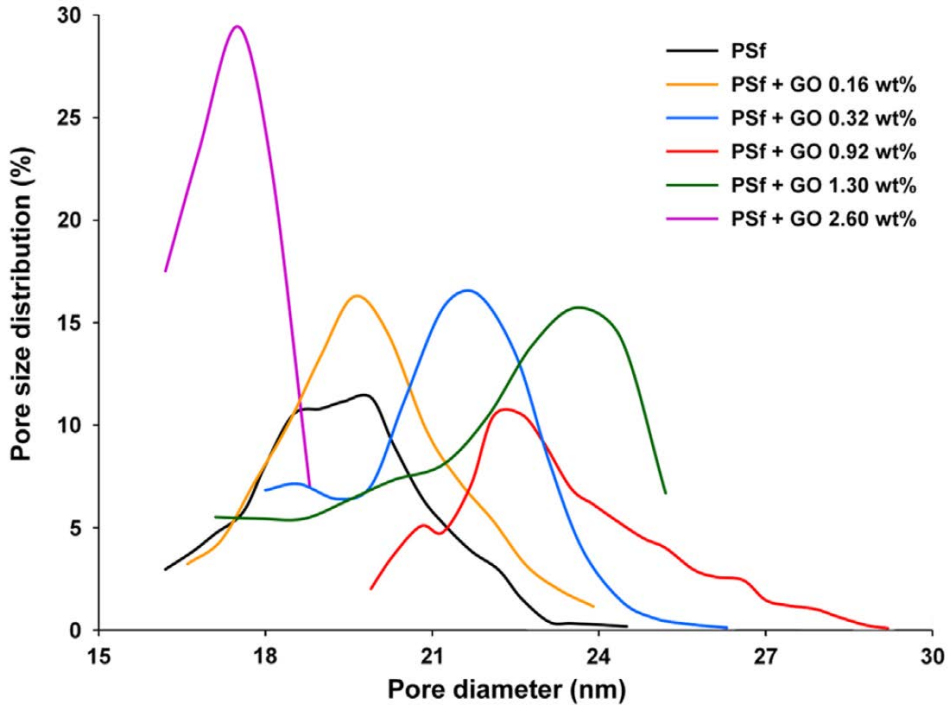

Figure III-10. Pore size distributions of the membranes with various GO contents.

also be supported by the increase of membrane pore size with increasing GO content up to 1.30 wt%. It is worth noting that those properties (i.e., larger pores and larger water flux) have nothing to do with membrane defects. It is because any defect was not detected on the SEM images of top surfaces of membranes with various GO contents (**Figure III-11**). Although the average pore size was increased by up to 20 % with increasing GO content up to 1.30 wt%, the rejection test with BSA (Bovine serum albumin) showed only 1 % decrease of the rejection rate up to the same GO content (**Figure III-12**).

On the other hand, the addition of excess GO could lead to an increase in polymer solution viscosity and a resultant delayed demixing to permit creep relaxation that relieves the stresses, which induces formation of smaller pores. Note in this regard that the viscosity markedly increased for the polymer solution with 0.39 wt% GO that corresponds to the membrane with 2.60 wt% GO relative to PSf weight (**Figure III-8 & Figure III-13**). This fact suggests that there is an optimum value of GO fraction for pure water flux.

The rheological hindrance by delayed demixing also appears in the cross-sectional structure of the membrane with 2.60 wt% GO (**Figure III-14**). The exchange of solvent and nonsolvent in the aforementioned fractured points is much faster than through the defect-free skin, so that solidification front moves much faster at the fractured points. This consequently leads to formation of finger-like structure accompanying movements of solidified polymer toward the side of finger-like void (Strathmann and Kock 1977). However, if the viscosity of polymer solution is too high, the propagation of solidification front is inhibited by delayed demixing. **Figure III-14** shows that there is little difference in the cross-sectional structure for the membranes with GO content ranging from 0 to 1.30 dry wt% (wt %

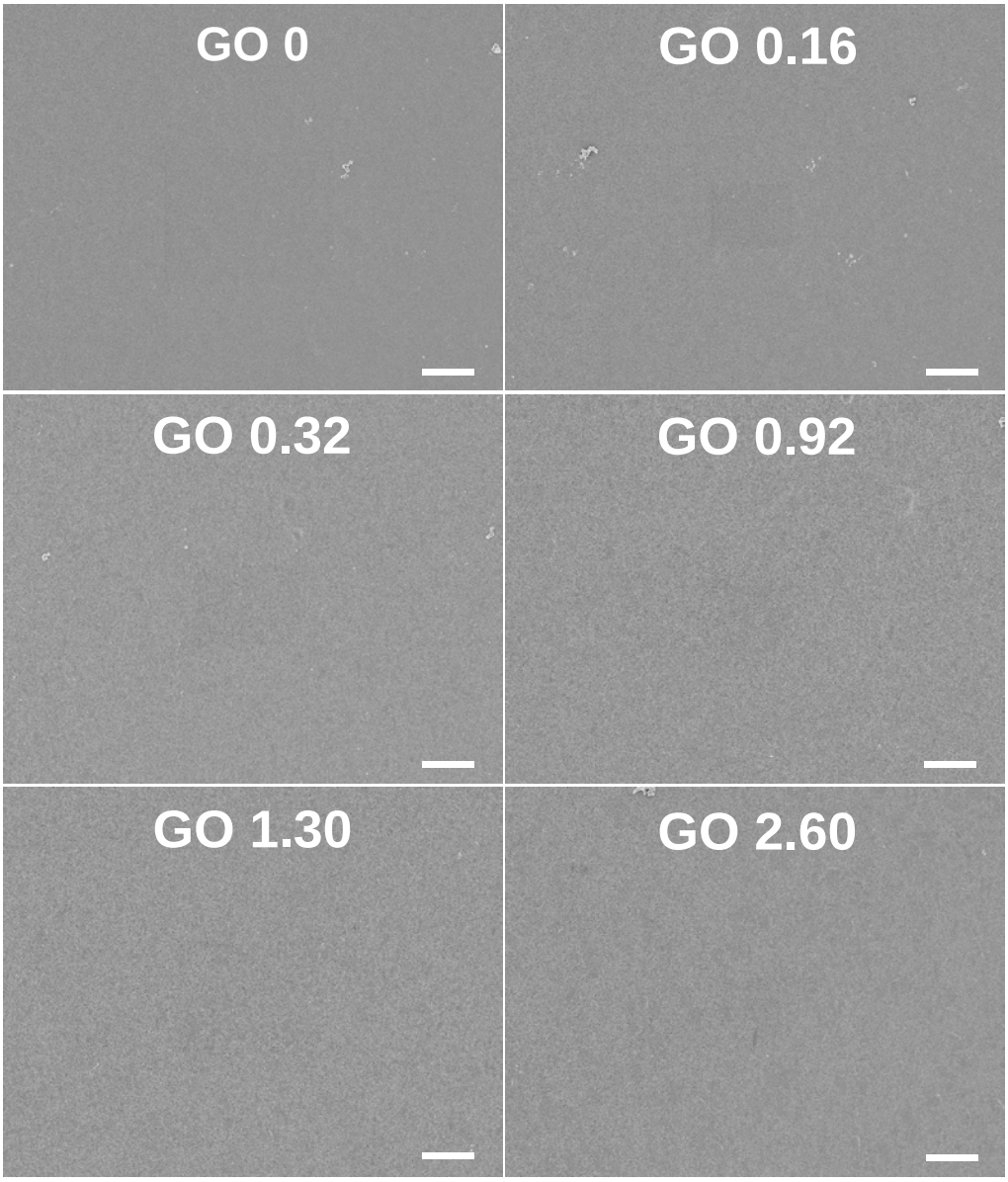

Figure III-11. SEM images of top surfaces of membranes with various GO contents. (Scale bar: 3 μm)

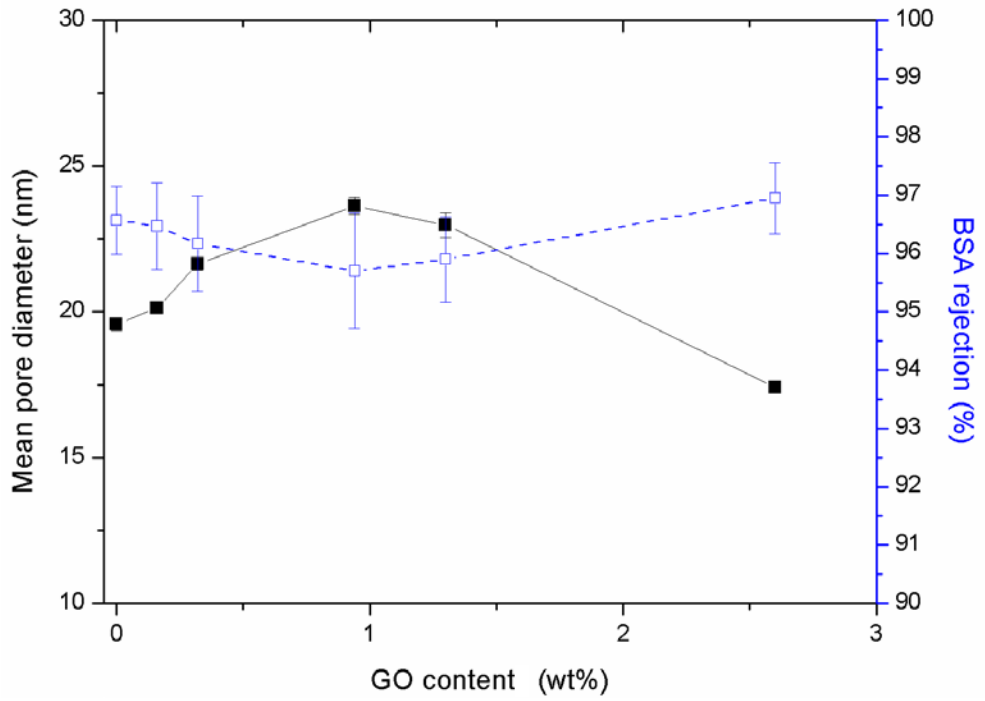

Figure III-12. Change of mean pore diameter and BSA rejection rate as a function of GO content.

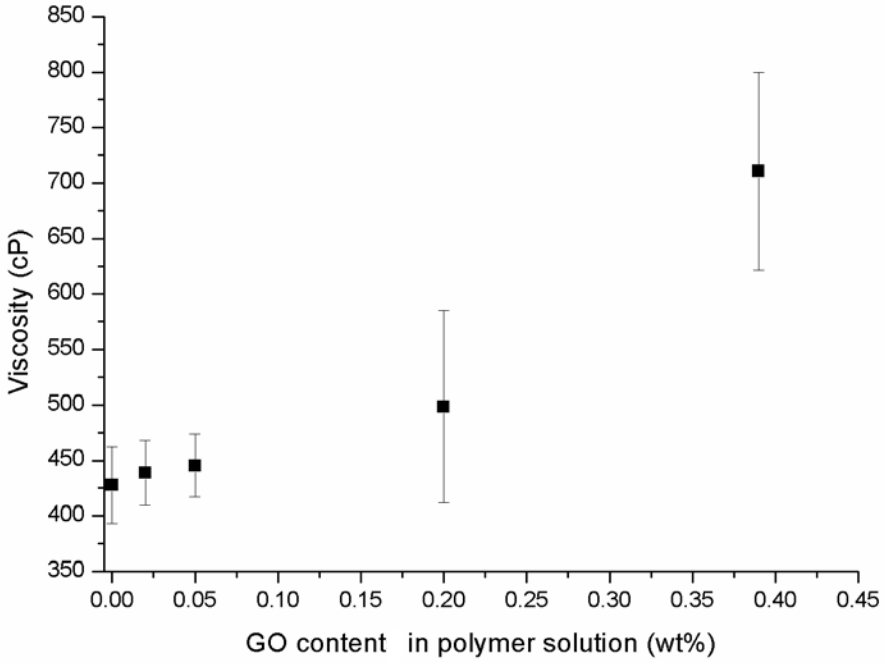

Figure III-13. Viscosity of polymer solution for various GO contents. (error bar: standard deviation, n=4) Note that the wt% here is based on polymer solution weight rather than the polymer weight.

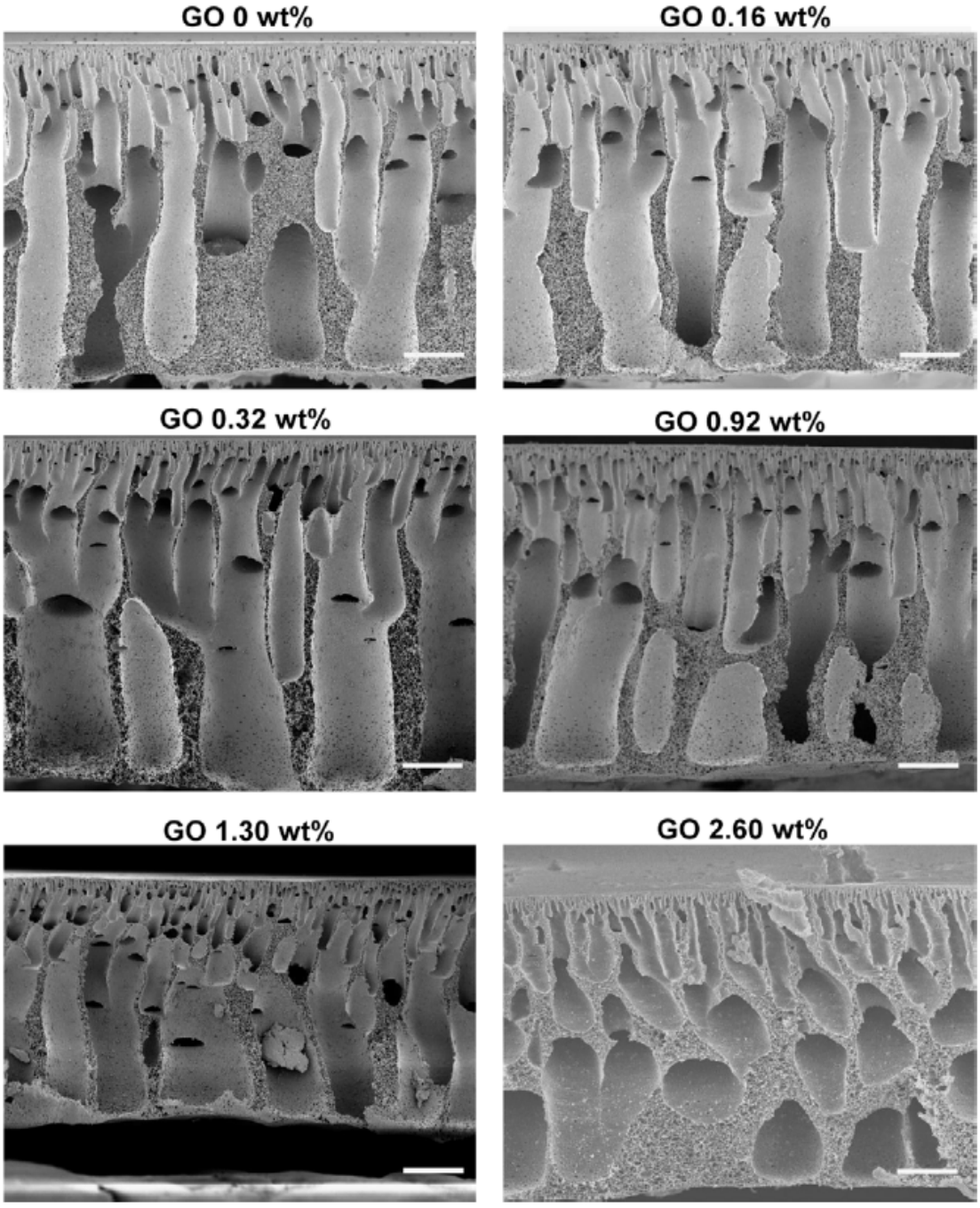

Figure III-14. Cross-sectional images of membranes. (scale bars, 20 μm.)

based on dry polymer weight). This fact coincides with the observation that there is no significant difference in the viscosity of the polymer solutions with GO content ranging from 0 to 0.2 wet wt% (wt % based on polymer solution weight) that were used to produce the membranes with 0-1.30 dry wt% GO. However, the membrane with 2.60 dry wt% GO had a dense sub-layer, because the propagation of finger toward bottom surface ceased due to unusual increase in the viscosity of polymer solution with 0.39 wet wt% GO that produced the membrane with 2.60 dry wt% GO. This dense sub-surface layer of the membrane with 2.60 wt% GO must have contributed to the decrease in its pure water flux.

Although a quantitative assessment cannot accurately be made with regard to the balancing effects of hydrophilicity and viscosity, the results obtained indicate that the dominant factor affecting the pore structure is hydrophilicity of polymer solution when the GO content is relatively low whereas it becomes viscosity of the solution when the content is larger than around 2 wt%.

III.3.5. Mechanical strength of polysulfone/graphene oxide membrane

Figure III-15 shows Young's modulus of PSf membrane for various GO contents. The mechanical strength of membrane increases with increasing GO content up to 1.30 wt% GO, which could be attributed to the very high aspect ratio of the graphene oxide. However, excessive GO in membrane might play the role of providing stress convergence points in the membrane that is caused by aggregation of GO in polymeric matrix, so that the membrane with 2.60 wt% GO showed brittle feature (Xu, Hong et al. 2009, Liu, Zhang et al. 2010).

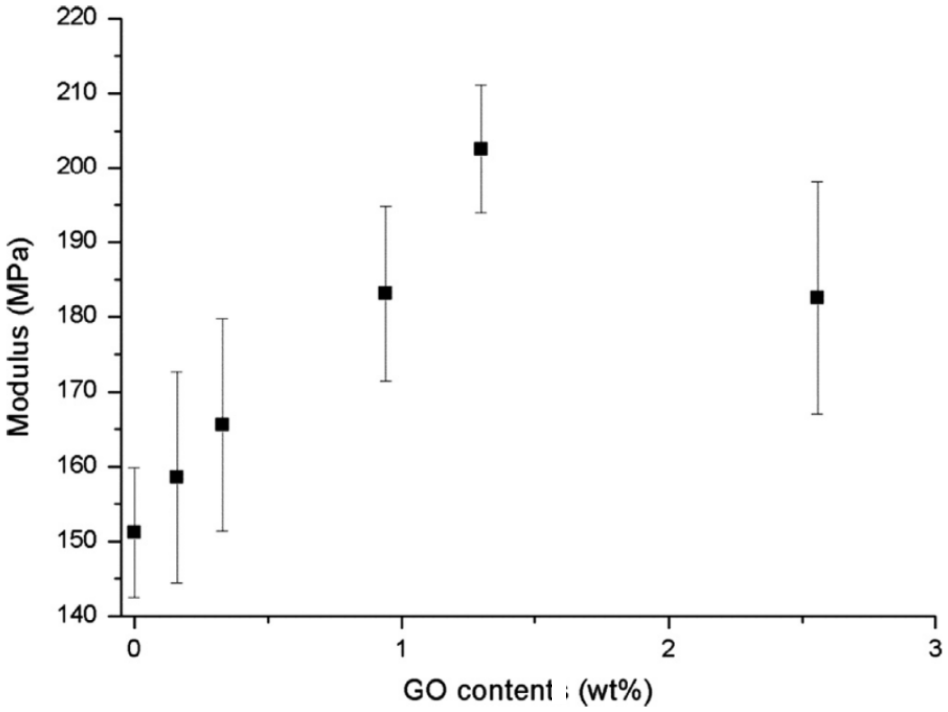

Figure III-15. Young's modulus of PSf membrane for various GO contents. (error bar: standard deviation, n=5.)

III.3.6. Membrane bioreactor operation

The TMP profiles for the three membranes are shown in **Figure III-16 (a).** The profiles show the TMP changes that were needed to maintain a permeate flux of 16 L/m^2/h at an aeration rate of 1.5 L/min. Since the experiments were for comparison and only a measure of membrane lifetime is needed, no cyclic operation was involved as in real MBR operation where cycles of operation/release or operation/back-flushing are repeated. The real MBR operation is typically ceased when TMP reaches 50 kPa for a chemical washing. Therefore, the profiles are given up to 50 kPa in the figure.

Quite apparent in the figure is a drastic change in the TMP profile as the GO content in membrane increases. It took only 10 h of operation for TMP to rise up to 50 kPa for the PSf membrane without GO. For the membrane with 1.30 wt% GO, in contrast, the TMP reached 50 kPa after 50 h of operation. This comparison implies that a fivefold increase can be realized in the operating time between back-flushings in the operation/back-flushing cycle. It also implies that a fivefold lengthening can be achieved of the time between chemical cleanings with only 1.30 wt% GO in it. Less chemical washing together with the increased mechanical strength of membrane by addition of GO (**Figure III-15**) should contribute to extended membrane lifetime. All these advantages with the addition of GO would substantially lower the operating cost of MBR.

To verify that graphene oxide with the functional groups, and not graphene, is responsible for the remarkable performance, TMP experiments were also carried out with rGO and the results are given in **Figure III-16 (b)**. In other words, detrimental effects of using rGO are apparent in the TMP profile when it is compared with that of the membrane without rGO, confirming the assertion.

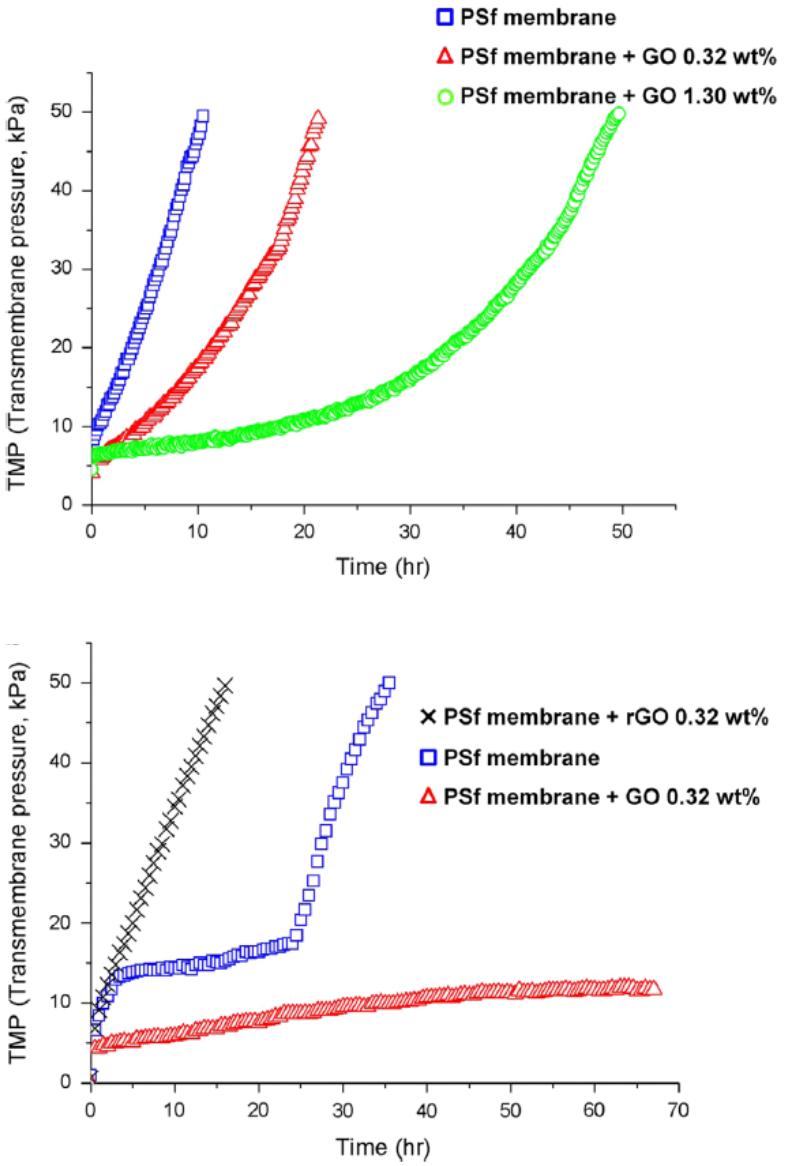

Figure III-16. Membrane bioreactor (MBR) operation with PSf/GO nanocomposite membrane (a) TMP profiles of the PSf/GO nanocomposite membranes with GO contents of 0 wt%, 0.32 wt%, and 1.30 wt% during the operation of continuous MBR at a constant flux of 16 L/m^2/h and an aeration rate of 1.5 L/min. (b) TMP profiles of PSf membrane for three cases: without GO, with 0.32 wt% GO, and with 0.32 wt% rGO (continuous operation of MBR at a constant flux of 16 L/m^2/h and an aeration rate of 4.0 L/min).

It is worth noting that the rates of TMP rise-up of polysulfone membrane and the membrane with 0.32% GO in the bottom panel is much slower than those in the top panel. It is because the stronger intensity of aeration (4 L/min) in the bottom panel than that in the top (1.5 L/min) could mitigate membrane fouling more effectively and thus slow down the rate of TMP rise-up. The reason for the plateau region in TMP rise up for the polysulfone membrane in the bottom panel is not so clear, but it is similar to the typical pattern of two phases-TMP rise up which is often observed in the MBR operation under a certain operating condition (Hwang, Lee et al. 2008, Yeon, Cheong et al. 2008).

III.4. Conclusions

Polysulfone ultrafiltration membrane including graphene oxide (GO) nanoplatelets was prepared for MBRs for wastewater treatment. The GO nanoplatelets can change the pore size and pore structure of porous medium formed by phase inversion. The GO membrane has anti-biofouling capability due to its hydrophilicity and electrostatic repulsion characteristics. It also has superior mechanical strength and water permeability. There is an optimum value of GO fraction to get higher water flux.

Chapter IV

IV. Impact of Support Layer on Thin-Film Composite Reverse Osmosis Membrane Performance

IV.1. Introduction

Water scarcity problem is increasingly accelerated by climate change and increasing demographic pressure. As a result, seawater desalination through advanced water treatment is becoming much more necessitated than ever before (Oki and Kanae 2006, Piao, Ciais et al. 2010, Green, Taniguchi et al. 2011). Reverse osmosis (RO) technology among several technologies for desalination has been actively sought to alleviate the problems caused by water deficiency because it consumes relatively low energy compared with any other desalination technologies such as thermal desalination (Elimelech and Phillip 2011). For the technology, however, there is still a need for reducing high operational costs associated with high hydraulic pressure that exceeds the osmotic pressure of feed solution (Sourirajan 1970). Therefore, high water permeability is desired in RO membrane to achieve high water flux under low operating pressure while retaining high salt rejection to reduce energy consumption in RO process.

To obtain high water permeability, various approaches have been taken. For instance, a wide variety of surface modification approaches involving radical-, photochemical-, radiation-, redox-, and plasma-induced grafting as well as polyvinyl alcohol coating have been taken to improve the water permeability by covalently attaching hydrophilic monomers or covering the membrane surface with more hydrophilic compounds (Lee, Arnot et al. 2011). Another approach is to add a nanomaterial such as zeolites or carbon nanotubes to provide more hydrophilic surfaces or preferential flow paths for high permeability (Pendergast and Hoek 2011). Recently, molecular layer-by-layer assembly was successfully applied to a process for creating polyamide (PA) layers on porous support layer to attain several

advantages such as thickness control at monomer length-scale, minimal surface roughness, and well-defined chemical composition (Gu, Lee et al. 2013).

It is not surprising that most of the studies on RO membrane are on the active layer with no consideration of the support layer, as apparent from the above discussion, because both salt rejection and most hydraulic resistance affecting the water permeability are believed to occur in the active layer. In contrast, the support layer of RO membrane has been regarded as a peripheral or irrelevant factor to membrane performance, because the role of the support layer has been considered only to enable active layer to endure high pressure compression. As a result, little work has been carried out on the support layer, and even when it was studied, it was in the context of examining the influence that the support layer characteristics have on the formation of the active layer during interfacial polymerization (IP) (Kim and Kim 2006, Singh, Joshi et al. 2006, Ghosh and Hoek 2009, Misdan, Lau et al. 2013). In addition, a theoretical modelling study was carried out for the effect of pore size and porosity of the support layer on the diffusive transport through the composite structure (Ramon, Wong et al. 2012).

In this work, we examine the role that the support layer plays and demonstrate that water flux of RO membrane can change depending on the pore structure of the support layer. We find that the influence of the support layer on RO membrane performance is more prominent than that of the active layer thickness. This finding implies that the water flux through RO membrane can significantly be altered by the way the support layer is formed. We also present an experimental method that is more appropriate to represent the characteristics of the support layer as related to water flux.

IV.2. Experimental section

IV.2.1. Fabrication of polysulfone porous support layer

To verify the influence of support layer on RO membrane performance, five types of support layers with distinctive structure were fabricated by varying the polymer solution concentration from 10 wt% to 30 wt% in light of the fact that typical polymer concentration used for conventional RO membranes is more than 20 wt% (Baker 2000, Lalia, Kochkodan et al. 2013). Polysulfone (PSf, Solvay Korea, Korea) in the amount corresponding to each concentration was dissolved in 1-methyl-2-pyrrolidinone (NMP, Sigma-Aldrich, USA) by stirring for 12h at 60 °C. After sonication for 1h, the polymer solutions were kept for 12h at 25 °C without stirring until bubbles disappear in the solution prior to casting. After a polyester non-woven fabric was wetted with solvent, the polymer solution was drawn down on the fabric using a micrometric film applicator (Elcometer 3570, Elcometer). The nascent support membranes were then immersed in a water bath for 24h at room temperature for entire liquid-liquid demixing.

IV.2.2. Fabrication of polyamide active layer by interfacial polymerization

Thin-film composite (TFC) membranes were prepared by forming PA selective layer on top of the porous PSf support membrane via the IP. Briefly, PSf support membranes were first immersed in a 3 wt% aqueous m-phenylenediamine (MPD, Woongjin Chemical, Korea) solution for 1 min. The MPD soaked support membranes were rolled with a rubber roller to remove the excess solution from the membrane surface, and then dried for 1 min at room temperature. The MPD saturated support membranes were then immersed in a 0.1 w/v% trimesoyl chloride (TMC, Aldrich, USA) in ISOL-C (SK innovation, Korea) solution for 1 min. The TFC membranes were stored for 10 min at room temperature after cured at 60 °C for 2 min. The fabricated TFC membranes were rinsed carefully and stored in deionized water for 30 min at room temperature prior to testing.

IV.2.3. Characterization

Tomograms of the prepared five support layers were obtained by non-destructive inspections employing an X-ray microfocus computed tomography (CT) system (phoenix v|tome|x m, GE, USA), and the tomograms were analyzed using a program called Image J which could calculate the cross-sectional area ratio of finger-like regions from the top view.

Micro-images were acquired by a Field Emission Scanning Electron Microscope (FESEM) (AURIGA, Carl Zeiss, Germany). Cross-sectional images of membranes were obtained by fracturing the samples immediately after immersing in liquid nitrogen to prevent them from being destroyed. A sputter coater (SCD 005, BAL-TEC, Germany) was used to coat all samples with platinum for 100 seconds. The topology of selective layer surface was probed by a Scanning Probe Microscope (SPM) (INNV-BASE, VEECO, USA).

The mean pore size can be estimated on the basis of the correlation between solute separation and solute diameter in solute transport based on the log-normal probability function.(Singh, Khulbe et al. 1998) Consequently, the mean pore size of a support layer of RO membrane was calculated to be the diameter of solute (Polyethylene glycol (PEG) or Polyethylene oxide (PEO)) corresponding to the solute separation of 50% (**Figure IV-1**). Stokes radii of PEG or PEO molecule were taken as the radii of solutes, which were obtained from the relationship between their molecular weights and the empirical equation reported in a previous work.(Singh, Khulbe et al. 1998) The amount of the separated solute was measured by total organic carbon analyzer (Sievers 5310, GE, USA).

Porosities and specific surface areas of support membranes were determined by mercury intrusion porosimetry (AutoPore IV 9500, Micromeritics,

USA). The viscosities of the polymer solutions were measured by an Advanced Rheometric Expansion System (ARES) (Rheometric Scientific ARES, Rheometric Scientific, USA). The relative atomic concentrations of N and O in active layers were investigated using X-ray photoelectron spectroscopy (XPS) (Axis-HSI, Kratos Analytical, UK) to compare the extent of cross-linking of PA.

Contact angle measurements were conducted using an OCA Contact Angle System (DataPhysics, Germany) and reported as an average of 9 measurements. The surface charge of each TFC membrane was determined by measuring the particle mobility induced only by the surface charge of membrane utilizing an electrophoretic light scattering spectrometer (ELS-Z2, Ostuka Electronic, Japan) equipped with a plated sample cell. The chemical structure of as-prepared membranes was characterized using an Fourier transform infrared (FTIR) spectrometers (Nicolet 6700, Thermo Scientific, USA) equipped with an attenuated total reflection (ATR).

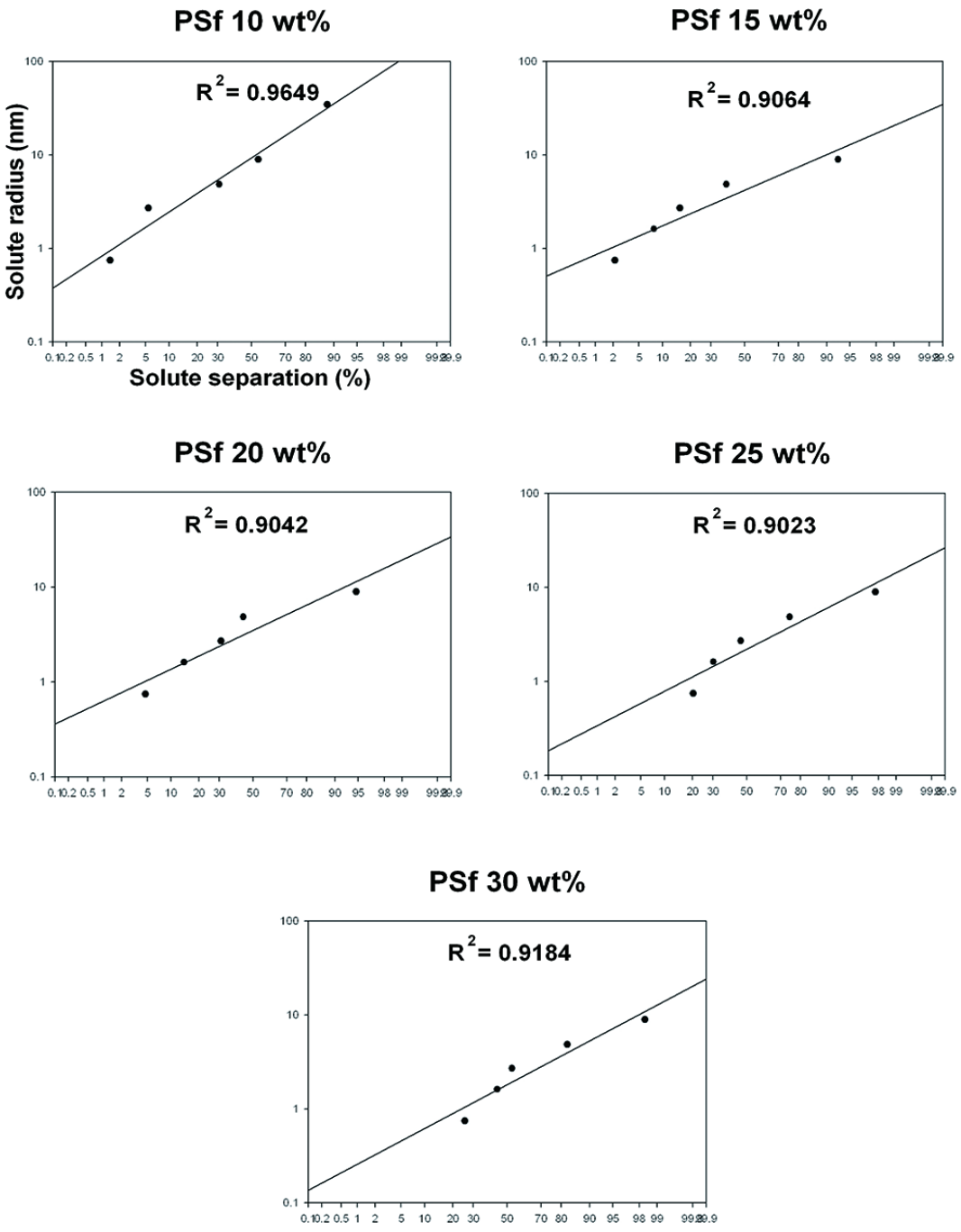

Figure Ⅳ-1. Solute radius curves plotted on a log-normal probability paper for the support layers prepared with different polymer solution concentrations. Solute: Polyethylene glycol (PEG) or Polyethylne Oxide (PEO), Polymer solution: 10 wt% - 30 wt % of PSf.

IV.2.4. Reverse osmosis test

Water flux and salt rejection of the prepared TFC membranes were assessed by a bench scale cross-flow system with a 2000 ppm NaCl solution. The effective membrane area is 29.1 cm^2. The system consists of a reservoir with working volume of 10 L, two pumps, and RO modules operated in parallel (**Figure IV-2 (a)**). The cross-flow rate was fixed at 20 cm/s, and the temperature was constant at 25 ± 0.5 °C. The RO system was stabilized only with the NaCl solution for 30 min at an applied pressure of 2410 kPa (24.1 bar), and then operated for 30 min at a constant pressure of 1550 kPa (15.5 bar) to measure water flux ($L \cdot m^{-2} \cdot h^{-1}$). The water flux was calculated by dividing the volume of the collected permeate for 30 min by membrane area. Observed salt rejection was determined by measuring the difference in the salt concentration of the feed (C_f) and the permeate (C_p) with a conductivity meter using the following equation: salt rejection (%) = $100 \times (1 - \frac{C_p}{C_f})$. The water flux and salt rejection values for each sample are the average of five different measurements, collected over a period of approximately 30 min.

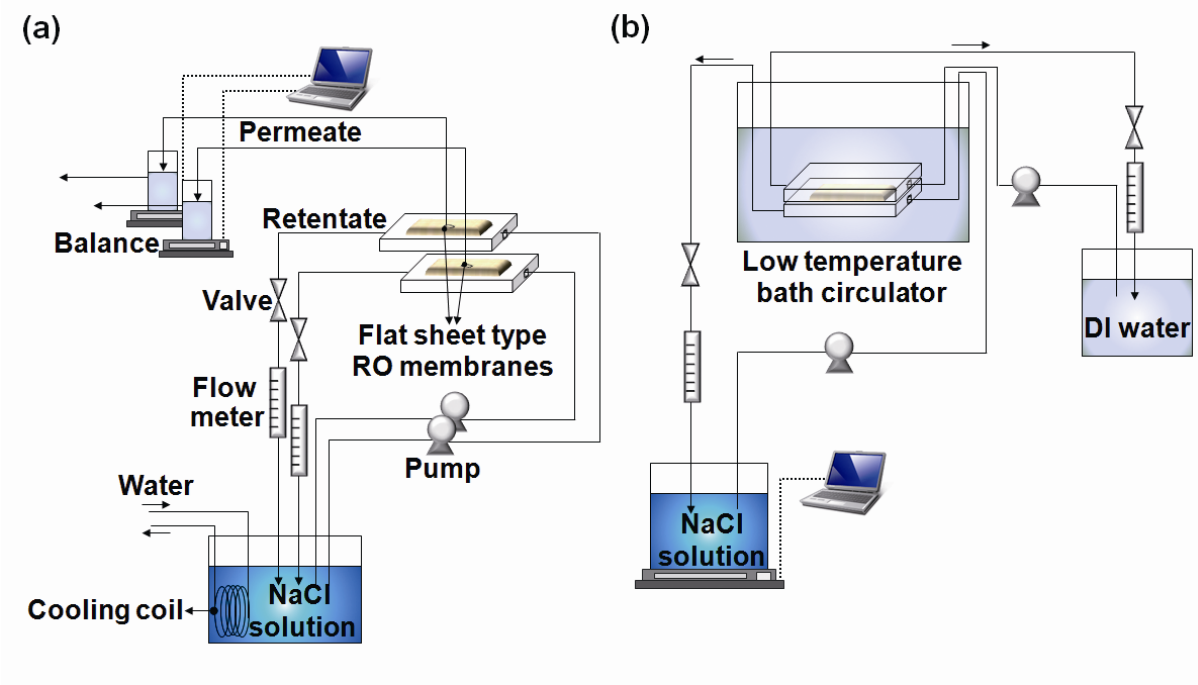

Figure Ⅳ-2. Schematic diagram of the lab-scale (a) reverse osmosis system and (b) forward osmosis system.

IV.2.5. Forward osmosis test

Pure water flux across the membrane was also evaluated in a bench scale forward osmosis (FO) system (**Figure IV-2 (b)**) equipped with a cross-flow membrane cell with the channel 49 mm long, 21 mm wide, and 3 mm deep to determine tortuosity of support membrane. Prior to FO test, the fabric layer was carefully removed by peeling them away from the other layer composed of the PA selective layer and the PSf support layer. In FO mode, the support layer and the active layer are against draw solution and feed solution, respectively. Feed solution was 6L of deionized water, and the draw solution was 1 L of 5M NaCl aqueous solution. The feed and draw solutions were circulated with pump at a cross-flow rate of 20 cm/s. The test temperature was maintained at 20 ℃ ± 0.5 ℃ using low temperature bath circulator. The osmotic water flux was the average of the volumetric change of NaCl solution during 1 h after the FO system was stabilized.

IV.3. Results and discussion

IV.3.1. Control of support layer structure using pore formation mechanism in phase inversion.

A membrane fabricated with a polymer solution consisting of PSf and NMP generally has larger surface pores and a finger-like structure underneath the skin layer (Strathmann and Kock 1977, Lee, Chae et al. 2013). Meanwhile, the rate of precipitation slows down as the viscosity of polymer solution increases, which results in a transition from a finger-like structure to a sponge-like structure as well as the decrease in surface pore size (Mulder 1996, Han and Nam 2002). Such explanations of earlier studies were in good agreement with our experimental results of PSf support membranes, which is well revealed in **Figure IV-3** and **Figure IV-4**.

It is clear from the micrographs that up to the polymer concentration of 20 wt%, the finger-like structure dominates although appears the region filled with the sponge-like structure between the fingers. As the concentration is further increased, the sponge-like structure starts asserting itself and it dominates for the concentration greater than 25 wt%. It should be noted in this regard that the viscosity increases with increasing polymer concentration (**Figure IV-3**). These micrographs show the progression of the change in the membrane structure as the polymer concentration (or the viscosity of polymer solution) is increased.

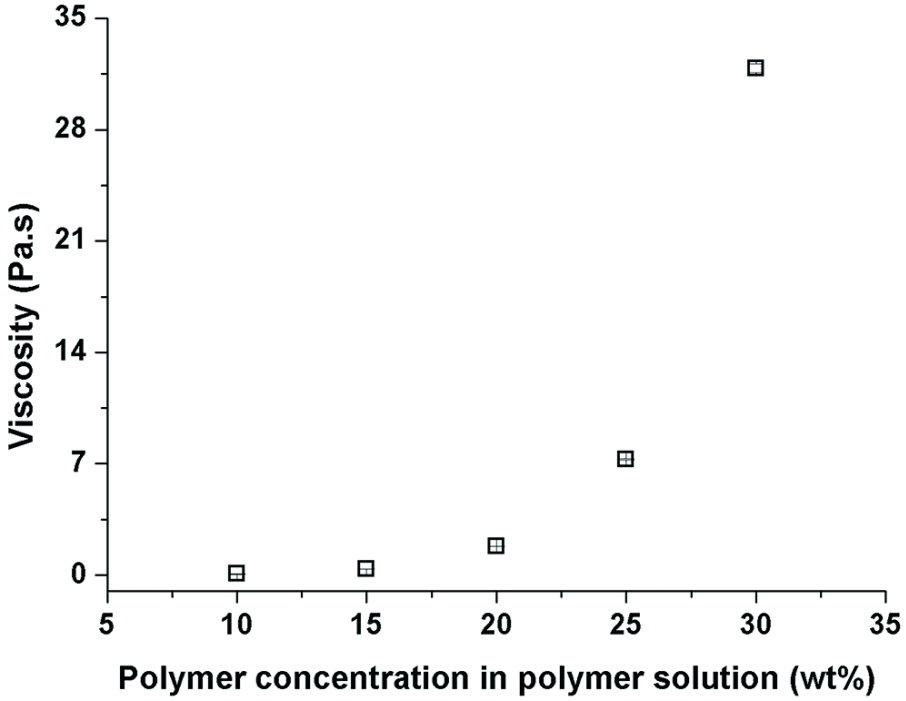

Figure Ⅳ-3. Viscosities of polymer solutions with various polymer concentrations (error bar: standard deviation, n=5).

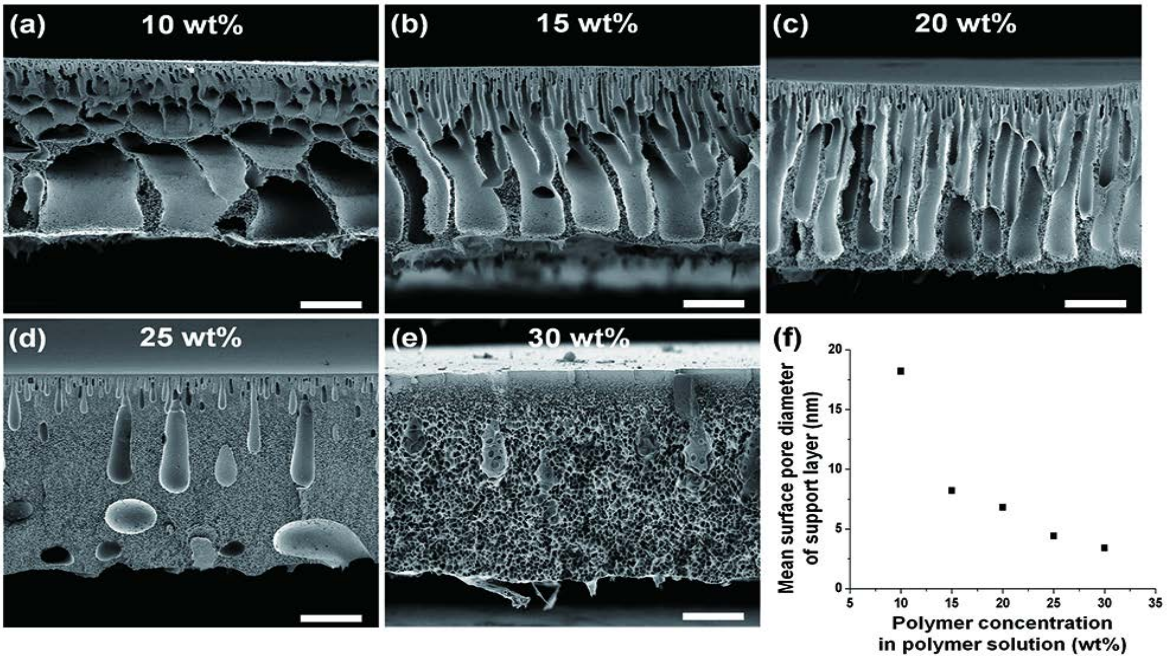

Figure Ⅳ-4. The micrographs are cross-sectional SEM images of support membranes (scale bar: 40 μm). In order from (a) to (e), the polymer concentrations in polymer solutions used to fabricate support membranes are 10 wt%, 15 wt%, 20 wt%, 25 wt%, and 30 wt%, respectively. (f) Mean surface pore size of each support membrane (error bar: standard deviation, n=3).

IV.3.2. Correlation between mean surface pore size of support layer and active layer thickness of reverse osmosis membrane.

Prior to testing the performances of RO membranes fabricated with the support membranes having different pore structure, we uncovered a correlation between surface pore size of support layer and active layer thickness of RO membrane. According to our results, the active layer thickness decreased with increasing polymer concentration (**Figure IV-5 (a) and Figure IV-6**). It is assumed to be caused by the fact that the PA layer is formed by "volcano-like" reaction accompanying MPD eruption from surface pores of the support layer during the IP (Freger 2005, Ghosh and Hoek 2009). In other words, the PA film could grow thicker as the surface pore size of the support layer becomes larger, because the larger surface pore is desirable to diffuse more MPD monomers (**Figure IV-7**). This was confirmed by the trend shown in **Figure IV-5 (b)** between active layer thickness and mean surface pore size of the support layer which were obtained by SEM image (**Figure IV-6**) and solute transport measurement (**Figure IV-1**), respectively.

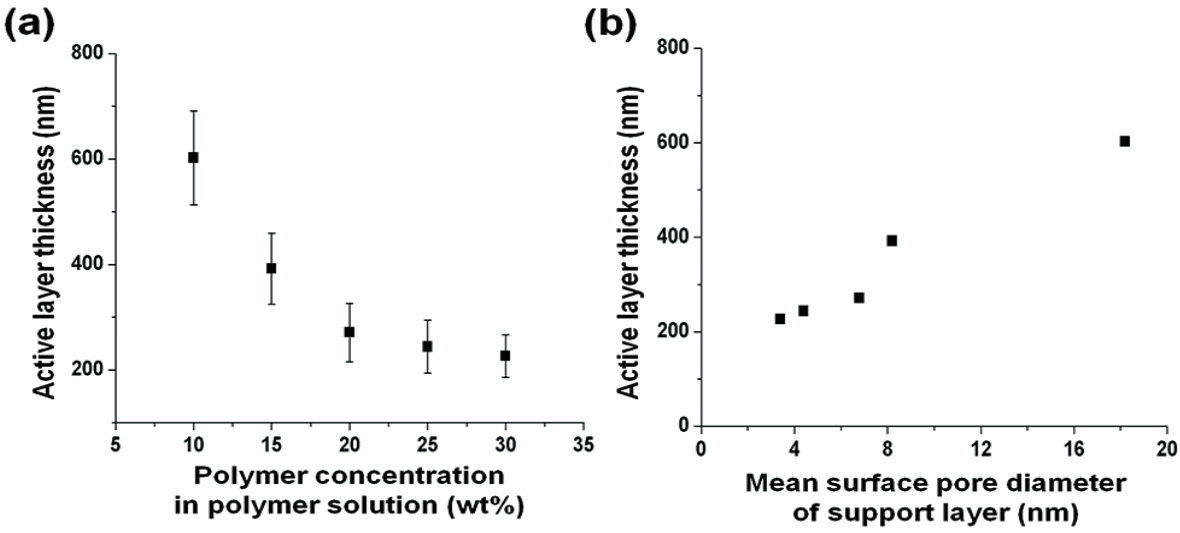

Figure Ⅳ-5. Active layer thickness governed by mean pore size of support layer. (a) Active layer thickness of each RO membrane (error bar: standard deviation, n=5), and (b) correlation between mean surface pore size of each support membrane and active layer thickness of RO membrane.

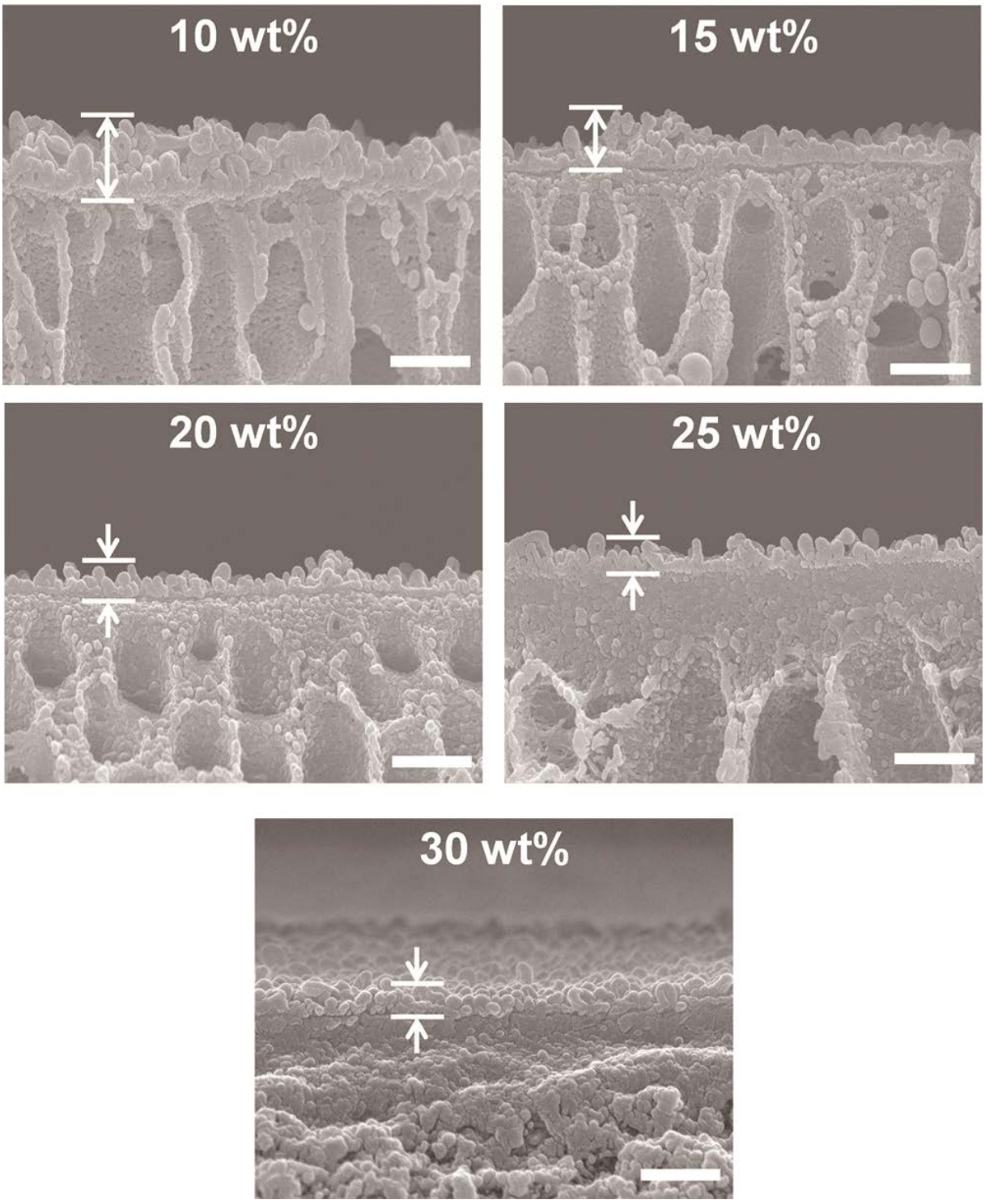

Figure Ⅳ-6. Cross-sectional SEM images including the active and support layers of RO membrane (scale bar: 1 μm).

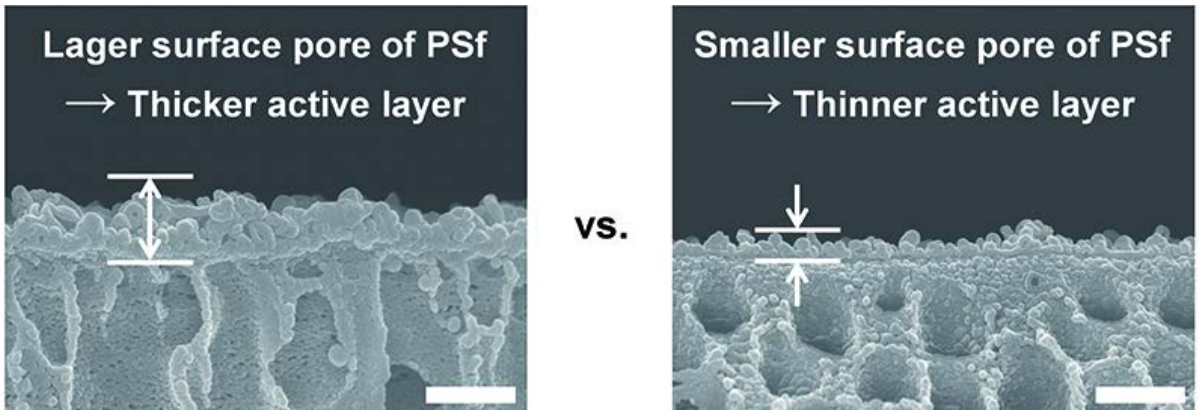

Figure Ⅳ-7. Micrographs of thicker and thinner active layer formed on PSf support layers with larger and smaller surface pores, respectively (scale bar: 1 μm).

IV.3.3. Correlation between active layer characteristics of reverse osmosis membrane and water flux.

It is generally known that the water flux increases with decreasing thickness of the active layer according to the solution diffusion model for transport through the RO membrane. For instance, a fivefold decrease in the active layer thickness resulted in an 80% increase in the water flux (Gu, Lee et al. 2013). In contrast, in our study here, the water flux increases with increasing thickness of the active layer while the salt rejection rate is almost unaffected (**Figure IV-8**). Comparing the TFC membrane produced by 10 wt% polymer solution against that by 30 wt% polymer solution, the active layer thickness for 10 wt% solution was 602 (± 88) nm whereas it was 226 (± 40) nm for 30 wt% solution (**Figure IV-5 (a)**). In spite of this much thicker active layer (602 nm vs. 226 nm), the water flux for the TFC prepared by 10 wt% solution is almost 30 times higher than that for the membrane made with 30 wt% solution (**Figure IV-8**), which indicates that the water flux was not dominated by the active layer thickness in this study. Moreover, there was no relationship between the density (or the extent of cross-linking) of active layer and the water flux of RO membrane according to XPS data (**Figure IV-9**), which also supports that the water flux was not dominated by the nature of active layer in this study. It is known that there is a positive correlation between the N/O ratio and the degee of cross-linking of polyamide active layer (Kim, Kwak et al. 2005). Also, it has been reported that the higher degree of cross-linking leads to increasing permeability of RO membrane because an increase of the interstitial space between linear polymer chains or the molecular-level free volume by cross-linking loosen polymer chain packing of the active layer (Kim, Kwak et al. 2005, Peng, Huang et al. 2010). Therefore, we examined the N/O ratio of each active layer using 20 wt%

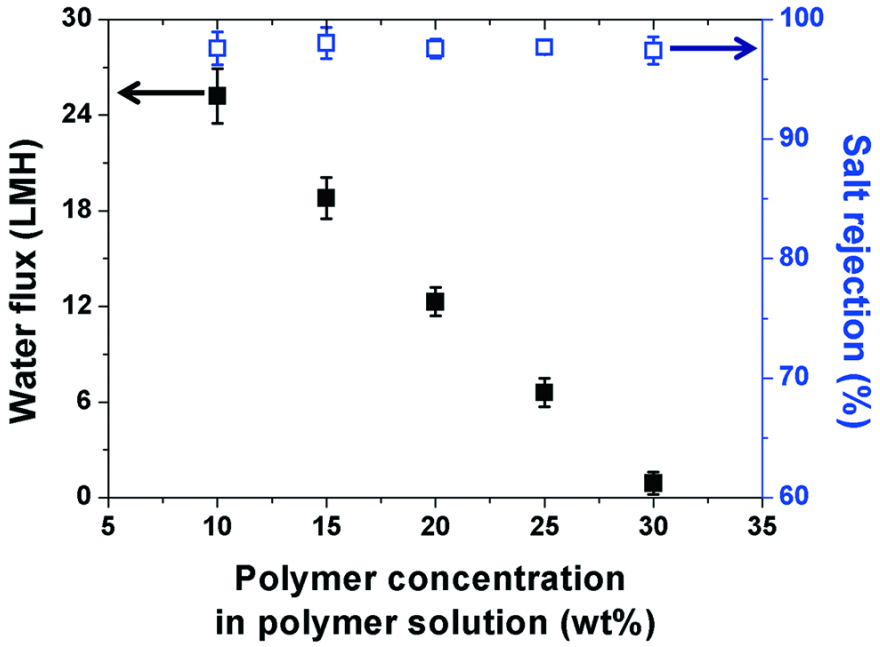

Figure Ⅳ-8. Water flux and salt rejection of RO membranes with the support layers prepared with different polymer concentrations (error bar: standard deviation, n=5).

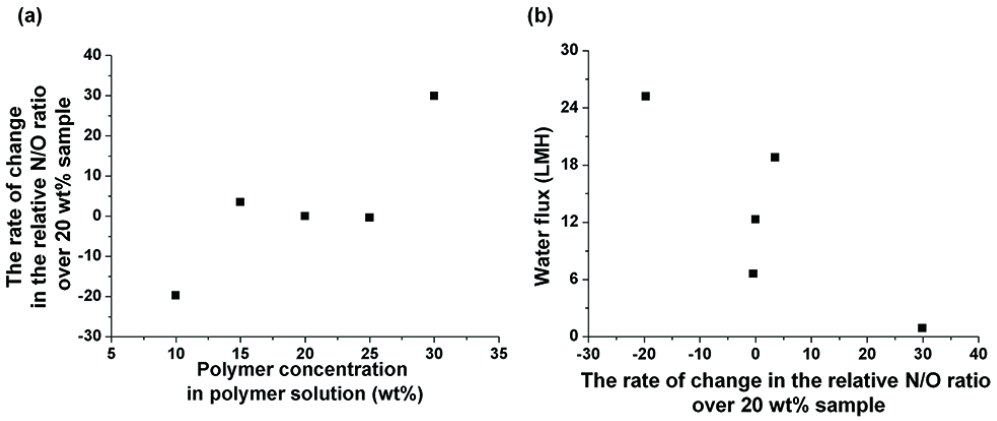

Figure Ⅳ-9. Evaluation of cross-linking degree of each active layer using N/O ratio. (a) The rate of change in the relative atomic concentration of N and O in each active layer over that of 20 wt% sample, and (b) The plot of water flux against the rate of change in the relative atomic concentration of N and O in each active layer over that of 20 wt% sample.

sample as a baseline to compare the extents of their cross-linking and to confirm the correlation between the extent of cross-linking and water flux trend in this study. (Note that 20 wt% corresponds to typical polymer concentration to prepare support membrane used for commercial RO membranes. (Baker 2000, Lalia, Kochkodan et al. 2013)) According to our result, the degree of cross-linking was not related to water flux of RO membrane in this study (**Figure IV-9 (b)**).

IV.3.4. Pressure drop and water transport behaviour in support layer during reverse osmosis operation.

As apparent from the above discussion, it is not the active layer that dictates water permeation through RO membrane within the range of the active layer thickness. It is this second belief on water flux of RO membrane that we put into question in this work. Here, we demonstrate that the support layer is not necessarily negligible although the pressure drop in the support layer is not a substantial portion.

The support layer consists mainly of sponge-like region and finger-like region. In the sponge-like region, the microvoids smaller than a few micrometers dominate whereas the macrovoids ranging from tens-of-micrometer to a hundred micrometer do in the finger-like region. Consequently, finger-like regions can provide water continuity within the support layer unlike sponge-like regions, thereby providing most pathways for water transport due to a substantially less resistance in the finger-like region than that in the sponge-like regions. Considering that fluids tend to mostly pass through the region with lower resistance, it can be inferred that finger-like regions are main pathways for water permeation. If the phenomenon appears in the support layer of TFC membrane during RO operation, the difference in characteristics of support layer might affect the overall water flux in RO regardless of the nature of active layer. This suggests the possibility that more water can be produced by RO membrane when finger-like regions account for a large proportion of the support membrane volume.

To ascertain whether significant difference in hydraulic resistance can lie in the support layer depending on the pore structure of the support layer during RO operation, we examined the pressure drops in the support layers based on Ergun

equation. The Ergun equation combines Blake-Kozeny equation that represents the viscous energy loss mainly in laminar flow with Burke-Plummer equation that describes the kinetic energy loss mainly in turbulent flow. It is often used to analyze the resistance or pressure drop that occurs when fluids flow through porous media (Vafai and Tien 1981, Wu, Yu et al. 2008). The Ergun equation could be written as follows:

$$\frac{\Delta P}{L} = \frac{72 \cdot \tau \cdot \mu \cdot (1-\varepsilon)^2 \cdot v_s}{D_p^2 \cdot \varepsilon^3} + \frac{3 \cdot f \cdot (1-\varepsilon)}{\varepsilon^3} \cdot \frac{\rho \cdot v_s^2}{D_p} \quad (1)$$

where P is the pressure, L is the length along the macroscopic pressure gradient in porous media, τ is the tortuosity, μ is the dynamic viscosity of fluid, ε is the porosity of porous media including both finger-like regions and sponge-like regions, D_p is the average diameter of particles, v_s is the superficial velocity (defined by v_s = Q/A, where Q is the total flow rate through a cross-section of area A), f is the friction coefficient, and ρ is the density of fluid (Wu, Yu et al. 2008).

It is helpful for the calculation of the pressure drop to know the range of modified Reynolds number ($Re_p = \frac{D_p \cdot \rho \cdot v_s}{\mu \cdot (1 - \varepsilon)}$) since the second term on the right hand side of Equation (1) can be neglected when the number is less than 10 whereas the first term can be neglected if the number is larger than 100 (Bird, Stewart et al. 1960). The modified Reynolds numbers were calculated using the specific surface area ($S_v = \frac{6 \cdot (1 - \varepsilon)}{D_p}$) as following:

$$Re_p = \frac{6 \cdot \rho \cdot v_s}{\mu \cdot S_v} \quad (2)$$

With experimentally determined parameters, it can be shown that the Reynolds

numbers of the support membranes used in osmotic separation range from 6.9×10^{-8} to 8.6×10^{-6} (**Table IV-1**). Therefore, only the first term in Equation (1) can be used for estimating the pressure drop, which can be rewritten for ΔP as follows with S_v instead of D_p:

$$\Delta P = \frac{2 \cdot \tau \cdot \mu \cdot S_v^2 \cdot v_s \cdot L}{\varepsilon^3} \tag{3}$$

The specific surface area and the porosity in the above equation can be obtained experimentally from mercury porosimetry and the water velocity from the amount of water collected over a period of time. The tortuosity factor, however, has to be estimated based on FO experiments.

According to literature studies (Cath, Childress et al. 2006, Yip, Tiraferri et al. 2010), the following relationships hold for FO membrane:

$$\tau = S \times \frac{\varepsilon}{t} \tag{4}$$

$$S = \frac{D}{J_w^{FO}} \cdot \ln\left(\frac{A \times \pi_{D,b} + B}{A \times \pi_{F,m} + B + J_w^{FO}}\right) \tag{5}$$

where S is the structure parameter, t is the membrane thickness, D is the salt diffusion coefficient, J_w^{FO} is the measured volumetric water flux in FO test, A is the intrinsic water permeability, B is the salt permeability, $\pi_{D,b}$ is the bulk osmotic pressure of the draw solution, and $\pi_{F,m}$ is the osmotic pressure at the membrane surface on the feed side (0 atm for deionized water feed). The parameters A and B are obtained from the following relationships:

$$A = \frac{J_w^{RO}}{\Delta P} \tag{6}$$

Table Ⅳ-1. Reynolds numbers and variations derived experimentally.

	Superficial velocity, v_s (m/s, n=5)	**Specific surface area, S_v (m^{-1}, n=3)**	**Reynolds number, Re_p**
10 wt%	7.0×10^{-6} ($\pm 0.5 \times 10^{-6}$)	4.9×10^{6} ($\pm 1.7 \times 10^{6}$)	8.6×10^{-6}
15 wt%	5.2×10^{-6} ($\pm 0.4 \times 10^{-6}$)	6.8×10^{6} ($\pm 1.5 \times 10^{6}$)	4.6×10^{-6}
20 wt%	3.4×10^{-6} ($\pm 0.2 \times 10^{-6}$)	14.2×10^{6} ($\pm 4.1 \times 10^{6}$)	1.4×10^{-6}
25 wt%	1.8×10^{-6} ($\pm 0.2 \times 10^{-6}$)	24.0×10^{6} ($\pm 6.2 \times 10^{6}$)	4.6×10^{-7}
30 wt%	0.3×10^{-6} ($\pm 0.2 \times 10^{-6}$)	21.8×10^{6} ($\pm 3.6 \times 10^{6}$)	6.9×10^{-8}

$$R = 1 - \frac{C_p}{C_f} \tag{7}$$

$$B = \frac{(1 - R) \cdot A \cdot (\Delta P - \Delta \pi)}{R} \tag{8}$$

where J_w^{RO} is the measured volumetric water flux in the RO test, R is the salt rejection, and $\Delta\pi$ is the osmotic pressure difference across the RO membrane.

The tortuosity factors calculated from FO experiments and the equations given above are shown in **Table IV-2**, along with experimentally determined values of the specific surface area, the linear velocity, and the porosity for two membranes prepared with 10 wt% and 25 wt% polymer solutions. The values can be used in Equation (3) to estimate the pressure drops across the two membranes.

According to the calculated results, the estimated pressure drop across the membrane corresponding to 10 wt% polymer solution is about 0.1 kPa whereas it is about 60 kPa for the membrane prepared with 25 wt% polymer solution. This huge difference reaching 600 fold in the pressure drop in support layer resulted mainly from the tortuosity and the specific surface area (refer to the values in **Table IV-2** and Equation (3)). It is noteworthy that the support membrane has a smaller tortuosity and specific surface area if finger-like regions account for a large proportion of the support membrane volume, since finger-like regions have smaller surface area per volume than sponge-like regions (**Figure IV-10**). Consequently, it can be concluded that finger-like regions are mainly used for water permeation due to much smaller pressure drop during RO operation as well, which in turn dictates the water flux through the membrane.

Table Ⅳ-2. Data for osmotic separation operations at 20 °C to evaluate the difference between pressure drops in 10 wt% and 25 wt% samples. Equations from (4) and (8) were used to determine tortuosity with a diffusivity of 1.33 × 10^{-9} $\frac{m^2}{s}$ for NaCl (McCutcheon and Elimelech 2006, Yip, Tiraferri et al. 2010). 30 wt% sample was not used to evaluate pressure drop, because it had the J_w^{FO} under detection limit.

Membrane	10 wt%	25 wt%
Tortuosity, τ [n=3]	1.91 (± 0.38)	122 (± 38)
Specific surface area, S_v [m^{-1}, n=3]	4.9 × 10^6 (± 1.7 × 10^6)	24.0 × 10^6 (± 6.2 × 10^6)
Superficial velocity, v_s [m/s, n=5]	7.0 × 10^{-6} (± 0.5 × 10^{-6})	1.8 × 10^{-6} (± 0.2 × 10^{-6})
Porosity, ε [n=3]	0.83 (± 0.05)	0.73 (± 0.07)
Structure parameter, S [μm, n=3]	231 (± 46)	16,744 (± 5,313)
Intrinsic water permeability, A [L·m^{-2}·h^{-1}·bar^{-1}, n=5]	1.63 (± 0.11)	0.43 (± 0.06)
Salt permeability, B [L·m^{-2}·h^{-1}, n=5]	0.54 (± 0.28)	0.13 (± 0.03)
Water flux in FO mode, J_w^{FO} [L·m^{-2}·h^{-1}, n=3]	46.4 (± 7.0)	1.36 (± 0.42)
Salt rejection, R [%, n=5]	97.6 (± 1.4)	97.7 (± 0.6)

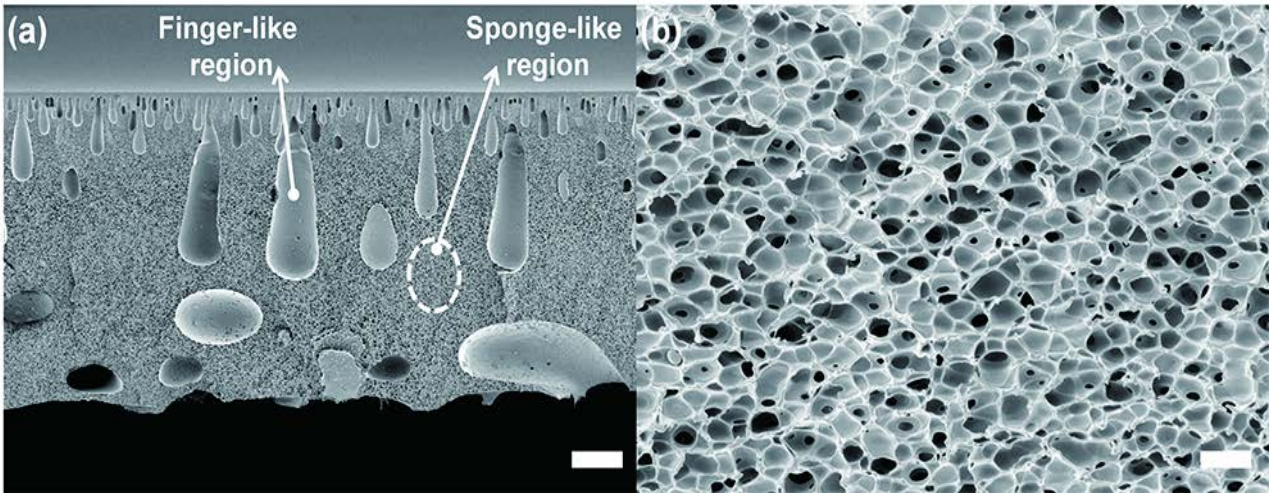

Figure Ⅳ-10. Cross-sectional SEM images of support membrane fabricated using 25 wt% polymer solution. (a) The support membrane fabricated using 25 wt% polymer solution (scale bar: 20 μm), and (b) the magified image of sponge region including microvoids in 25 wt% support membrane (scale bar: 2 μm). Sponge-like region comprised of microvoids with the width of a few micrometers has a larger surface area per volume than finger-like region.

IV.3.5. Correlation between the characteristics of support layer and water flux of reverse osmosis membrane.

For the experimental clarification of the correlation between the characteristics of the support layer and water flux of RO membrane, we used X-ray microfocus CT system to measure the proportion of the finger-like region in the support layer. Since most voids in sponge-like regions are smaller than the detection limit of the X-ray microfocus CT system used in this study, finger-like regions can exclusively be distinguishable in tomograms (**Figure IV-11**).

We obtained 25 tomograms of each support membrane in the depth direction at 25 different depths, as determined by a program called Image J on the basis of the tomogram (**Figure IV-12 (a)**). An averaged proportion value of all the finger-like regions at different positions at each polymer concentration is given in **Figure IV-12 (b)**. The figure shows that the averaged proportion value of finger-like regions decreases linearly with increasing concentration of polymer in the polymer solution used to fabricate the support membrane, and the trend in the proportion of finger-like region is considerably similar to that of water flux through the RO membrane.

This result signifies that the characteristics of support layer could affect directly water flux of RO membrane without discernible difference in salt rejection when the RO membrane is prepared with a given polymer solution. Such a plot is shown in **Figure IV-12 (c)** where the water flux is plotted against the averaged proportion value of finger-like regions. Actually, it has a linear relationship with water flux, revealing a high correlation between them.

From the above results, it can be inferred that the finger-like regions dictate effective area available for water permeation through active layer, because the

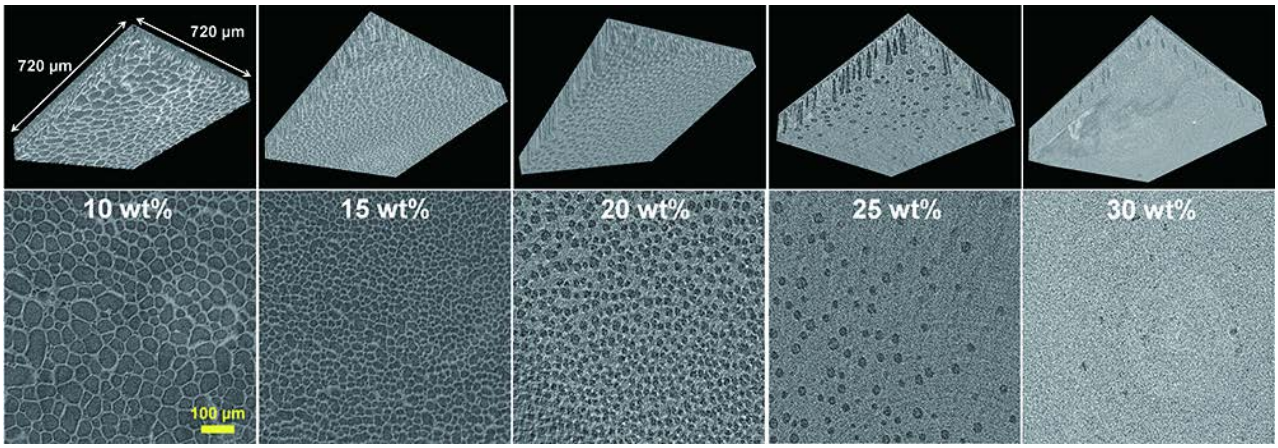

Figure Ⅳ-11. The micrographs in the top line and in the bottom line are 3D images and tomograms of support membranes obtained by non-destructive inspections, respectively. In order from left to right, the polymer concentrations in polymer solutions used to fabricate support membranes are 10 wt%, 15 wt%, 20 wt%, 25 wt%, and 30 wt%, respectively. In the 3D images and tomograms, the dark part represents finger-like region.

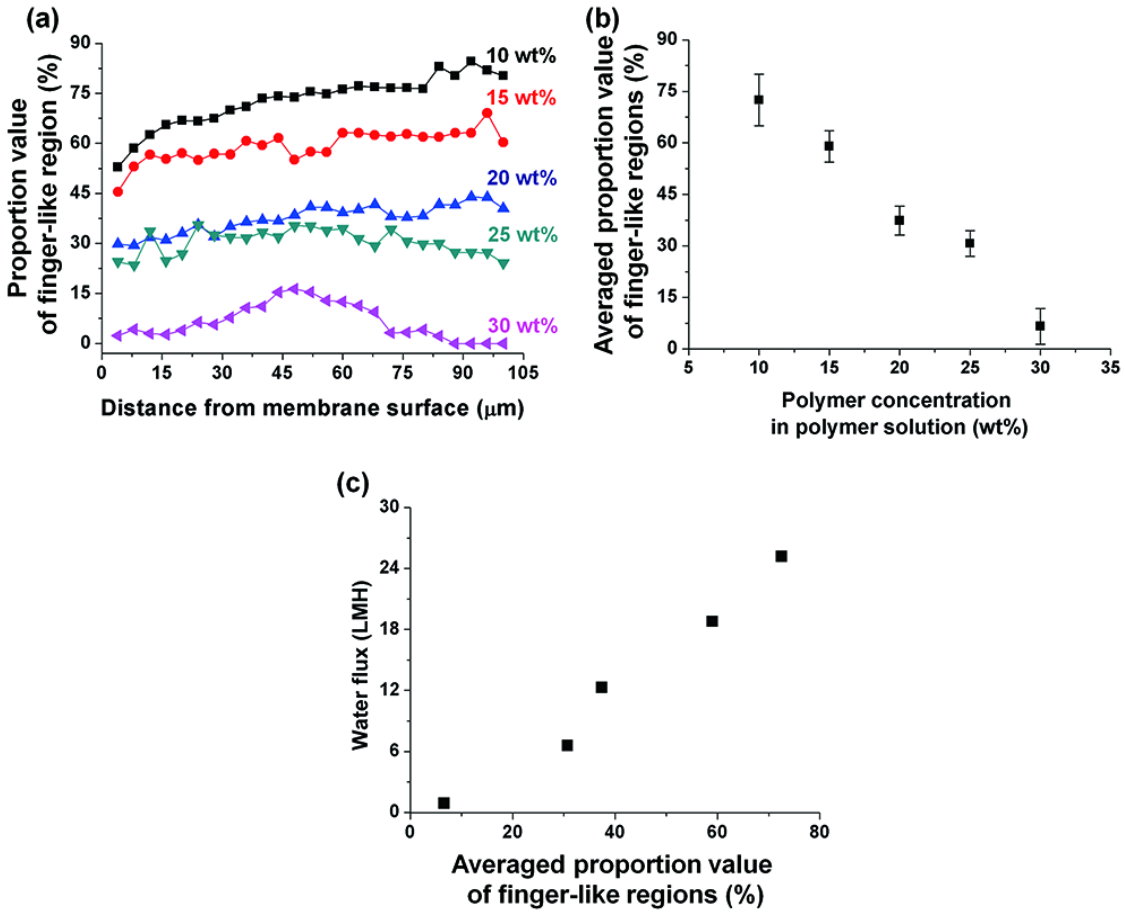

Figure Ⅳ-12. Estimation of proportion of finger-like region in each support layer. (a) Proportion of finger-like region in support membranes at different heights, (b) averaged proportion value of finger-like region in support membranes (error bar: standard deviation, n=25), and (c) correlation between averaged proportion value of finger-like region in support membranes and water fluxes of RO membranes.

finger-like regions and only fractions of active layer area right above them are exclusively used for filtration due to significantly smaller resistance in finger-like regions. In other word, effective area of active layer is predetermined by distribution of finger-like region in support layer regardless of active layer property.

IV.3.6. Various characteristics of a thin-film composite membrane on water flux of reverse osmosis membrane

Although we showed that the support layer plays a dominant role in determining the water flux of RO membrane, we also examined several factors that were reported relevant to the water flux in the literature.

It has been reported (Hirose, Ito et al. 1996) that an increase in the roughness of the upper surface of the active layer results in an increase in the surface area or effective area in contact with salt water, which in turn leads to an increase in the water flux. Although this trend holds for our case (**Figure IV-13 (a) and Figure IV-14**), the increase in the surface area from 14.4 (±0.9) μm^2 (as determined by atomic force microscopy for an area of 3 μm × 3 μm) to 15.0 (±1.8) μm^2, as the concentration of polymer solution is decreased from 25 to 10 wt%, is too small to cause a more than threefold increase in the water flux.

Another factor to consider is the surface chemistry effect of active layer on the water permeability of RO membrane. Chemical compositions of the active layer formed on each support layer obtained by FTIR were almost identical (**Figure IV-13 (b)**), but contact angles were marginally dissimilar (**Figure IV-13 (c)**). It is inferred that small differences in contact angles only resulted from the difference in the roughness of active layer, because contact angle decreases with rougher surface according to Wenzel's model. Despite some discrepancies, however, it was considered that the difference in contact angle also did not have a great influence on the water flux of RO membrane since it was too little to cause the big difference in water flux.

Membrane surface charge can also affect the water permeability of RO membrane due to its negative impacts such as electroviscous effect inducing charge

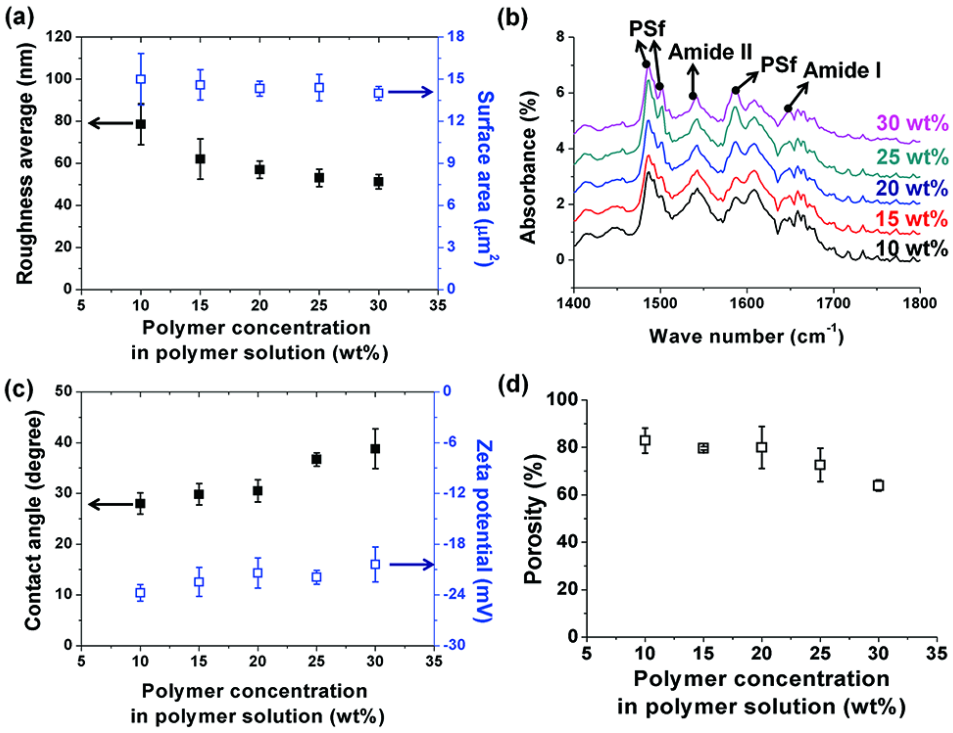

Figure Ⅳ-13. Various characteristics of a TFC membrane as a function of polymer concentration: (a) roughness and surface area (error bar: standard deviation, n=5), (b) absorbance in FTIR spectra, (c) contact angle and zeta potential (error bar: standard deviation, n=9 and n=3, respectively), and (d) porosity of support layer (error bar: standard deviation, n=3).

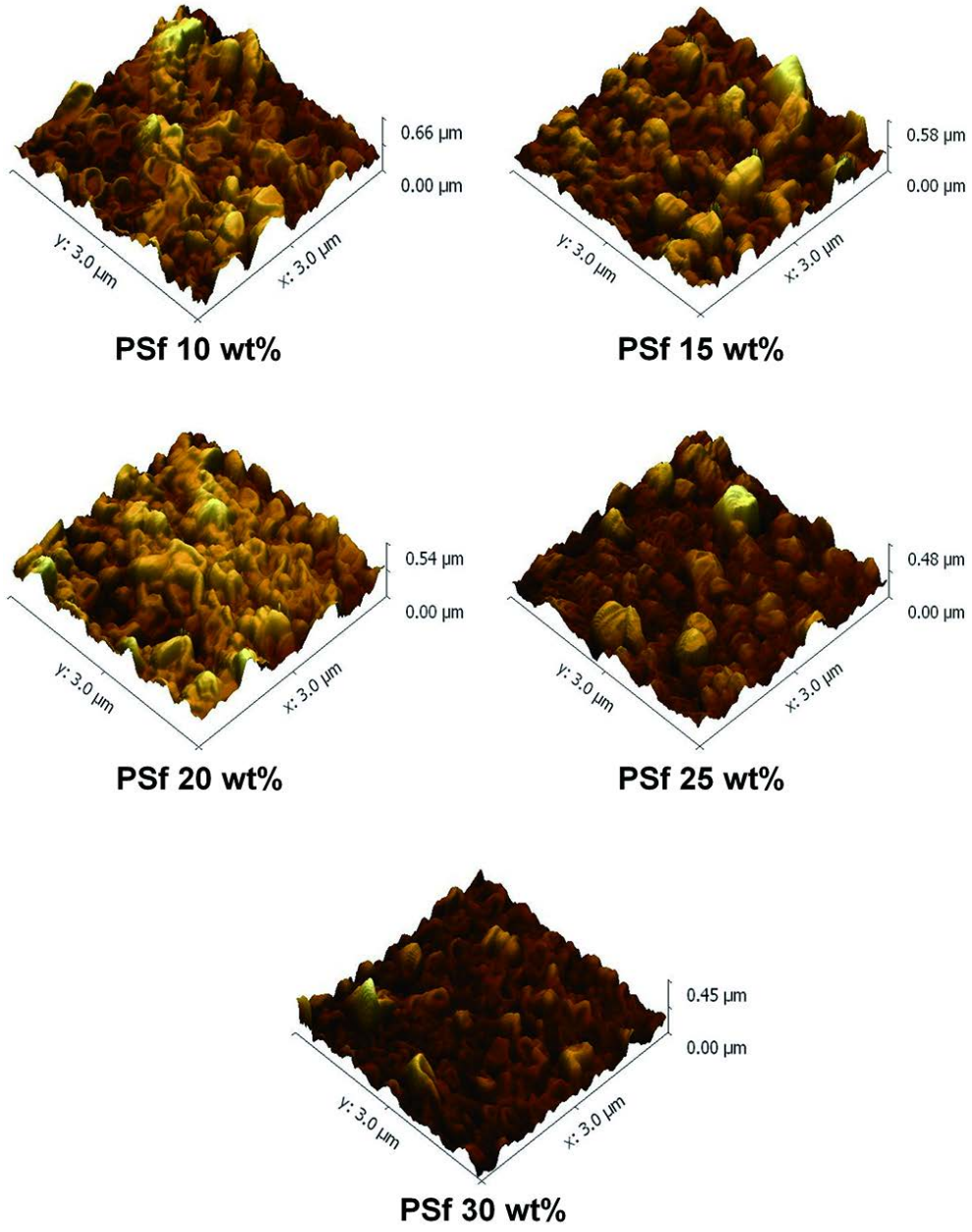

Figure Ⅳ-14. SPM surface images of active layers formed on support layers.

drag on water (Childress and Elimelech 2000). It is known that the water flux decreases with increasing value of absolute zeta potential (Childress and Elimelech 2000). It was believed that membrane surface charge also did not have an influence on the water flux of RO membrane, because the result in **Figure IV-13 (c)** shows exactly the opposite trend, i.e., increasing water flux with increasing absolute zeta value.

Lastly, we investigated porosities of support layers to verify other influenceable factors of support layer for the water permeability of RO membrane. There was also little correlation between the porosities of support layers and the water flux (**Figure IV-13 (d)**).

IV.4. Conclusions

In summary, we have found that it is not the active layer thickness, at least when its thickness is larger than 200 nm, but it is the support layer that determines the water flux delivered by RO membrane. When the polymer concentration of the solution for preparing the support layer was varied from 10 wt% to 30 wt% in the fabrication of TFC RO membrane, almost a thirtyfold increase in the flux resulted. Little change was observed in the salt rejection efficiency due to the change. The change in the polymer concentration leads to a significant change in the porous structure of the prepared support layer, which is mainly responsible for the difference in the water flux. It is noted that the structural character of support layer has a greater effect on water flux than that of active layer thickness. We have uncovered and developed a non-intrusive experimental method that can be used to represent the characteristics of the support layer, and these experimental values were used to relate the quantity to the water flux with success.

The findings here suggest that the porosity of support layer be maximized to the extent it does not compromise the mechanical strength of support layer for best performance of RO membrane. We expect that the versatility of these findings potentially provides useful insight into the direction to take for improving performance on a wide range of thin-film composite membrane applications, including brackish water and seawater desalination, water treatment and reuse, gas separation, and pressure retarded osmosis for energy generation.

Chapter V

V. Size-Controlled Graphene Oxide Enabling Thin-Film Composite Reverse Osmosis Membrane to Have Highly Porous Support Layer for High Performance

V.1. Introduction

Today a third of the global population lives in water shortage country (SERVICE 2006), one of the pressing needs of people throughout the world is adequate supply of drinking water. To satisfy the demand for an enormous amount of water required by the expanding global population, sea water desalination can be the suitable alternative to solve water scarcity problem. Among several approaches for desalination, reverse osmosis (RO) process has been widely used due to various strengths such as relatively low energy consumption, high quality of treated water and a small footprint (Elimelech and Phillip 2011). However, low energy efficiency still remains unanswered as a serious challenge in RO process over the past few decades. For this reason, exploring a critical attribute to improve the performance of membranes for desalination is one of the most important issues.

Recently, the studies addressing the influence of support layer on RO membrane performance have gradually increased to develop the enhancing strategy of the membrane performance as part of an effort to avoid inundating patents regarding active layer (Kim and Kim 2006, Singh, Joshi et al. 2006, Ghosh and Hoek 2009, Ramon, Wong et al. 2012, Misdan, Lau et al. 2013). We also examined the effect of support layer on the RO membrane performance in the previous study, and reached the conclusion that maximizing the porosity of support layer would be desirable to draw best performance of RO membrane. It is distinctly facile approach to enhance performance of RO membrane through the only increasing porosity of support layer. However, the mechanical strength of support layer cannot help weakening inevitably if the support layer becomes more porous to induce the increase in water flux of RO membrane. It must cause merely nominal water

production because RO membrane consisting of highly porous support layer should only be operated under much lower condition than normal pressure due to its low mechanical properties. Therefore, it is necessary for highly porous support layer to be operationally feasible by ensuring its mechanical strength for its application to the fabrication of RO membrane with improved performance.

In terms of reinforcing the mechanical strength of highly porous support layer, graphene oxide (GO) can provide an excellent option because GO has not only a superior intrinsic strength due to sp^2 carbon bonding network but can also effectually transfer their outstanding mechanical property to the polymer matrix in nanocomposites due to their high specific surface area, interlocking ability stemming from their wrinkled surface, and their two-dimensional geometry (Lee, Wei et al. 2008, Rafiee, Rafiee et al. 2009). Actually, GO has been proved effective in enhancing mechanical property of GO/polymer nanocomposites at low GO content in several studies (Stankovich, Dikin et al. 2006, Xu, Hong et al. 2009, Satti, Larpent et al. 2010, Han, Yan et al. 2011, Potts, Dreyer et al. 2011) and has also shown to be efficient for its purpose in membrane fabrication (Wang, Yu et al. 2012, Lee, Chae et al. 2013, Zhang, Xu et al. 2013). In particular, when the lateral dimensions of GO platelets are larger, this exceptional mechanical property of GO becomes better due to relatively fewer defects on the larger GO platelets (Lin, Shen et al. 2012). For this reason, the size control of GO platelets has been regarded as an important issue and attempted through several approaches such as adjusting oxidation path and mechanical energy input including shaking and sonication (Pan and Aksay 2011), chemical exfoliation by controlling oxidation time, temperature and the amount of oxidants (Zhang, Liang et al. 2009, Kang and Shin 2012), selective precipitation of GO sheets by pH control (Wang, Bai et al. 2011), and

electrochemical control over reaction parameters such as the applied voltage, electrical current and reduction time (Peng, Liu et al. 2011). Aside from this issue with the size effect of GO platelets, their reinforcing effect correlates with dispersibility, aspect ratio, and interfacial interaction between GO platelets and polymer matrix when the GO platelets are added to polymer composite as fillers (Alexandre and Dubois 2000, Fornes and Paul 2003, Lv, Xue et al. 2010, Potts, Dreyer et al. 2011). Therefore, the size effect of GO platelets should be considered along with the above-mentioned parameters when GO platelets are used to improve mechanical properties of polymer composite.

In this report, we demonstrate that a facile method to prepare high performance RO membrane consisting of support layer with maximized porosity and mechanical strength by incorporating GO platelets. For the purpose of the preparation of GO platelets with more suitable characteristics to ameliorate porous polymer nanocomposites' strength, we fabricated different size of GO platelets by simply adjusting mechanical energy input per volume of graphite oxide (GtO) solution without additional oxidants, oxidation time, and mechanical energy input. We verified diverse significant characteristics of GO platelets in relation to mechanical properties of nanocomposite membranes by evaluating Raman D/G-band peak intensity ratio, zeta potential, thickness, and aspect ratio of GO platelets according to their sizes. GO platelets with the most desirable characteristics were used to fabricate PSf/GO nanocomposite support layer with both mechanical strength comparable to existing support layer and highly porous structure simultaneously. As-prepared PSf/GO nanocomposite support layer allowed thin-film composite (TFC) RO membrane to have higher water permeability with comparable salt rejection without side effects concomitant with the addition of GO

platelets, and the TFC RO membrane made of the PSf/GO nanocomposite support layer outperformed others including commercial membranes as well as the previously reported membranes in open literature.

V.2. Experimental section

V.2.1. Preparation of size-controlled graphene oxide platelets

The preparation procedures of precursor graphene oxide (GO) are similar to that described in our previous study (Lee, Chae et al. 2013). GO platelets were prepared from natural graphite powders (100 mesh, Alfar Aesar, USA) via modified Hummers method (Hummers Jr and Offeman 1958). Natural graphite powders, sulfuric acid (H_2SO_4, 95%, DAEJUNG, Korea), and nitric acid (HNO_3, 60%, DC chemical Co. Ltd., Korea) first were mixed and then potassium permanganate ($KMnO_4$, Sigma-Aldrich, USA) was gradually added into the mixture under stirring. After stirring at 35-40 °C for 2 h, de-ionized (DI) water was added slowly into the mixture. The mixture was continually stirred at 100 °C until the dark green color of the mixture turned into light brownish. After the mixture was transferred into an ice bath, and DI water and H_2O_2 (DUKSAN, Korea) were slowly added into the mixture with vigorous stirring to remove the excess permanganate (Zhao, Li et al. 2011). The resultant mixture was washed using 5% HCl aqueous solution to eliminate metal ions followed by DI water several times (Wang, Feng et al. 2011). The obtained graphite oxide (GtO) particles were added to N-methyl-2-pyrrolidone (NMP, Sigma-Aldrich, USA). To prepare different size of GO platelets, the as-prepared GtO solution was sonicated by simply adjusting mechanical energy input per volume of GtO solution (**Figure V-1**). In detail, 92 kJ was applied to 20, 80, and 240 mL of GtO solutions (4 $mg \cdot mL^{-1}$) using a tip sonicator (Sonic VCX-750, Sonics & Materials, Inc., USA) in ice water bath for 30 min. GO platelets exfoliated by applying 4.6, 1.2, and 0.4 $kJ \cdot mL^{-1}$ were marked as small (*s*-GO), medium (*m*-GO), and large GO (*l*-GO), respectively.

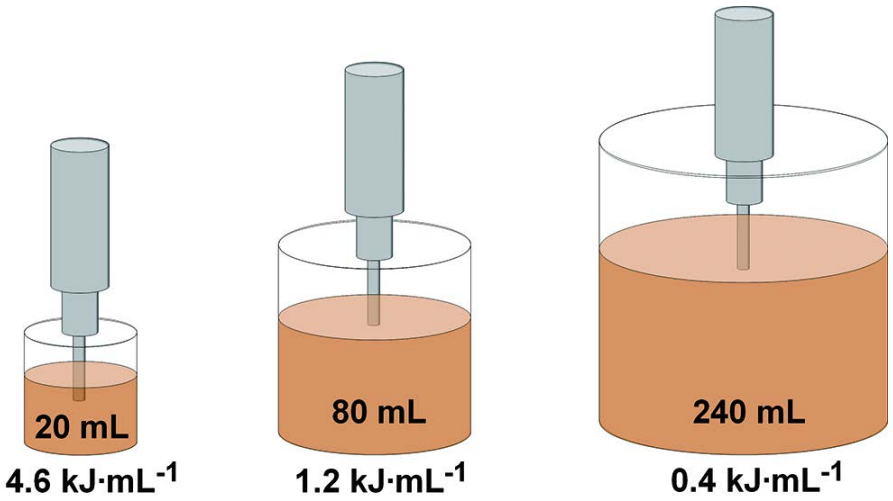

Figure V-1. Preparation of different size of GO platelets by varying mechanical energy input per volume of GtO solution.

V.2.2. Fabrication of size-controlled graphene oxide platelets composite reverse osmosis membrane

To utilize highly porous polysulfone (PSf, Solvay Korea, Korea) membrane as a support layer of thin-film composite (TFC) reverse osmosis (RO) membrane for the purpose of enhancing performance, the as-produced GO platelets were incorporated in the highly porous PSf membrane according to the following procedure regardless of their sizes. The polymer solution consisting of 10 wt% of PSf and 90 wt% of NMP including various concentrations of GO platelets (0.5, 1, 2 and 4 $mg \cdot mL^{-1}$) was casted to prepare the PSf/GO nanocomposite membranes with the following contents of GO platelets relative to PSf weight: 0.45, 0.89, 1.77, and 3.47 wt%. After optimum size and addition amount of GO platelets to enhance mechanical strength of highly porous support layers were determined by tensile tests, GO-reinforced support layers were produced via nonsolvent induced phase separation (NIPs) and used to fabricate TFC RO membranes. PSf membrane made from 15 wt% polymer solution also was prepared as a reference for a comparison purpose. TFC RO membrane with highly porous support layer were made via conventional interfacial polymerization (IP) of 2 wt% m-phenylenediamine (MPD, Woongjin Chemical, Korea) in DI water and 0.1 w/v% trimesoyl chloride (TMC, Aldrich, USA) in Hexane (DUKSAN, Korea). 2 wt% triethylamine (TEA, SAMCHUN, Korea), 4 wt% camphor sulfonic acid (CSA, Aldrich, USA), and 1.5 wt% dimethyl sulfoxide (DMSO, DAEJUNG, Korea) were added to the MPD aqueous solution to prepare TFC RO membrane with excellent baseline performance. After cured at 60 °C for 10 min, the as-prepared TFC membranes were washed thoroughly with DI water and stored in DI water for 30 min at room temperature prior to RO operation.

V.2.3. Characterization

To evaluate quantitatively the influence of structural characteristics of support layers on RO membrane performance, non-destructive inspections were conducted using an X-ray microfocus computed tomography (CT) system (phoenix v|tome|x m, GE, USA), and the tomograms obtained from the non-destructive inspections were processed employing the software Image J to analyze the ratio of the finger-like region cross-sectional area to the total membrane cross-sectional area from the top view. Field Emission Scanning Electron Microscope (FESEM) (AURIGA, Carl Zeiss, Germany) was used to acquire cross-sectional images of active and support layers. All the samples were flash-freezed in liquid nitrogen and then fractured to prevent them from being damaged. The fractured samples were sputter-coated with platinum for 100 seconds by a sputter coater to prevent charging (SCD 005, BAL-TEC, Germany). The particle size distributions of GO platelets corresponding to *s*-GO, *m*-GO, and *l*-GO were obtained by a particle size analyzer (S 3500, Microtrac, USA). Capillary flow porometer (CFP-1500AEL, PMI, USA) was used to measure the pore size distribution of the as-prepared membranes based on gas flow/liquid displacement method. A micro-Raman spectrometer (LabRam 300, JY-Horiba, USA) combined a 100X objective lens was utilized to analyze the carbon structure of GO platelets according to different sizes using a 532 nm laser source. The thicknesses of GO platelets were examined by a Scanning Probe Microscope (SPM) (INNV-BASE, VEECO, USA). Zeta potential measurements of the GO dispersions were carried out using electrophoretic light scattering spectrometer (ELS-Z2, Ostuka Electronic, Tokyo, Japan) at room temperature. The tensile properties of PSf/GO composite membranes were measured by Universal testing machine (Instron, USA). All the specimens were

measured at a rate of 1 mm/min using 50 N load cells. Advanced Rheometric Expansion System (ARES) (Rheometric Scientific ARES, Rheometric Scientific, USA) was used to measure the viscosities of the polymer solutions including different contents of GO platelets.

V.2.4. Reverse osmosis test

Reverse osmosis (RO) membrane performance was assessed using a cross-flow system with a 2000 ppm NaCl at a constant temperature (25 ± 0.5 °C). After stabilized with feed solution for 1 h at an operating pressure of 2410 kPa (24.1 bar), the RO apparatus was operated for 1 h at a constant pressure of 1550 kPa (15.5 bar) to measure water flux and salt rejection. The collected permeate volume for 1h was used to determine the water flux in terms of liters per square meter per hour ($L \cdot m^{-2} \cdot h^{-1}$). Salt rejections were calculated by measuring the salt concentrations of the feed and permeate solution with a conductance meter as given below in equation (1):

$$\text{Salt rejection (\%)} = 100 \times \left(1 - \frac{C_p}{C_f}\right) \quad (1)$$

where C_f and C_p are the salt concentrations of feed and permeate solution, respectively.

V.3. Results and discussion

V.3.1. Size control of graphene oxide platelets by applying different mechanical energy input per volume

Different mechanical energy input per volume of GtO solution can lead to difference in structural characteristics such as size, degree of damage or the number of layers of GO platelets although the same precursor GtO was used to prepare each GO platelet. **Figure V-2** presents the particle size distributions of GO platelets with three different sizes, namely small GO (*s*-GO), medium GO (*m*-GO), and large GO (*l*-GO) and scanning electron microscope (SEM) images corresponding to each size of GO platelets. The *s*- GO, *m*-GO, and *l*-GO had statistical mean size of 3.8, 7.8, and 18.6 μm, respectively, which demonstrates that change of mechanical energy input per volume of GtO solution is an effective way to control the size of final GO products.

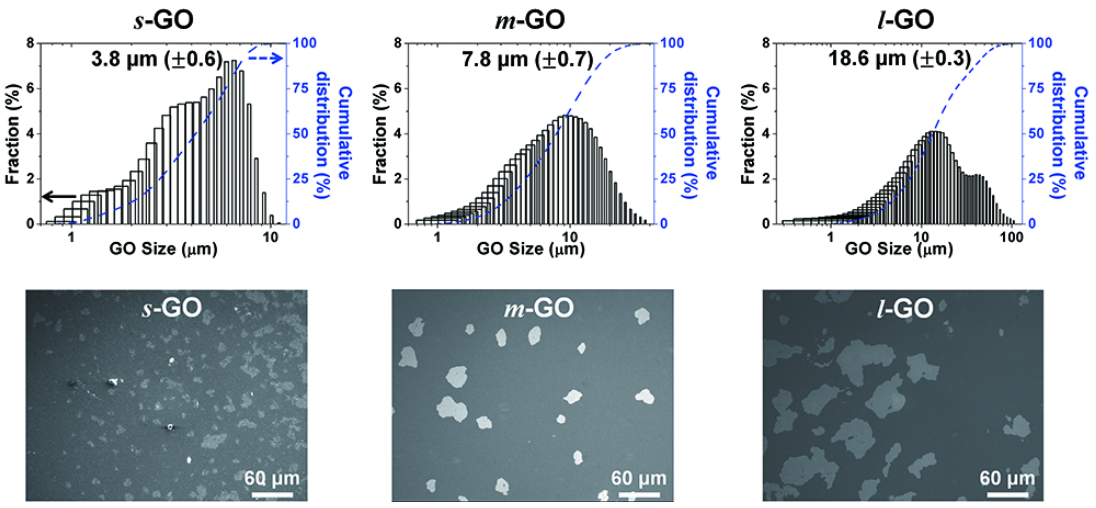

Figure V-2. Particle size distributions of three different groups of GO platelets (the top line) and the corresponding SEM images (the bottom line). (Number in parenthesis: standard deviation, n=15)

V.3.2. Structural integrities of graphene oxide platelets according to different sizes

Besides size of GO platelets, structural integrity of as-prepared GO platelets can also vary significantly depending on mechanical energy input per volume of the solution because sonication in aqueous solution or polar organic media causes considerable damage to the GO platelets (Dreyer, Park et al. 2009, Pan and Aksay 2011). It is effective to identify Raman D/G-band peak intensity ratios in order to estimate the structural integrity of GO platelets, since the D-band in Raman spectroscopy stems from the structural imperfections generated by epoxide and hydroxyl groups on the carbon basal plane while the G-band is caused by in-plane bond stretching of pairs of sp^2 C atoms (Pimenta, Dresselhaus et al. 2007, Su, Xu et al. 2009, Yang, Velamakanni et al. 2009). As shown in **Figure V-3**, the intensity ratios of the two bands decreased with increasing the size of GO platelets, which seems to be a concomitant result of fewer defects with increasing GO size as mentioned in the previous studies (Su, Xu et al. 2009, Lin, Shen et al. 2012).

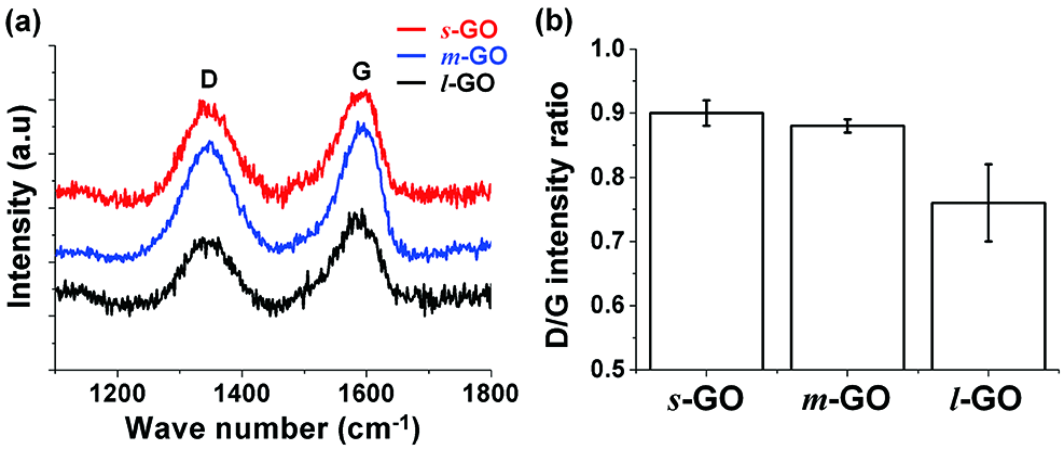

Figure V-3. Identification of Raman D/G-band peak intensity ratios. (a) Raman spectra of D and G band, and (b) the corresponding Raman D/G-band peak intensity ratios for GO platelets of three different size groups. (error bars: standard deviation, n=3)

V.3.3. Mechanical properties of polysulfone/graphene oxide nanocomposite membranes

Although larger graphene derivatives could have higher intrinsic stiffness due to fewer defects (Lin, Shen et al. 2012), *s*-GO was more effectual than *l*-GO in increasing mechanical properties of PSf/GO nanocomposite membrane. **Figure V-4 (a)** shows the ultimate tensile strengths for PSf/GO nanocomposite support layers prepared with 10 wt% of PSf and different amount of *l*-GO and *s*-GO. The tensile strength (~1.42 MPa) of support layer with 0.9 wt% *s*-GO was larger by about 78% than that (~0.80 MPa) without GO. On the contrary, the tensile strength (~1.07 MPa) of support layer with 0.9 wt% *l*-GO was larger by about 34% than that without GO, indicating *s*-GO is more efficient than *l*-GO in improving the tensile strength. The content of PSf used for the support layer of conventional RO membrane ranges between 15 wt% and 25 wt% (Yip, Tiraferri et al. 2010). Taking into account the tensile strength of 1.62 MPa for the support layer prepared with 15 wt% of PSf, with the addition of 0.9 wt % of *s*-GO, the tensile strength of support layer prepared with only 10 wt% of PSf could reach about 88% of that with 15 wt% of PSf.

A similar trend to tensile strength is observable in Young's modulus as well (**Figure V-4 (b)).** Whereas the Young's modulus (~94 MPa) of support layer with 0.9 wt% *l*-GO was larger only 21% than that (~77 MPa) without GO, the modulus (~112 MPa) of support layer with *s*-GO was increased by 45% at the same weight fraction. The moduluses of support layer w/ and w/o *s*-GO corresponded to about 82% and 60% of that prepared with 15 wt% of PSf (~130 MPa), respectively.

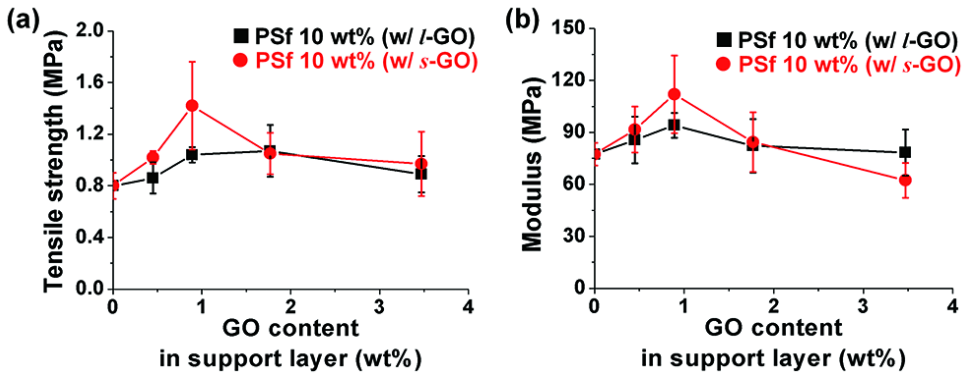

Figure V-4. Mechanical properties of PSf/GO nanocomposite support layers prepared with 10 wt% of PSf and different amount of *l*-GO and *s*-GO: (a) tensile strength and (b) Young's modulus (error bars: standard deviation, n=5).

V.3.4. Effective characteristics of graphene oxide platelets to improve mechanical properties of polymer nanocomposites

It is noteworthy that *s*-GO augmented mechanical properties of PSf nanocomposite membrane at a level comparable to those of support layers for conventional RO membranes. Several researches have ascribed this phenomenon to the fact that load-bearing capability of nanofillers depends on the dispersion and interfacial interaction between the nanofillers and polymer matrix as well as their inherent modulus (Yu, Ramesh et al. 2007, Ramanathan, Abdala et al. 2008, Cai and Song 2009, Das, Prasad et al. 2009, Fang, Wang et al. 2009, Lv, Xue et al. 2010).

We evaluated indirectly the aspect ratio and specific surface area of GO platelets by measuring their thicknesses according to the size. The aspect ratio of nanofillers is the key attribute in relation to the increasing load transfer of the nanofillers according to several micromechanical model such as Halpin-Tsai, Mori-Tanaka, and Shear Lag models (Cox 1952, Halpin 1969, Mori and Tanaka 1973, Halpin 1992, Chatterjee, Nafezarefi et al. 2012). The large specific surface area of nanofillers is also significant factor dominating the reinforcing capabilities of the polymer nanocomposites, because it also facilitates the stress transfer from polymer matrix to the nanofillers by increasing contact area with the polymer matrix (Chatterjee, Nafezarefi et al. 2012). These properties depend on the exfoliation degree of GO platelets. This signifies that large-size GO platelets can have smaller aspect ratio or specific surface area rather than small-size GO platelets if they have relatively large platelet thicknesses due to insufficient exfoliation. **Figure V-5** presents top-view and cross-sectional atomic force microscope (AFM) images of three different sizes of GO platelets. The well

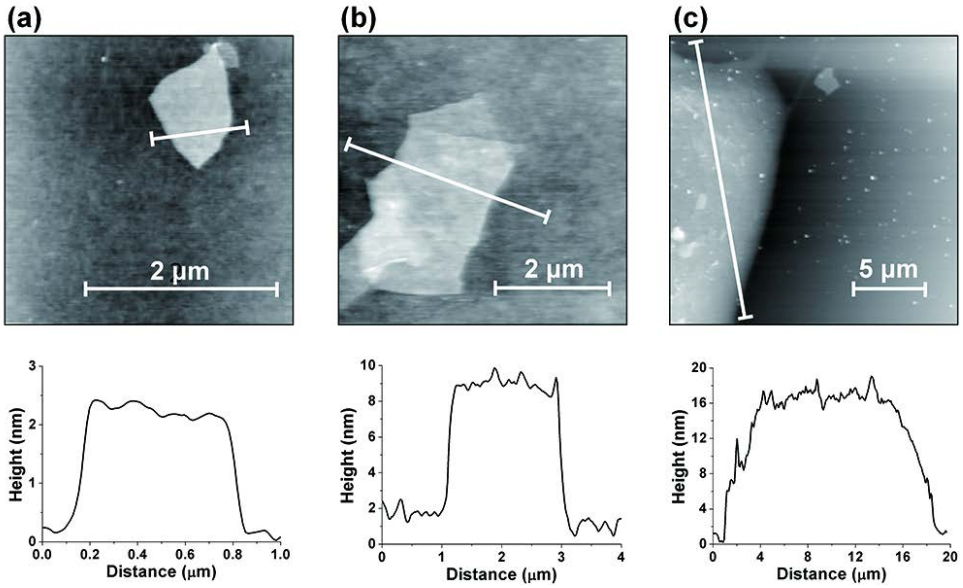

Figure V-5. AFM images of (a) *s*-GO, (b) *m*-GO, and (c) *l*-GO deposited onto a silicon wafer from an organic solvent (the top line) and the corresponding cross-sectional images taken along the white line indicating each platelet thickness (the bottom line).

exfoliated *s*-GO platelets closely approximated to monolayer whereas *m*-GO platelets had a few nanometer-thick layers (**Figure V-5**). Even *l*-GO platelets had the thickness more than 10 layers (**Figure V-5**). As a result, *s*-GO had the largest aspect ratio among as-prepared GO platelets although its size corresponded to nearly a quarter of the lateral platelet dimension of *l*-GO (**Figure V-6**). In addition, it is assumed that *s*-GO has much larger specific surface area than other GO platelets at equivalent loadings due to their relatively complete exfoliation.

Dispersibility of nanofillers in polymer solution is also one of the vital factors in enhancing mechanical properties of polymer nanocomposites, because the nanofillers with poor dispersibility can be agglomerated in the colloidal dispersion followed by the attenuation of their reinforcing effects due to the decrease in their aspect ratio or formation of stress convergence points (or defects) within polymer matrix (Potts, Dreyer et al. 2011, Lee, Chae et al. 2013). Especially, nanofillers such as GO platelets are susceptible to the agglomeration due to their unusually large surface area and additional π-π bonding (Gojny, Wichmann et al. 2004, Chatterjee, Nafezarefi et al. 2012). Moreover, such characteristics might be facilitated in the system accompanying solidification by desolvation of solvent such as phase separation, since the nanofillers could undergo a sharp increase of their concentration in polymer solution as phase separation processes. Accordingly, it has to be confirmed whether GO platelets to be used to enhance mechanical performance of polymer nanocomposites have excellent dispersibility prior to their applications. We measured the zeta potential of GO platelets to estimate the stabilities of GO dispersion according to the size, and the values are revealed in **Figure V-7**. It is advantageous to incorporate well exfoliated *s*-GO into highly porous PSf membrane in the view of dispersibility of GO platelets as well, because

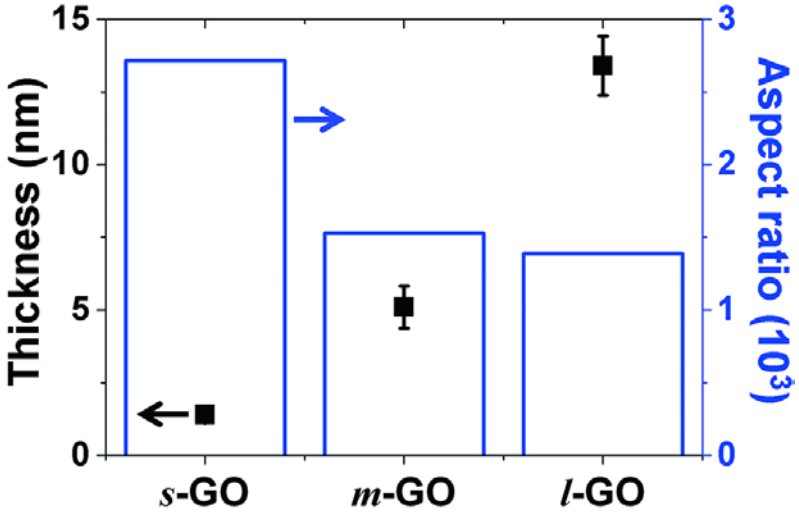

Figure V-6. Thicknesses and aspect ratios of GO platelets according to different size.

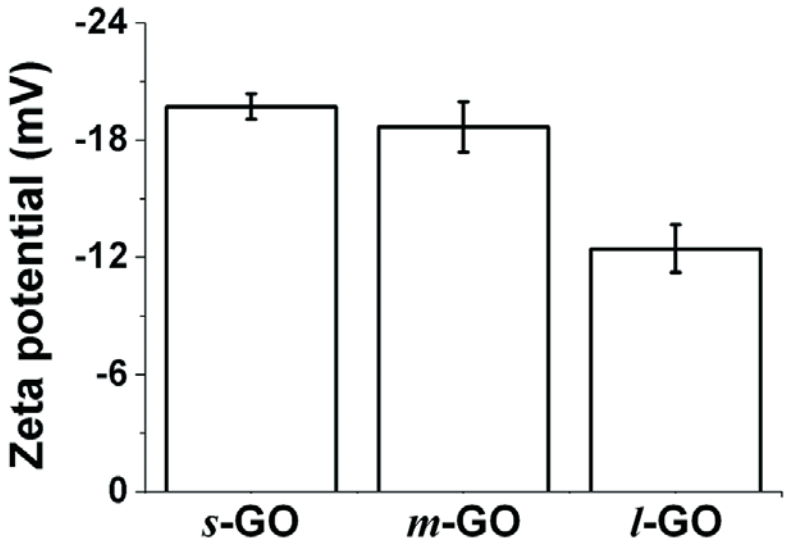

Figure V-7. Zeta potentials of three different groups of GO platelets in organic solvent.

a large number of exposed oxygenated functional groups in *s*-GO can contribute to more stable dispersion of GO platelets by inducing strong electrostatic repulsion among them unlike insufficiently exfoliated *l*-GO (Lin, Shen et al. 2012). From the above-mentioned results, it is inferred that *s*-GO could provide better load-bearing capability than *l*-GO at equivalent loading due to the characteristics of *s*-GO such as relatively higher dispersibility, aspect ratio, and specific surface area.

V.3.5. Influence of graphene oxide addition on structural characteristics of active and support layers

According to our previous study, TFC RO membranes comprised of active layer with comparable cross-linking degree and highly porous support layer are favorable for higher water permeability, because regions with lower resistance such as finger-like region could be exclusively used for water permeation during RO operation as shown in **Figure V-8**. Based on the above study, there is the potential for *s*-GO to contribute to materialization of high performance RO membrane by enhancing mechanical properties of highly porous support layer. Although *s*-GO endows highly porous support layer with excellent mechanical properties, however, it cannot be desirable alternative to enhance RO membrane performance if it adversely affects the formation of active or support layer with favorable structure for water permeation. Thus, it is required to confirm how *s*-GO influences the formation of active or support layer prior to testing RO membrane performance. We compared structural characteristics of RO membranes made with PSf 15 wt% membrane, PSf 10 wt% membrane, and PSf 10 wt% membrane w/ s-GO.

We confirmed support layer with larger mean pore size leads to the formation of thicker active layer based on 'volcano-like reaction' in our previous study. This means that the change in surface pore size of support layer concomitant with the addition of *s*-GO can induce variation in active layer thickness. **Figure V-9 (a)** and **(b)** show pore size distribution and mean pore size of each support layer. Mean pore size of PSf 10 wt% membrane was almost two times larger than that of PSf 15 wt% membrane. Moreover, the addition of *s*-GO into PSf 10 wt% membrane led to about 13% increase in mean pore size, which implies that much

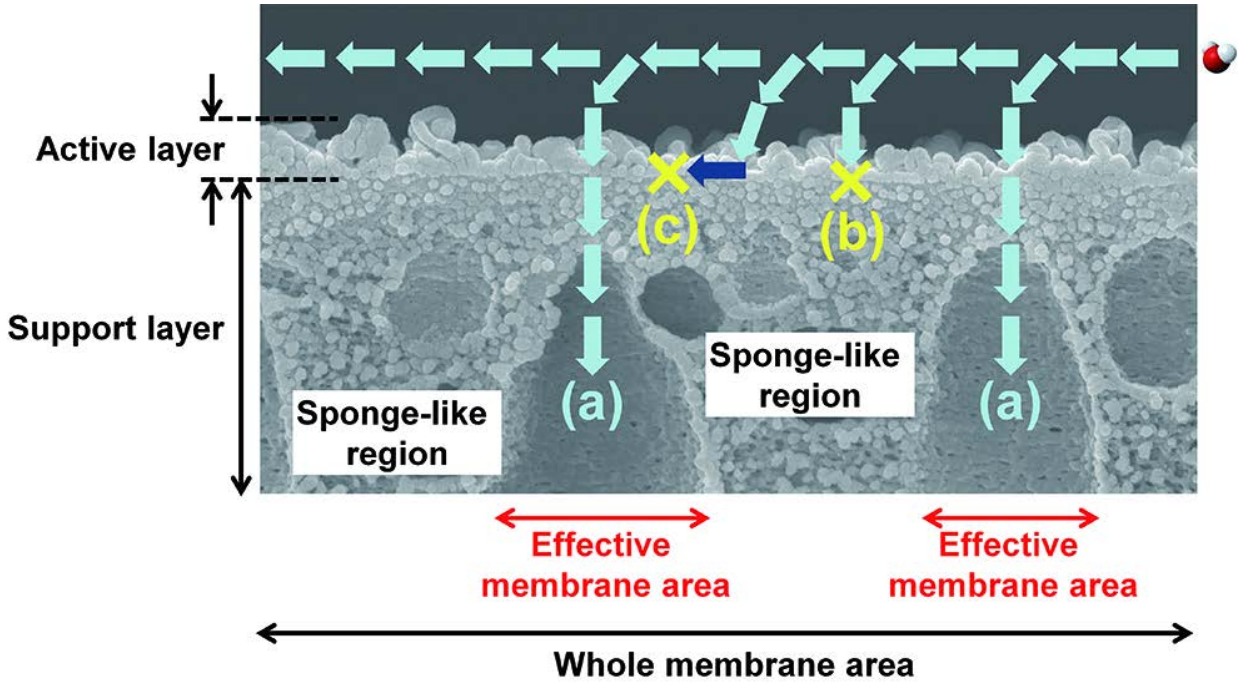

Figure V-8. Schematic of water transport through RO membrane. (a) Water molecules permeating active layer right above finger-like region in support layer, (b) water molecules unable to diffuse into active layer right above sponge-like region in support layer. Water molecules would pass by active layer right above sponge-like region in support layer due to relatively larger resistance than finger-like region, and (c) impossible lateral diffusion of water molecules in active layer by its huge hydraulic resistance.

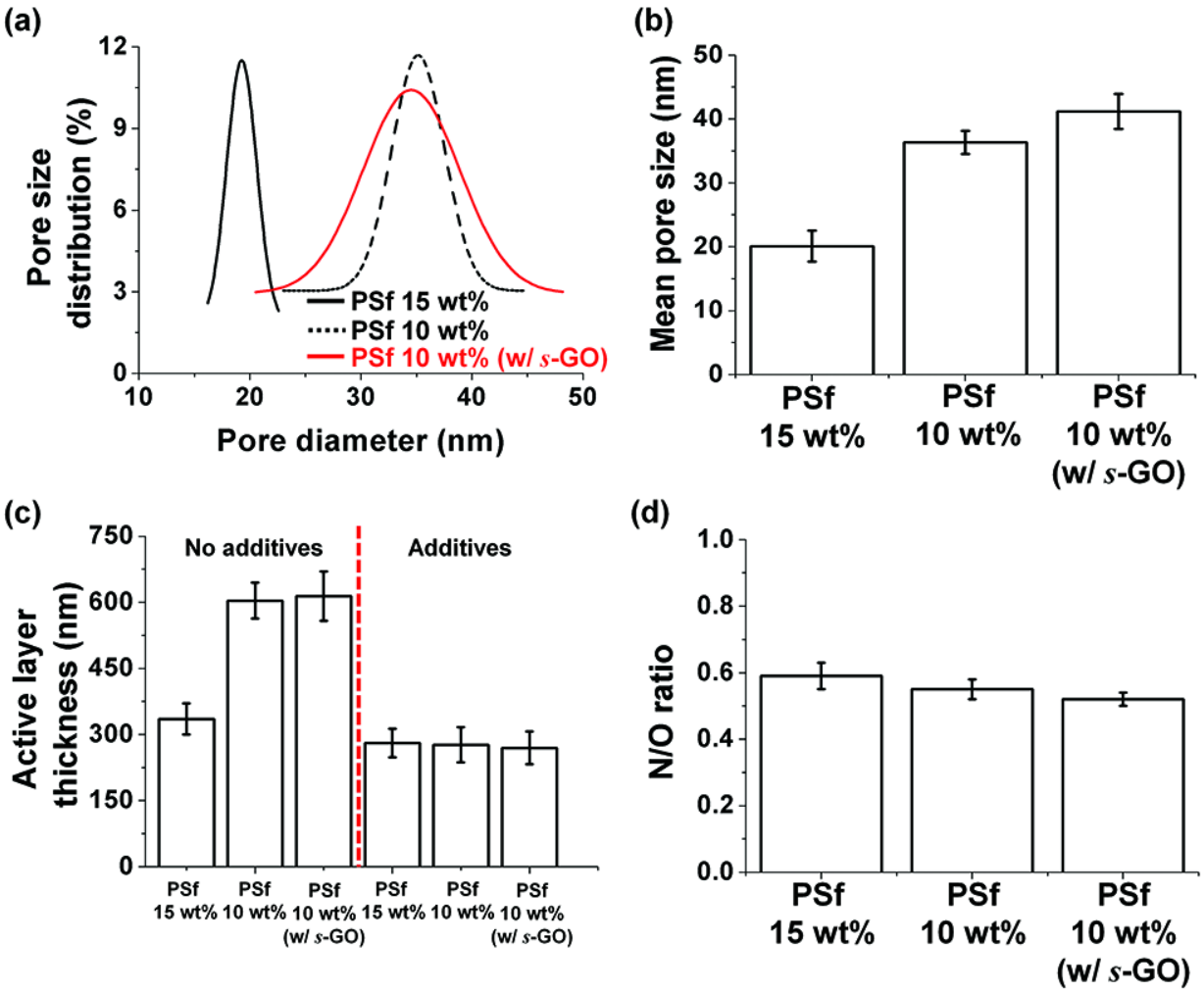

Figure V-9. Influence of mean pore size of support layer on the formation of active layer. (a) Pore size distribution of each support membrane, (b) mean pore size of each support membrane, (c) active layer thickness of each RO membrane according to use of additives in the aqueous-MPD solution, and (d) composition ratios of each active layer.

thicker active layer can be formed by PSf 10 wt% membrane w/ s-GO during IP compared to PSf 15 wt% membrane. This prediction was accordance with the trend in thickness of the active layer formed from TMC solution with MPD solution without additives (**Figure V-9 (c) and Figure V-10**). However, all the RO membranes had a similar level of active layer thickness when they were prepared from MPD solution containing additives (**Figure V-9 (c) and Figure V-10**). This is ascribed to the fact that enhanced MPD diffusivity by the addition of DMSO leads to the formation of a thinner active layer during IP (Kwak, Jung et al. 2001, Kim, Kwak et al. 2005, Ghosh, Jeong et al. 2008). This tendency also appeared in the cross-linking degree of active layer. According to the previous study (Kim, Kwak et al. 2005), the cross-linking degree of polyamide (PA) active layer can be estimated by the atomic concentration ratio of N and O based on the fact that the partially cross-linked PA consists of the linear part ($C_{15}H_{10}N_2O_4$) with free pendant carboxylic acid and the cross-linked part ($C_{18}H_{12}N_3O_3$) with amide linkage as shown in **Figure V-11**, and the increase in N/O ratio means the increasing cross-linking degree of active layer. In shown in **Figure V-9 (d)**, N/O ratios (or cross-linking degrees) of each active layer are almost identical, which also results from DMSO used in IP since DMSO allows cross-linking degree to increase by changing the distribution of reaction sites (Kim, Kwak et al. 2005). From the above results, it is confirmed that additives determine nature of active layer and *s*-GO incorporated in support layer does not affect the formation or characteristics of active layer.

Next, we examined the possibility that *s*-GO has a negative effect on the formation of support layer with desired structure in water permeation. We verified

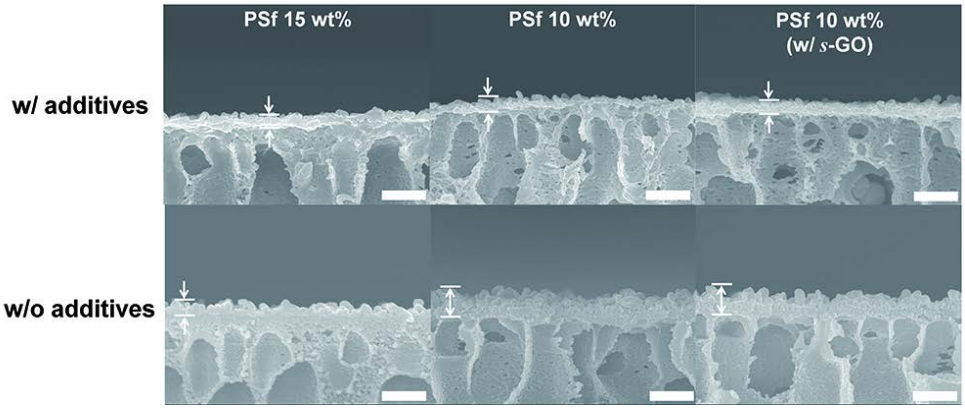

Figure V-10. Cross-sectional SEM images including the active and support layers of RO membranes according to use of additives in the aqueous-MPD solution (scale bar: 1 μm).

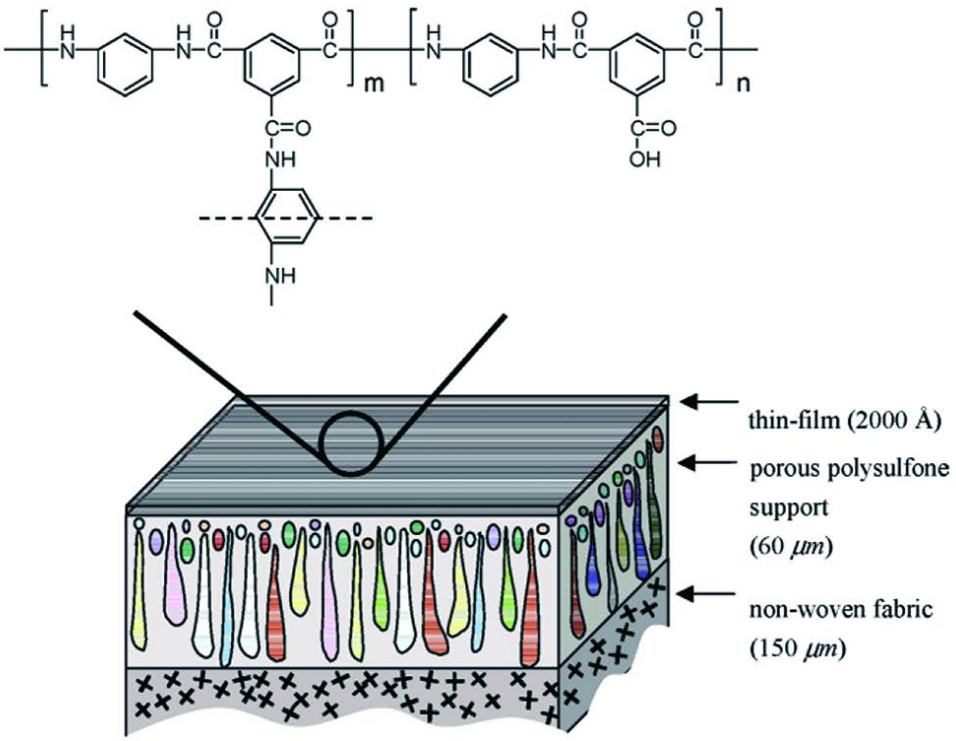

Figure V-11. Schematic of TFC RO membrane and the chemical structure of polyamide active layer (Kim, Kwak et al. 2005).

highly porous support layer can lead to the improving water permeability of RO membrane regardless of nature of active layer in our previous study. In other words, permeability of RO membrane can deteriorate due to *s*-GO if the *s*-GO results in the support layer with a more or less dense structure in sub-surface layer, although it makes no difference in the properties of active layer. We performed non-destructive inspection using X-ray microfocus CT system to compare quantitatively the proportions of finger-like region in each support layer as well as observation of cross-sectional structures by SEM. **Figure V-12** shows the micrographs of three kinds of support layers obtained from various points of view. It is evident from the cross-sectional SEM images that pore structure of support layer is dictated by polymer concentration in polymer solution irrespective of the addition of *s*-GO. The quantitative comparison of the proportion of finger-like region also reveals that a distinct difference in structural characteristics of support layer results from only polymer concentration, namely rheological characteristics of polymer solution used in the fabrication of support membranes (**Figure V-13**). **T**aking into account the viscosity of 0.48 Pa.s for the polymer solution prepared with 15 wt% of PSf, the viscosity of polymer solution with 0.9 wt% *s*-GO are almost 5 times lower than that with 15 wt% of PSf. It is noted in this regard that *s*-GO does not cause rheological hindrance due to the increasing viscosity of polymer solution and the resultant delayed phase separation inducing the formation of dense structure at the contents level of *s*-GO used in this study as shown in **Figure V-13 (c).** These results imply that *s*-GO can improve mechanical properties of highly porous support layer without adverse effects on the formation of favorable structure for water permeation.

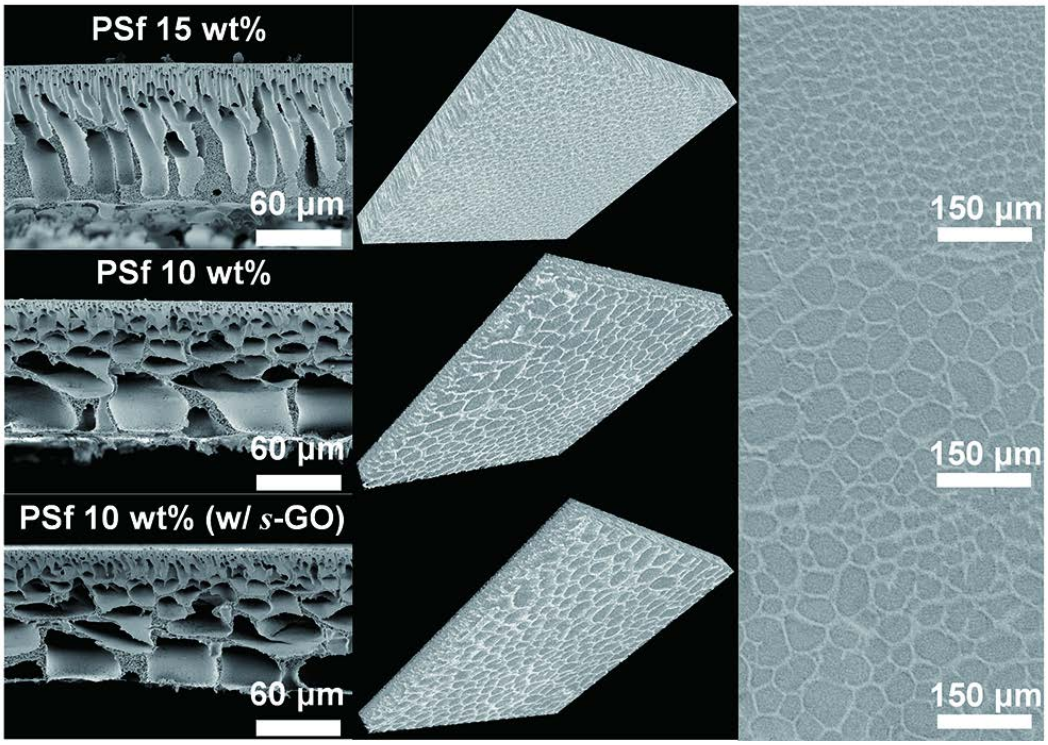

Figure V-12. The micrographs in the left column are cross-sectional SEM images of support membranes, and those in the central column and in the right column are 3D images and tomograms of support membranes acquired by non-intrusive inspections, respectively. In order from top to bottom, the polymer solutions used to fabricate support membranes are PSf 15 wt%, PSf 10 wt%, and PSf 10 wt% including about 0.1 wt% *s*-GO, respectively. The dark region in the 3D images and tomograms indicates finger-like region.

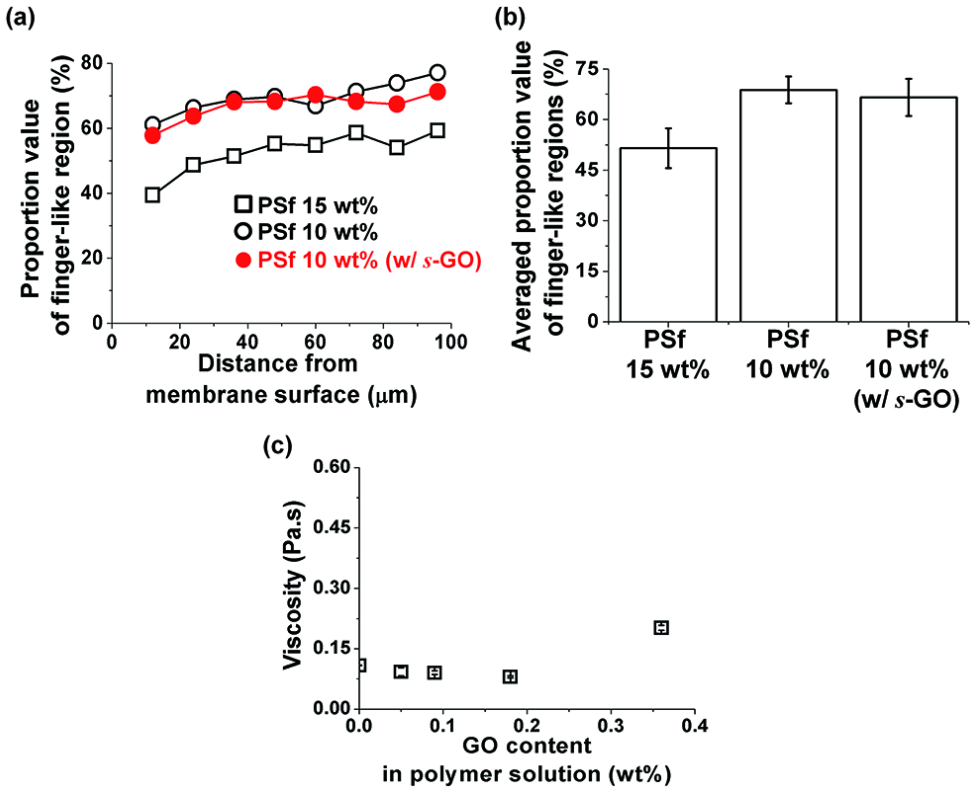

Figure V-13. Estimation of proportion of finger-like region in each support layer. (a) Proportion of finger-like region in support layers at different positions, (b) mean proportion of finger-like region in support layers (error bar: standard deviation, n=8), and (c) variation in viscosity of polymer solution according to the addition amount of *s*-GO. (error bar: standard deviation, n=3) Note that the GO content (wt%) here is based on the weight of polymer solution.

V.3.6. Performance of reverse membrane made of polysulfone/graphene oxide nanocomposites support layer

We measured water flux and salt rejection of RO membrane (PA-*s*-GO membrane) made of highly porous support layer (PSf 10 wt% membrane) reinforced with *s*-GO using cross-flow system and compared the values to those of RO membrane (PA membrane) prepared from PSf 15 wt%. We also compared PA-*s*-GO membrane to RO membranes consisting of active layer with improved permselectivity via CNT incorporation or molecular layer-by-layer (mLBL) to verify the validity of maximizing porosity of support layer as the enhancing strategy of RO membrane performance. Lastly, we evaluated the performance of several commercial RO membranes for comparison against PA-*s*-GO membrane for the purpose of examining its potential for industrial application. **Figure V-14** reveals that PA-*s*-GO membrane had almost 50 % increased water flux compared to PA membrane, and the flux of PA-*s*-GO went as far as to surpass reported literature values for CNT composite RO membranes or mLbL RO membrane. In addition, PA-*s*-GO exhibited outstanding membrane performances rather than diverse commercial RO membranes with comparable salt rejection. These results suggest that GO-reinforced highly porous support layer alone enables hand-made RO membranes to have performance level high enough to outperform commercial membranes, and it can lead to further improvement by combining existing technologies to prepare preferable active layer for water permeation.

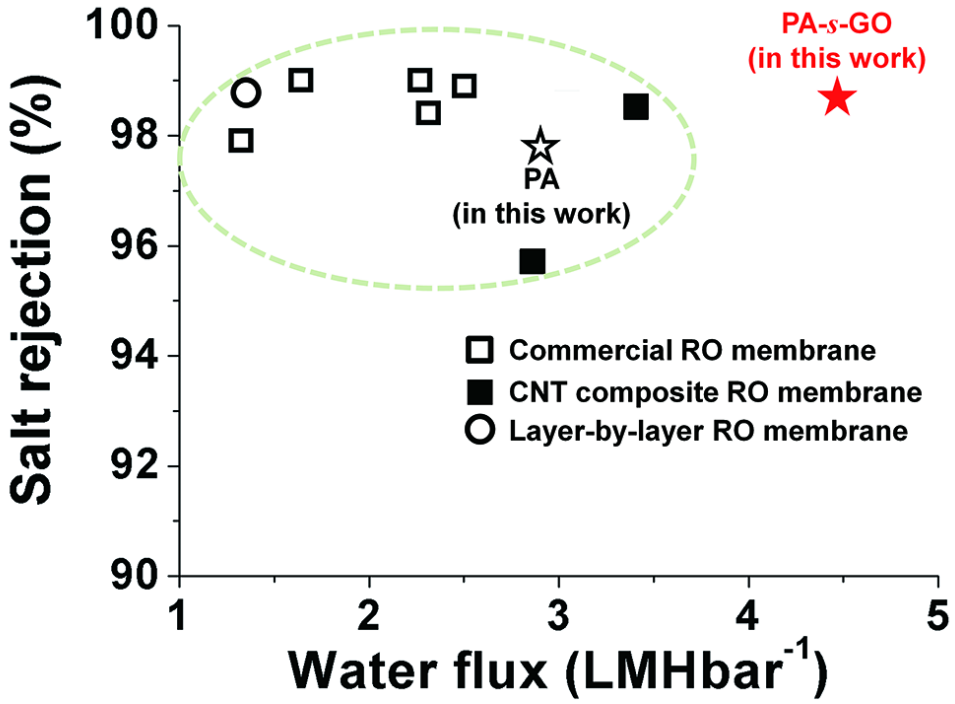

Figure V-14. Comparison of RO membranes developed in current work with CNT composite, mLbL, and commercial RO membranes. Detailed information is in Table V-1.

Table V-1. Comparison of performance of PA-*s*-GO membrane with others.

Membrane	Unit water flux [$L \cdot m^{-2} \cdot h^{-1} \cdot bar^{-1}$]	Rejection [%]	References
PA-*s*-GO	**4.48**	**98.7**	**This work**
PA	2.88	97.7	Tested in this work
mLbL	1.34	98.7	(Gu, Lee et al. 2013)
CNT composite 1	3.41	98.5	(Lee, Kim et al. 2014)
CNT composite 2	2.86	95.7	(Kim, Choi et al. 2014)
Dow-filmte SW30HR	1.65	99	Tested in this work
Hydranautics LFC-1	2.32	98.4	Tested in this work
Hydranautics SWC5	1.33	97.9	Tested in this work
Nano H2O SW400ES	2.27	99	Tested in this work
Woongjin FE	2.50	98.9	Tested in this work

V.4. Conclusions

We demonstrate a novel and facile strategy to enhance RO membrane performance through optimization of support layer, not through active layer. The critical attribute of this approach is based on the fact that the distribution of resistance in support layer affects the overall water flux in RO, in other words, highly porous support layer can lead to higher water flux of RO membrane without discernible difference in salt rejection. The mechanical reinforcement of highly porous support layer must take precedence in order for its application to RO process. We confirmed that small GO (*s*-GO) platelets with higher dispersibility, larger specific surface area, and aspect ratio are more desirable to improve mechanical properties of nanocomposite support layer irrespective of defects on them, when the polymer nanocomposites are prepared by phase inversion accompanying continuous desolvation by liquid-liquid demixing between solvent and nonsolvent. *s*-GO platelets were produced by a straightforward method based on adjusting mechanical energy input per volume of precursor solution. The mechanical properties of the support layer prepared with 10 wt% of PSf and 0.9 wt% s-GO were comparable to those of the support layer of conventional RO membrane. Also, as-prepared GO platelets did not hinder the formation of active or support layer with proper structure for water permeation. As a result, they could contribute to the preparation of highly porous support layer with mechanical strength comparable to typical support layer used for commercial RO membrane and the resultant fabrication of TFC RO membrane outperforming both the current upper bounds of RO membranes prepared by modification of active layer and commercial RO membranes. The versatility and availability of this approach provide a practical

and feasible way to accomplish bulk production of high performance TFC membrane applicable to sea water desalination via reverse or forward osmosis, pressure retarded osmosis for energy production, and gas separation.

Chapter VI

VI. Conclusions

VI. Conclusions

VI-1. Polysulfone (PSf) ultrafiltration (UF) membrane including graphene oxide (GO) nanoplatelets was prepared for MBRs for wastewater treatment, and the characteristics of the membrane were investigated. The following conclusion can be drawn:

(1) The GO nanoplatelets can change the pore size and pore structure of porous medium formed by phase inversion.

(2) The GO membrane has anti-biofouling capability due to its hydrophilicity and electrostatic repulsion characteristics.

(3) The GO membrane also has superior mechanical strength and water permeability.

(4) There is an optimum value of GO fraction which yields the highest water flux.

VI-2. Impact of support layer on water flux of thin-film composite (TFC) reverse osmosis (RO) membrane was investigated. The following conclusion can be drawn:

(1) The change in the polymer concentration of the solution for preparing the support layer leads to a significant change in the porous structure of the prepared support layer, which is mainly responsible for the difference in the water flux of TFC RO membrane.

(2) The structural character of support layer has a greater effect on water flux than that of active layer thickness, at least when its thickness is larger than 200 nm.

(3) A non-intrusive experimental method (X-ray microfocus computed tomography system) can be used to represent the characteristics of the

support layer, and these experimental values can be used to relate the quantity to the water flux with success.

VI-3. Highly porous GO nanoplatelets incorporated support layer was fabricated to prepare high performance TFC RO membrane consisting of the support layer with both mechanical strength comparable to the support layer of conventional RO membrane and highly porous structure simultaneously, and the characteristics of the membrane were investigated. The following conclusion can be drawn:

(1) Small GO (*s*-GO) platelets with higher dispersibility, larger specific surface area, and aspect ratio are more desirable to improve mechanical properties of highly porous support layer prepared with 10 wt% of PSf.

(2) *s*-GO platelets can be produced by a straightforward method based on adjusting mechanical energy input per volume of precursor solution.

(3) The mechanical properties of the support layer prepared with 10 wt% of PSf and 0.9 wt% *s*-GO are comparable to those of the support layer of conventional RO membrane.

(4) TFC RO membrane prepared with the *s*-GO nanocomposite support layer has water permeability outperforming both the current upper bounds of RO membranes prepared by modification of active layer and commercial RO membranes.

Nomenclature

A	intrinsic water permeability
AFM	atomic force microscope
ARES	advanced rheometric expansion system
ATR	attenuated total reflection
B	salt permeability
BSA	bovine serum albumin
C_f	salt concentration of the feed
C_p	salt concentration of the permeate
CA	cellulose acetate
CDC	cocurrent downflow contactor
CFP	capillary flow porometer
CFSTR	continuous flow stirred tank reactor
CLSM	confocal laser scanning microscopy
CNT	carbon nanotube
CSA	camphor sulfonic
CT	computed tomography
D	salt diffusion coefficient
D_p	average diameter of particles
DMA	dimethylacetamide
DMF	dimethylformamide
DMSO	dimethyl sulfoxide
EDS	energy dispersive X-ray spectrometer
EIPs	evaporation induced phase separation

f	friction coefficient
FESEM	field emission scanning electron microscopy
FO	forward osmosis
FTIR	Fourier transform infrared
GFP	green fluorescent protein
GNP	graphite nanoplatelets
GO	graphene oxide
GtO	graphite oxide
IP	interfacial polymerization
J_w^{FO}	measured volumetric water flux in FO test
J_w^{RO}	measured volumetric water flux in the RO test
L	length along the macroscopic pressure gradient in porous media
l-GO	large graphene oxide platelets
L-L	liquid-liquid
MBR	membrane bioreactor
MD	membrane distillation
MF	microfiltration
m-GO	medium graphene oxide platelets
mLbL	molecular layer-by-layer
MMM	mixed matrix membranes
MPD	m-phenylenediamine
NF	nanofiltration
NIPs	nonsolvent induced phase separation
NMP	N-methyl-2-pyrrolidone
OD	optical density

P	pressure
PA	polyamide
PAN	polyacrylonitrile
PAO1	Pseudomonas aeruginosa
PE	polyethylene
PEEK	polyetheretherketone
PEG	poly(ethylene glycol)
PEO	poly(ethylene oxide)
PES	polyethersulfone
PIP	piperazine
PP	polypropylene
PPESK	poly(phthazine ether sulfone ketone)
PSf	polysulfone
PTFE	poly(tetrafluorethylene)
PVA	polyvinyl alcohol
PVDF	polyvinylidene fluoride
PVP	polyvinyl pyrrolidone
PWF	pure water flux
R	salt rejection
rGO	reduced graphene oxide
s-GO	small graphene oxide platelets
SPM	scanning probe microscope
Re_p	Reynolds number
RO	reverse osmosis
S	structure parameter

S_v	specific surface area
t	membrane thickness
TEA	triethylamine
TFC	thin-film composite
TIPs	thermally induced phase separation
TMC	trimesoyl chloride
TMP	transmembrane pressure
TSB	tryptic soy broth
UF	ultrafiltration
v_s	superficial velocity
VIPs	vapor induced phase separation
XPS	X-ray photoelectron spectroscopy

Greek letters

ε	porosity of porous media
μ	dynamic viscosity of fluid
$\Delta\pi$	osmotic pressure difference across the RO membrane
$\pi_{D,b}$	bulk osmotic pressure of the draw solution
$\pi_{F,m}$	osmotic pressure at the membrane surface on the feed side
ρ	density of fluid
τ	tortuosity

References

(1975). Reverse osmosis membrane, US Patent 3,926,798.

Agre, P. (2004). "Aquaporin water channels (Nobel lecture)." Angewandte Chemie International Edition **43**(33): 4278-4290.

Agre, P. (2005). "Membrane water transport and aquaporins: looking back." Biology of the Cell **97**(6): 355-356.

Agre, P., S. Sasaki and M. Chrispeels (1993). "Aquaporins: a family of water channel proteins." American Journal of Physiology-Renal Physiology **265**(3): F461-F461.

Aizawa, T., R. Souda, S. Otani, Y. Ishizawa and C. Oshima (1990). "Anomalous bond of monolayer graphite on transition-metal carbide surfaces." Physical review letters **64**(7): 768.

Akcora, P., S. K. Kumar, J. Moll, S. Lewis, L. S. Schadler, Y. Li, B. C. Benicewicz, A. Sandy, S. Narayanan and J. Ilavsky (2009). ""Gel-like" mechanical reinforcement in polymer nanocomposite melts." Macromolecules **43**(2): 1003-1010.

Akcora, P., H. Liu, S. K. Kumar, J. Moll, Y. Li, B. C. Benicewicz, L. S. Schadler, D. Acehan, A. Z. Panagiotopoulos and V. Pryamitsyn (2009). "Anisotropic self-assembly of spherical polymer-grafted nanoparticles." Nature materials **8**(4): 354-359.

Alexandre, M. and P. Dubois (2000). "Polymer-layered silicate nanocomposites: preparation, properties and uses of a new class of materials." Materials Science and Engineering: R: Reports **28**(1): 1-63.

Amirilargani, M., E. Saljoughi, T. Mohammadi and M. Moghbeli (2010). "Effects

of coagulation bath temperature and polyvinylpyrrolidone content on flat sheet asymmetric polyethersulfone membranes." Polymer Engineering & Science **50**(5): 885-893.

Arthanareeswaran, G., P. Thanikaivelan, J. A. Raguime, M. Raajenthiren and D. Mohan (2007). "Metal ion separation and protein removal from aqueous solutions using modified cellulose acetate membranes: Role of polymeric additives." Separation and purification technology **55**(1): 8-15.

Baker, R. W. (2000). Membrane technology, Wiley Online Library.

Bartels, C. R. (1989). "A surface science investigation of composite membranes." Journal of membrane science **45**(3): 225-245.

Becerril, H. A., J. Mao, Z. Liu, R. M. Stoltenberg, Z. Bao and Y. Chen (2008). "Evaluation of solution-processed reduced graphene oxide films as transparent conductors." ACS nano **2**(3): 463-470.

Berger, C., Z. Song, X. Li, X. Wu, N. Brown, C. Naud, D. Mayou, T. Li, J. Hass and A. N. Marchenkov (2006). "Electronic confinement and coherence in patterned epitaxial graphene." Science **312**(5777): 1191-1196.

Bird, R. B., W. E. Stewart and E. N. Lightfoot (1960). Transport phenomena, Wiley New York.

Bolotin, K. I., K. Sikes, Z. Jiang, M. Klima, G. Fudenberg, J. Hone, P. Kim and H. Stormer (2008). "Ultrahigh electron mobility in suspended graphene." Solid State Communications **146**(9): 351-355.

Buchsteiner, A., A. Lerf and J. Pieper (2006). "Water dynamics in graphite oxide investigated with neutron scattering." The Journal of Physical Chemistry B **110**(45): 22328-22338.

Cadotte, J., R. Petersen, R. Larson and E. Erickson (1980). "A new thin-film

composite seawater reverse osmosis membrane." Desalination **32**: 25-31.

Cadotte, J. E. (1977). Reverse osmosis membrane, Google Patents.

Cadotte, J. E. (1981). Interfacially synthesized reverse osmosis membrane, Google Patents.

Cai, D. and M. Song (2009). "A simple route to enhance the interface between graphite oxide nanoplatelets and a semi-crystalline polymer for stress transfer." Nanotechnology **20**(31): 315708.

Cath, T. Y., A. E. Childress and M. Elimelech (2006). "Forward osmosis: Principles, applications, and recent developments." Journal of membrane science **281**(1): 70-87.

Celik, E., H. Park, H. Choi and H. Choi (2011). "Carbon nanotube blended polyethersulfone membranes for fouling control in water treatment." Water research **45**(1): 274-282.

Chan, W.-F., H.-y. Chen, A. Surapathi, M. G. Taylor, X. Shao, E. Marand and J. K. Johnson (2013). "Zwitterion functionalized carbon nanotube/polyamide nanocomposite membranes for water desalination." ACS nano **7**(6): 5308-5319.

Chang, I. S., P. Le Clech, B. Jefferson and S. Judd (2002). "Membrane fouling in membrane bioreactors for wastewater treatment." Journal of environmental engineering **128**(11): 1018-1029.

Chatterjee, S., F. Nafezarefi, N. Tai, L. Schlagenhauf, F. Nüesch and B. Chu (2012). "Size and synergy effects of nanofiller hybrids including graphene nanoplatelets and carbon nanotubes in mechanical properties of epoxy composites." Carbon **50**(15): 5380-5386.

Cheryan, M. (1998). Ultrafiltration and microfiltration handbook, CRC press.

Childress, A. E. and M. Elimelech (2000). "Relating nanofiltration membrane

performance to membrane charge (electrokinetic) characteristics." Environmental science & technology **34**(17): 3710-3716.

Choi, J. H., J. Jegal and W. N. Kim (2006). "Fabrication and characterization of multi-walled carbon nanotubes/polymer blend membranes." Journal of Membrane Science **284**(1): 406-415.

Chuang, W.-Y., T.-H. Young, W.-Y. Chiu and C.-Y. Lin (2000). "The effect of polymeric additives on the structure and permeability of poly (vinyl alcohol) asymmetric membranes." Polymer **41**(15): 5633-5641.

Compton, O. C. and S. T. Nguyen (2010). "Graphene Oxide, Highly Reduced Graphene Oxide, and Graphene: Versatile Building Blocks for Carbon-Based Materials." Small **6**(6): 711-723.

Congjie, G. (2003). "Development and extension of seawater desalination by reverse osmosis." Chinese Journal of Oceanology and Limnology **21**(1): 40-45.

Cox, H. (1952). "The elasticity and strength of paper and other fibrous materials." British journal of applied physics **3**(3): 72.

Das, B., K. E. Prasad, U. Ramamurty and C. Rao (2009). "Nano-indentation studies on polymer matrix composites reinforced by few-layer graphene." Nanotechnology **20**(12): 125705.

Dikin, D. A., S. Stankovich, E. J. Zimney, R. D. Piner, G. H. Dommett, G. Evmenenko, S. T. Nguyen and R. S. Ruoff (2007). "Preparation and characterization of graphene oxide paper." Nature **448**(7152): 457-460.

Dikin, D. A., S. Stankovich, E. J. Zimney, R. D. Piner, G. H. B. Dommett, G. Evmenenko, S. B. T. Nguyen and R. S. Ruoff (2007). "Preparation and characterization of graphene oxide paper." Nature **448**(7152): 457-460.

Drewsa, A., C. H. Leeb and M. Kraumea (2006). "Membrane fouling–a review on

the role of EPS." Desalination **200**: 186-188.

Dreyer, D. R., S. Park, C. W. Bielawski and R. S. Ruoff (2009). "The chemistry of graphene oxide." Chem. Soc. Rev. **39**(1): 228-240.

Eizenberg, M. and J. Blakely (1979). "Carbon monolayer phase condensation on Ni (111)." Surface Science **82**(1): 228-236.

Elimelech, M. and W. A. Phillip (2011). "The future of seawater desalination: energy, technology, and the environment." Science **333**(6043): 712-717.

Fang, M., K. Wang, H. Lu, Y. Yang and S. Nutt (2009). "Covalent polymer functionalization of graphene nanosheets and mechanical properties of composites." Journal of Materials Chemistry **19**(38): 7098-7105.

Fierro, D., K. Buhr, C. Abetz, A. Boschetti-de-Fierro and V. Abetz (2009). "New insights into the control of self-assembly of block copolymer membranes." Australian journal of chemistry **62**(8): 885-890.

Fontananova, E., J. C. Jansen, A. Cristiano, E. Curcio and E. Drioli (2006). "Effect of additives in the casting solution on the formation of PVDF membranes." Desalination **192**(1): 190-197.

Fornes, T. and D. Paul (2003). "Modeling properties of nylon 6/clay nanocomposites using composite theories." Polymer **44**(17): 4993-5013.

Francis, P. S. (1966). "Fabrication and evaluation of new ultrathin reverse osmosis membranes." Available from the National Technical Information Service, Springfield VA 22161 as PB-177 083, Price codes: A 04 in paper copy, A 01 in microfiche. OSW Research and Development Progress Report(177).

Freger, V. (2003). "Nanoscale heterogeneity of polyamide membranes formed by interfacial polymerization." Langmuir **19**(11): 4791-4797.

Freger, V. (2005). "Kinetics of film formation by interfacial polycondensation."

Langmuir **21**(5): 1884-1894.

Gómez-Navarro, C., R. T. Weitz, A. M. Bittner, M. Scolari, A. Mews, M. Burghard and K. Kern (2007). "Electronic transport properties of individual chemically reduced graphene oxide sheets." Nano letters **7**(11): 3499-3503.

Geim, A. K. (2009). "Graphene: status and prospects." Science **324**(5934): 1530-1534.

Geim, A. K. and K. S. Novoselov (2007). "The rise of graphene." Nature materials **6**(3): 183-191.

Ghosh, A. K. and E. Hoek (2009). "Impacts of support membrane structure and chemistry on polyamide–polysulfone interfacial composite membranes." Journal of Membrane Science **336**(1): 140-148.

Ghosh, A. K., B.-H. Jeong, X. Huang and E. Hoek (2008). "Impacts of reaction and curing conditions on polyamide composite reverse osmosis membrane properties." Journal of Membrane Science **311**(1): 34-45.

Glater, J., M. Zachariah, S. McCray and J. McCutchan (1983). "Reverse osmosis membrane sensitivity to ozone and halogen disinfectants." Desalination **48**(1): 1-16.

Gojny, F., M. Wichmann, U. Köpke, B. Fiedler and K. Schulte (2004). "Carbon nanotube-reinforced epoxy-composites: enhanced stiffness and fracture toughness at low nanotube content." Composites Science and Technology **64**(15): 2363-2371.

Graf, D., F. Molitor, K. Ensslin, C. Stampfer, A. Jungen, C. Hierold and L. Wirtz (2007). "Spatially resolved Raman spectroscopy of single-and few-layer graphene." Nano letters **7**(2): 238-242.

Green, T. R., M. Taniguchi, H. Kooi, J. J. Gurdak, D. M. Allen, K. M. Hiscock, H. Treidel and A. Aureli (2011). "Beneath the surface of global change: Impacts of climate change on groundwater." Journal of Hydrology.

Gu, J. E., S. Lee, C. M. Stafford, J. S. Lee, W. Choi, B. Y. Kim, K. Y. Baek, E. P. Chan, J. Y. Chung and J. Bang (2013). "Molecular Layer-by-Layer Assembled Thin-Film Composite Membranes for Water Desalination." Advanced Materials.

Halpin, J. (1969). "Stiffness and expansion estimates for oriented short fiber composites." Journal of Composite Materials **3**(4): 732-734.

Halpin, J. C. (1992). Primer on Composite Materials Analysis, (revised), CRC Press.

Han, D., L. Yan, W. Chen and W. Li (2011). "Preparation of chitosan/graphene oxide composite film with enhanced mechanical strength in the wet state." Carbohydrate Polymers **83**(2): 653-658.

Han, M. J. and S. T. Nam (2002). "Thermodynamic and rheological variation in polysulfone solution by PVP and its effect in the preparation of phase inversion membrane." Journal of membrane science **202**(1): 55-61.

Hansen, C. M. (2007). Hansen solubility parameters: a user's handbook, CRC press.

He, H., J. Klinowski, M. Forster and A. Lerf (1998). "A new structural model for graphite oxide." Chemical Physics Letters **287**(1): 53-56.

Higuchi, A. and T. Nakagawa (1990). "Surface modified polysulfone hollow fibers. III. Fibers having a hydroxide group." Journal of Applied Polymer Science **41**(9-10): 1973-1979.

Himeshima, Y., M. Kurihara and T. Uemura (1988). Interfacially synthesized reverse osmosis membrane, Google Patents.

Hirose, M., H. Ito and Y. Kamiyama (1996). "Effect of skin layer surface structures on the flux behaviour of RO membranes." Journal of Membrane Science **121**(2): 209-215.

Hu, W., C. Peng, W. Luo, M. Lv, X. Li, D. Li, Q. Huang and C. Fan (2010).

"Graphene-based antibacterial paper." Acs nano **4**(7): 4317-4323.

Huang, J., K. S. Zhang, K. Wang, Z. L. Xie, B. Ladewig and H. T. Wang (2012). "Fabrication of polyethersulfone-mesoporous silica nanocomposite ultrafiltration membranes with antifouling properties." Journal of Membrane Science **423**: 362-370.

Hummer, G., J. C. Rasaiah and J. P. Noworyta (2001). "Water conduction through the hydrophobic channel of a carbon nanotube." Nature **414**(6860): 188-190.

Hummers Jr, W. S. and R. E. Offeman (1958). "Preparation of graphitic oxide." Journal of the American Chemical Society **80**(6): 1339-1339.

Hwang, B. K., W. N. Lee, K. M. Yeon, P. K. Park, C. H. Lee, S. Chang, A. Drews and M. Kraume (2008). "Correlating TMP increases with microbial characteristics in the bio-cake on the membrane surface in a membrane bioreactor." Environmental science & technology **42**(11): 3963-3968.

Jarusutthirak, C. and G. Amy (2006). "Role of soluble microbial products (SMP) in membrane fouling and flux decline." Environmental science & technology **40**(3): 969-974.

Jensen, M. Ø. and O. G. Mouritsen (2006). "Single-Channel Water Permeabilities of< i> Escherichia coli</i> Aquaporins AqpZ and GlpF." Biophysical journal **90**(7): 2270-2284.

Jeong, B.-H., E. Hoek, Y. Yan, A. Subramani, X. Huang, G. Hurwitz, A. K. Ghosh and A. Jawor (2007). "Interfacial polymerization of thin film nanocomposites: a new concept for reverse osmosis membranes." Journal of Membrane Science **294**(1): 1-7.

Judd, S. (2008). "The status of membrane bioreactor technology." Trends in biotechnology **26**(2): 109-116.

Kalaitzidou, K., H. Fukushima and L. T. Drzal (2007). "Mechanical properties and morphological characterization of exfoliated graphite–polypropylene nanocomposites." Composites Part A: applied science and manufacturing **38**(7): 1675-1682.

Kalaitzidou, K., H. Fukushima and L. T. Drzal (2007). "A new compounding method for exfoliated graphite–polypropylene nanocomposites with enhanced flexural properties and lower percolation threshold." Composites Science and Technology **67**(10): 2045-2051.

Kalra, A., S. Garde and G. Hummer (2003). "Osmotic water transport through carbon nanotube membranes." Proceedings of the National Academy of Sciences **100**(18): 10175-10180.

Kang, D.-W. and H.-S. Shin (2012). "Control of size and physical properties of graphene oxide by changing the oxidation temperature." Carbon Letters **13**: 39-43.

Kang, S. T., A. Subramani, E. Hoek, M. A. Deshusses and M. R. Matsumoto (2004). "Direct observation of biofouling in cross-flow microfiltration: mechanisms of deposition and release." Journal of membrane science **244**(1): 151-165.

Kim, H., R. Tyagi, A. Fouda and K. Jonasson (1996). "The kinetic study for asymmetric membrane formation via phase-inversion process." Journal of applied polymer science **62**(4): 621-629.

Kim, H. I. and S. S. Kim (2006). "Plasma treatment of polypropylene and polysulfone supports for thin film composite reverse osmosis membrane." Journal of membrane science **286**(1): 193-201.

Kim, H. J., K. Choi, Y. Baek, D.-G. Kim, J. Shim, J. Yoon and J.-C. Lee (2014). "High-Performance Reverse Osmosis CNT/Polyamide Nanocomposite Membrane by Controlled Interfacial Interactions." ACS applied materials & interfaces **6**(4):

2819-2829.

Kim, I. C., H. G. Yoon and K. H. Lee (2002). "Formation of integrally skinned asymmetric polyetherimide nanofiltration membranes by phase inversion process." Journal of applied polymer science **84**(6): 1300-1307.

Kim, K., K. Lee, K. Cho and C. Park (2002). "Surface modification of polysulfone ultrafiltration membrane by oxygen plasma treatment." Journal of Membrane Science **199**(1): 135-145.

Kim, S., I. Do and L. T. Drzal (2010). "Thermal stability and dynamic mechanical behavior of exfoliated graphite nanoplatelets-LLDPE nanocomposites." Polymer composites **31**(5): 755-761.

Kim, S. and L. T. Drzal (2009). "Comparison of exfoliated graphite nanoplatelets (xGnP) and CNTs for reinforcement of EVA nanocomposites fabricated by solution compounding method and three screw rotating systems." Journal of Adhesion Science and Technology **23**(12): 1623-1638.

Kim, S. H., S.-Y. Kwak and T. Suzuki (2005). "Positron annihilation spectroscopic evidence to demonstrate the flux-enhancement mechanism in morphology-controlled thin-film-composite (TFC) membrane." Environmental science & technology **39**(6): 1764-1770.

Kirsh, Y. E. and Y. M. Popkov (1988). "New Trends in the Development of Polymeric Materials for Reverse Osmosis Membranes." Russian Chemical Reviews **57**(6): 566.

Klüppel, M. (2003). The role of disorder in filler reinforcement of elastomers on various length scales. Filler-Reinforced Elastomers/Sanning Force Microscopy, Springer**:** 1-86.

Koo, J., R. Petersen and J. Cadotte (1986). ESCA characterization of chlorine-

damaged polyamide reverse-osmosis membrane. ABSTRACTS OF PAPERS OF THE AMERICAN CHEMICAL SOCIETY, AMER CHEMICAL SOC 1155 16TH ST, NW, WASHINGTON, DC 20036.

Kotsalis, E., J. H. Walther and P. Koumoutsakos (2004). "Multiphase water flow inside carbon nanotubes." International Journal of Multiphase Flow **30**(7): 995-1010.

Kraume, M. and A. Drews (2010). "Membrane bioreactors in waste water treatment–Status and trends." Chemical engineering & technology **33**(8): 1251-1259.

Krishnan, S., C. J. Weinman and C. K. Ober (2008). "Advances in polymers for anti-biofouling surfaces." Journal of Materials Chemistry **18**(29): 3405-3413.

Kumar, A. and C. H. Lee (2013). "Synthesis and Biomedical Applications of Graphene: Present and Future Trends."

Kurihara, M., N. Kanamaru, N. Harumiya, K. Yoshimura and S. Hagiwara (1980). "Spiral-wound new thin film composite membrane for a single-stage seawater desalination by reverse osmosis." Desalination **32**: 13-23.

Kuznetsova, A., I. Popova, J. T. Yates Jr, M. J. Bronikowski, C. B. Huffman, J. Liu, R. E. Smalley, H. H. Hwu and J. G. Chen (2001). "Oxygen-containing functional groups on single-wall carbon nanotubes: NEXAFS and vibrational spectroscopic studies." Journal of the American Chemical Society **123**(43): 10699-10704.

Kwak, S.-Y., S. G. Jung and S. H. Kim (2001). "Structure-motion-performance relationship of flux-enhanced reverse osmosis (RO) membranes composed of aromatic polyamide thin films." Environmental science & technology **35**(21): 4334-4340.

Lafreniere, L. Y., F. D. Talbot, T. Matsuura and S. Sourirajan (1987). "Effect of

poly (vinylpyrrolidone) additive on the performance of poly (ether sulfone) ultrafiltration membranes." Industrial & engineering chemistry research **26**(11): 2385-2389.

Lalia, B. S., V. Kochkodan, R. Hashaikeh and N. Hilal (2013). "A review on membrane fabrication: Structure, properties and performance relationship." Desalination **326**: 77-95.

Larson, R., J. Cadotte and R. Petersen (1981). "The FT-30 seawater reverse osmosis membrane--element test results." Desalination **38**: 473-483.

Lau, W., A. F. Ismail, N. Misdan and M. Kassim (2012). "A recent progress in thin film composite membrane: a review." Desalination **287**: 190-199.

Le-Clech, P. (2010). "Membrane bioreactors and their uses in wastewater treatments." Applied microbiology and biotechnology **88**(6): 1253-1260.

Le-Clech, P., V. Chen and T. A. G. Fane (2006). "Fouling in membrane bioreactors used in wastewater treatment." Journal of Membrane Science **284**(1): 17-53.

Lee, C., X. Wei, J. W. Kysar and J. Hone (2008). "Measurement of the elastic properties and intrinsic strength of monolayer graphene." science **321**(5887): 385-388.

Lee, H. D., H. W. Kim, Y. H. Cho and H. B. Park (2014). "Experimental Evidence of Rapid Water Transport through Carbon Nanotubes Embedded in Polymeric Desalination Membranes." Small.

Lee, H. J., J. Won, H. Lee and Y. S. Kang (2002). "Solution properties of poly (amic acid)–NMP containing LiCl and their effects on membrane morphologies." Journal of membrane science **196**(2): 267-277.

Lee, J., H.-R. Chae, Y. J. Won, K. Lee, C.-H. Lee, H. H. Lee, I.-C. Kim and J.-m. Lee (2013). "Graphene Oxide Nanoplatelets Composite Membrane with

Hydrophilic and Antifouling Properties for Wastewater Treatment." Journal of Membrane Science.

Lee, K. P., T. C. Arnot and D. Mattia (2011). "A review of reverse osmosis membrane materials for desalination—development to date and future potential." Journal of Membrane Science **370**(1): 1-22.

Lee, W., S. Kang and H. Shin (2003). "Sludge characteristics and their contribution to microfiltration in submerged membrane bioreactors." Journal of Membrane Science **216**(1): 217-227.

Lerf, A., H. He, M. Forster and J. Klinowski (1998). "Structure of graphite oxide revisited." The Journal of Physical Chemistry B **102**(23): 4477-4482.

Li, D., M. B. Müller, S. Gilje, R. B. Kaner and G. G. Wallace (2008). "Processable aqueous dispersions of graphene nanosheets." Nature Nanotechnology **3**(2): 101-105.

Li, Z., W. Zhang, Y. Luo, J. Yang and J. G. Hou (2009). "How graphene is cut upon oxidation?" Journal of the American Chemical Society **131**(18): 6320-6321.

Liang, S., K. Xiao, Y. Mo and X. Huang (2011). "A novel ZnO nanoparticle blended polyvinylidene fluoride membrane for anti-irreversible fouling." Journal of Membrane Science.

Light, W., H. Chu and C. Tran (1987). "Reverse osmosis TFC magnum elements for chlorinated/dechlorinated feedwater processing." Desalination **64**: 411-421.

Lin, X., X. Shen, Q. Zheng, N. Yousefi, L. Ye, Y.-W. Mai and J.-K. Kim (2012). "Fabrication of highly-aligned, conductive, and strong graphene papers using ultralarge graphene oxide sheets." ACS nano **6**(12): 10708-10719.

Lind, M. L., A. K. Ghosh, A. Jawor, X. Huang, W. Hou, Y. Yang and E. M. Hoek (2009). "Influence of zeolite crystal size on zeolite-polyamide thin film

nanocomposite membranes." Langmuir **25**(17): 10139-10145.

Liu, C., D. Zhang, Y. He, X. Zhao and R. Bai (2010). "Modification of membrane surface for anti-biofouling performance: Effect of anti-adhesion and anti-bacteria approaches." Journal of Membrane Science **346**(1): 121-130.

Liu, H. and L. C. Brinson (2008). "Reinforcing efficiency of nanoparticles: a simple comparison for polymer nanocomposites." Composites Science and Technology **68**(6): 1502-1512.

Liu, H., L. Zhang, J. Li, Q. Zou, Y. Zuo, W. Tian and Y. Li (2010). "Physicochemical and Biological Properties of Nano-hydroxyapatite-Reinforced Aliphatic Polyurethanes Membranes." Journal of Biomaterials Science, Polymer Edition **21**(12): 1619-1636.

Liu, S., T. H. Zeng, M. Hofmann, E. Burcombe, J. Wei, R. Jiang, J. Kong and Y. Chen (2011). "Antibacterial activity of graphite, graphite oxide, graphene oxide, and reduced graphene oxide: membrane and oxidative stress." Acs Nano **5**(9): 6971-6980.

Liu, Y. and H. H. Fang (2003). "Influences of extracellular polymeric substances (EPS) on flocculation, settling, and dewatering of activated sludge."

Loeb, S. and S. Sourirajan (1962). Sea water demineralization by means of an osmotic membrane, ACS Publications.

Lv, C., Q. Xue, D. Xia, M. Ma, J. Xie and H. Chen (2010). "Effect of chemisorption on the interfacial bonding characteristics of graphene− polymer composites." The Journal of Physical Chemistry C **114**(14): 6588-6594.

Marchese, J., M. Ponce, N. Ochoa, P. Prádanos, L. Palacio and A. Hernández (2003). "Fouling behaviour of polyethersulfone UF membranes made with different PVP." Journal of Membrane Science **211**(1): 1-11.

McAllister, M. J., J.-L. Li, D. H. Adamson, H. C. Schniepp, A. A. Abdala, J. Liu, M. Herrera-Alonso, D. L. Milius, R. Car and R. K. Prud'homme (2007). "Single sheet functionalized graphene by oxidation and thermal expansion of graphite." Chemistry of Materials **19**(18): 4396-4404.

McCutcheon, J. R. and M. Elimelech (2006). "Influence of concentrative and dilutive internal concentration polarization on flux behavior in forward osmosis." Journal of Membrane Science **284**(1): 237-247.

Meinild, A.-K., D. A. Klaerke and T. Zeuthen (1998). "Bidirectional water fluxes and specificity for small hydrophilic molecules in aquaporins 0–5." Journal of Biological Chemistry **273**(49): 32446-32451.

Mejías Carpio, I. E., C. M. Santos, X. Wei and D. F. Rodrigues (2012). "Toxicity of a polymer-graphene oxide composite against bacterial planktonic cells, biofilms, and mammalian cells." Nanoscale **4**: 4746-4756.

Misdan, N., W. Lau, A. Ismail and T. Matsuura (2013). "Formation of thin film composite nanofiltration membrane: Effect of polysulfone substrate characteristics." Desalination **329**: 9-18.

Moniruzzaman, M. and K. I. Winey (2006). "Polymer nanocomposites containing carbon nanotubes." Macromolecules **39**(16): 5194-5205.

Morgan, P. W. (1965). Condensation polymers: by interfacial and solution methods, Interscience Publishers New York.

Mori, T. and K. Tanaka (1973). "Average stress in matrix and average elastic energy of materials with misfitting inclusions." Acta metallurgica **21**(5): 571-574.

Mulder, M. (1996). Basic principles of membrane technology, Springer.

Mysels, K. J. and W. Wrasidlo (1991). "Strength of interfacial polymerization films." Langmuir **7**(12): 3052-3053.

Nair, R., H. Wu, P. Jayaram, I. Grigorieva and A. Geim (2012). "Unimpeded Permeation of Water Through Helium-Leak–Tight Graphene-Based Membranes." Science **335**(6067): 442-444.

Novoselov, K., A. Geim, S. Morozov, D. Jiang, Y. Zhang, S. Dubonos, I. Grigorieva and A. Firsov (2004). "Electric field effect in atomically thin carbon films." Science **306**(5696): 666-669.

Noy, A., H. G. Park, F. Fornasiero, J. K. Holt, C. P. Grigoropoulos and O. Bakajin (2007). "Nanofluidics in carbon nanotubes." Nano Today **2**(6): 22-29.

Oki, T. and S. Kanae (2006). "Global hydrological cycles and world water resources." Science **313**(5790): 1068-1072.

Pan, S. and I. A. Aksay (2011). "Factors controlling the size of graphene oxide sheets produced via the graphite oxide route." ACS nano **5**(5): 4073-4083.

Paredes, J., S. Villar-Rodil, A. Martinez-Alonso and J. Tascon (2008). "Graphene oxide dispersions in organic solvents." Langmuir **24**(19): 10560-10564.

Park, J. Y., M. H. Acar, A. Akthakul, W. Kuhlman and A. M. Mayes (2006). "Polysulfone-< i> graft</i>-poly (ethylene glycol) graft copolymers for surface modification of polysulfone membranes." Biomaterials **27**(6): 856-865.

Park, S. and R. S. Ruoff (2009). "Chemical methods for the production of graphenes." Nature nanotechnology **4**(4): 217-224.

Pendergast, M. M. and E. M. Hoek (2011). "A review of water treatment membrane nanotechnologies." Energy & Environmental Science **4**(6): 1946-1971.

Peng, F., X. Huang, A. Jawor and E. Hoek (2010). "Transport, structural, and interfacial properties of poly (vinyl alcohol)–polysulfone composite nanofiltration membranes." Journal of Membrane Science **353**(1): 169-176.

Peng, X.-Y., X.-X. Liu, D. Diamond and K. T. Lau (2011). "Synthesis of

electrochemically-reduced graphene oxide film with controllable size and thickness and its use in supercapacitor." Carbon **49**(11): 3488-3496.

Petersen, R. J. (1993). "Composite reverse osmosis and nanofiltration membranes." Journal of membrane science **83**(1): 81-150.

Petersen, R. J. and J. E. Cadotte (1990). "Thin film composite reverse osmosis membranes." Handbook of Industrial Membrane Technology: 307-348.

Piao, S., P. Ciais, Y. Huang, Z. Shen, S. Peng, J. Li, L. Zhou, H. Liu, Y. Ma and Y. Ding (2010). "The impacts of climate change on water resources and agriculture in China." Nature **467**(7311): 43-51.

Pimenta, M., G. Dresselhaus, M. S. Dresselhaus, L. Cancado, A. Jorio and R. Saito (2007). "Studying disorder in graphite-based systems by Raman spectroscopy." Phys. Chem. Chem. Phys. **9**(11): 1276-1290.

Pinnau, I. and B. Freeman (2000). "Formation and modification of polymeric membranes: overview." Membrane Formation and Modification **744**: 1-22.

Potts, J. R., D. R. Dreyer, C. W. Bielawski and R. S. Ruoff (2011). "Graphene-based polymer nanocomposites." Polymer **52**(1): 5-25.

Qiu, S., L. Wu, X. Pan, L. Zhang, H. Chen and C. Gao (2009). "Preparation and properties of functionalized carbon nanotube/PSF blend ultrafiltration membranes." Journal of Membrane Science **342**(1): 165-172.

Rafiee, M. A., J. Rafiee, Z. Wang, H. Song, Z.-Z. Yu and N. Koratkar (2009). "Enhanced mechanical properties of nanocomposites at low graphene content." ACS nano **3**(12): 3884-3890.

Ramanathan, T., A. Abdala, S. Stankovich, D. Dikin, M. Herrera-Alonso, R. Piner, D. Adamson, H. Schniepp, X. Chen and R. Ruoff (2008). "Functionalized graphene sheets for polymer nanocomposites." Nature nanotechnology **3**(6): 327-331.

Ramanathan, T., S. Stankovich, D. Dikin, H. Liu, H. Shen, S. Nguyen and L. Brinson (2007). "Graphitic nanofillers in PMMA nanocomposites—an investigation of particle size and dispersion and their influence on nanocomposite properties." Journal of Polymer Science Part B: Polymer Physics **45**(15): 2097-2112.

Ramon, G. Z., M. C. Wong and E. Hoek (2012). "Transport through composite membrane, part 1: Is there an optimal support membrane?" Journal of Membrane Science **415**: 298-305.

Ratto, T. V., J. K. Holt and A. W. Szmodis (2011). Membranes with embedded nanotubes for selective permeability, Google Patents.

Reid, C. and E. Breton (1959). "Water and ion flow across cellulosic membranes." Journal of Applied Polymer Science **1**(2): 133-143.

Riley, R., H. Lonsdale and C. Lyons (1971). "Composite membranes for seawater desalination by reverse osmosis." Journal of Applied Polymer Science **15**(5): 1267-1276.

Roy, S., S. A. Ntim, S. Mitra and K. K. Sirkar (2011). "Facile fabrication of superior nanofiltration membranes from interfacially polymerized CNT-polymer composites." Journal of Membrane Science **375**(1): 81-87.

Satti, A., P. Larpent and Y. Gun'ko (2010). "Improvement of mechanical properties of graphene oxide/poly (allylamine) composites by chemical crosslinking." Carbon **48**(12): 3376-3381.

Schaefer, D. W. and R. S. Justice (2007). "How nano are nanocomposites?" Macromolecules **40**(24): 8501-8517.

SERVICE, R. F. (2006). "Desalination freshens up." Science(Washington, D. C.) **313**(5790): 1088-1090.

Shannon, M. A., P. W. Bohn, M. Elimelech, J. G. Georgiadis, B. J. Mariñas and A. M. Mayes (2008). "Science and technology for water purification in the coming decades." Nature **452**(7185): 301-310.

Shi, L., R. Wang, Y. Cao, D. T. Liang and J. H. Tay (2008). "Effect of additives on the fabrication of poly (vinylidene fluoride-< i> co</i>-hexafluropropylene)(PVDF-HFP) asymmetric microporous hollow fiber membranes." Journal of Membrane Science **315**(1): 195-204.

Singh, P. S., S. Joshi, J. Trivedi, C. Devmurari, A. P. Rao and P. Ghosh (2006). "Probing the structural variations of thin film composite RO membranes obtained by coating polyamide over polysulfone membranes of different pore dimensions." Journal of membrane science **278**(1): 19-25.

Singh, S., K. Khulbe, T. Matsuura and P. Ramamurthy (1998). "Membrane characterization by solute transport and atomic force microscopy." Journal of Membrane Science **142**(1): 111-127.

Smolders, C., A. Reuvers, R. Boom and I. Wienk (1992). "Microstructures in phase-inversion membranes. Part 1. Formation of macrovoids." Journal of Membrane Science **73**(2): 259-275.

Sourirajan, S. (1970). Reverse osmosis, London, UK: Logos Press Ltd.

Stankovich, S., D. A. Dikin, G. H. Dommett, K. M. Kohlhaas, E. J. Zimney, E. A. Stach, R. D. Piner, S. T. Nguyen and R. S. Ruoff (2006). "Graphene-based composite materials." Nature **442**(7100): 282-286.

Stankovich, S., D. A. Dikin, G. H. B. Dommett, K. M. Kohlhaas, E. J. Zimney, E. A. Stach, R. D. Piner, S. B. T. Nguyen and R. S. Ruoff (2006). "Graphene-based composite materials." Nature **442**(7100): 282-286.

Stankovich, S., D. A. Dikin, R. D. Piner, K. A. Kohlhaas, A. Kleinhammes, Y. Jia,

Y. Wu, S. T. Nguyen and R. S. Ruoff (2007). "Synthesis of graphene-based nanosheets via chemical reduction of exfoliated graphite oxide." Carbon **45**(7): 1558-1565.

Stankovich, S., R. D. Piner, X. Chen, N. Wu, S. T. Nguyen and R. S. Ruoff (2006). "Stable aqueous dispersions of graphitic nanoplatelets via the reduction of exfoliated graphite oxide in the presence of poly (sodium 4-styrenesulfonate)." Journal of Materials Chemistry **16**(2): 155-158.

Stankovich, S., R. D. Piner, S. T. Nguyen and R. S. Ruoff (2006). "Synthesis and exfoliation of isocyanate-treated graphene oxide nanoplatelets." Carbon **44**(15): 3342-3347.

Strathmann, H. (1985). Production of microporous media by phase inversion processes. ACS symposium series, Oxford University Press.

Strathmann, H. and K. Kock (1977). "The formation mechanism of phase inversion membranes." Desalination **21**(3): 241-255.

Su, C.-Y., Y. Xu, W. Zhang, J. Zhao, X. Tang, C.-H. Tsai and L.-J. Li (2009). "Electrical and spectroscopic characterizations of ultra-large reduced graphene oxide monolayers." Chemistry of Materials **21**(23): 5674-5680.

Tang, C. Y., Y.-N. Kwon and J. O. Leckie (2009). "Effect of membrane chemistry and coating layer on physiochemical properties of thin film composite polyamide RO and NF membranes: II. Membrane physiochemical properties and their dependence on polyamide and coating layers." Desalination **242**(1): 168-182.

Tiraferri, A., N. Y. Yip, W. A. Phillip, J. D. Schiffman and M. Elimelech (2011). "Relating performance of thin-film composite forward osmosis membranes to support layer formation and structure." Journal of Membrane Science **367**(1): 340-352.

Tomaschke, J. E. (1990). Interfacially synthesized reverse osmosis membrane containing an amine salt and processes for preparing the same, Google Patents.

Ulbricht, M. (2006). "Advanced functional polymer membranes." Polymer **47**(7): 2217-2262.

Vafai, K. and C. Tien (1981). "Boundary and inertia effects on flow and heat transfer in porous media." International Journal of Heat and Mass Transfer **24**(2): 195-203.

Vaia, R. A. and J. F. Maguire (2007). "Polymer nanocomposites with prescribed morphology: going beyond nanoparticle-filled polymers." Chemistry of Materials **19**(11): 2736-2751.

Van de Witte, P., P. Dijkstra, J. Van den Berg and J. Feijen (1996). "Phase separation processes in polymer solutions in relation to membrane formation." Journal of Membrane Science **117**(1): 1-31.

Van der Bruggen, B. (2013). "Preparation and characterization of thin-film nanocomposite membranes embedded with poly (methyl methacrylate) hydrophobic modified multiwalled carbon nanotubes by interfacial polymerization." Journal of Membrane Science **442**: 18-26.

Van Loosdrecht, M., J. Lyklema, W. Norde, G. Schraa and A. Zehnder (1987). "Electrophoretic mobility and hydrophobicity as a measured to predict the initial steps of bacterial adhesion." Applied and Environmental Microbiology **53**(8): 1898-1901.

Van Loosdrecht, M., W. Norde and A. Zehnder (1990). "Physical chemical description of bacterial adhesion." Journal of biomaterials applications **5**(2): 91-106.

Vatanpour, V., S. S. Madaeni, R. Moradian, S. Zinadini and B. Astinchap (2011).

"Fabrication and characterization of novel antifouling nanofiltration membrane prepared from oxidized multiwalled carbon nanotube/polyethersulfone nanocomposite." Journal of Membrane Science **375**(1): 284-294.

Wang, C., C. Feng, Y. Gao, X. Ma, Q. Wu and Z. Wang (2011). "Preparation of a graphene-based magnetic nanocomposite for the removal of an organic dye from aqueous solution." Chemical Engineering Journal **173**(1): 92-97.

Wang, D., K. Li and W. Teo (2000). "Porous PVDF asymmetric hollow fiber membranes prepared with the use of small molecular additives." Journal of Membrane Science **178**(1): 13-23.

Wang, H., T. Yu, C. Zhao and Q. Du (2009). "Improvement of hydrophilicity and blood compatibility on polyethersulfone membrane by adding polyvinylpyrrolidone." Fibers and polymers **10**(1): 1-5.

Wang, X., H. Bai and G. Shi (2011). "Size fractionation of graphene oxide sheets by pH-assisted selective sedimentation." Journal of the American Chemical Society **133**(16): 6338-6342.

Wang, Z., H. Yu, J. Xia, F. Zhang, F. Li, Y. Xia and Y. Li (2012). "Novel GO-blended PVDF ultrafiltration membranes." Desalination.

Wu, H., B. Tang and P. Wu (2010). "Novel ultrafiltration membranes prepared from a multi-walled carbon nanotubes/polymer composite." Journal of Membrane Science **362**(1): 374-383.

Wu, H., B. Tang and P. Wu (2013). "Optimization, characterization and nanofiltration properties test of MWNTs/polyester thin film nanocomposite membrane." Journal of Membrane Science **428**: 425-433.

Wu, J., B. Yu and M. Yun (2008). "A resistance model for flow through porous media." Transport in Porous Media **71**(3): 331-343.

Wu, S. (1982). Polymer interface and adhesion, CRC.

Xu, Y., W. Hong, H. Bai, C. Li and G. Shi (2009). "Strong and ductile poly (vinyl alcohol)/graphene oxide composite films with a layered structure." Carbon **47**(15): 3538-3543.

Yang, D., A. Velamakanni, G. Bozoklu, S. Park, M. Stoller, R. D. Piner, S. Stankovich, I. Jung, D. A. Field and C. A. Ventrice Jr (2009). "Chemical analysis of graphene oxide films after heat and chemical treatments by X-ray photoelectron and micro-Raman spectroscopy." Carbon **47**(1): 145-152.

Yang, Y., P. Wang and Q. Zheng (2006). "Preparation and properties of polysulfone/TiO2 composite ultrafiltration membranes." Journal of Polymer Science Part B: Polymer Physics **44**(5): 879-887.

Yang, Y., H. Zhang, P. Wang, Q. Zheng and J. Li (2007). "The influence of nano-sized TiO< sub> 2</sub> fillers on the morphologies and properties of PSF UF membrane." Journal of Membrane Science **288**(1): 231-238.

Yeon, K.-M., W.-S. Cheong, H.-S. Oh, W.-N. Lee, B.-K. Hwang, C.-H. Lee, H. Beyenal and Z. Lewandowski (2008). "Quorum sensing: a new biofouling control paradigm in a membrane bioreactor for advanced wastewater treatment." Environmental science & technology **43**(2): 380-385.

Yip, N. Y., A. Tiraferri, W. A. Phillip, J. D. Schiffman and M. Elimelech (2010). "High performance thin-film composite forward osmosis membrane." Environmental science & technology **44**(10): 3812-3818.

Yu, A., P. Ramesh, M. E. Itkis, E. Bekyarova and R. C. Haddon (2007). "Graphite nanoplatelet-epoxy composite thermal interface materials." The Journal of Physical Chemistry C **111**(21): 7565-7569.

Zhang, J., Z. Xu, W. Mai, C. Min, B. Zhou, M. Shan, Y. Li, C. Yang, Z. Wang and

X. Qian (2013). "Improved hydrophilicity, permeability, antifouling and mechanical performance of PVDF composite ultrafiltration membranes tailored by oxidized low-dimensional carbon nanomaterials." Journal of Materials Chemistry A **1**(9): 3101-3111.

Zhang, L., J. Liang, Y. Huang, Y. Ma, Y. Wang and Y. Chen (2009). "Size-controlled synthesis of graphene oxide sheets on a large scale using chemical exfoliation." Carbon **47**(14): 3365-3368.

Zhao, G., J. Li, X. Ren, C. Chen and X. Wang (2011). "Few-layered graphene oxide nanosheets as superior sorbents for heavy metal ion pollution management." Environmental science & technology **45**(24): 10454-10462.

Zhao, H., S. Qiu, L. Wu, L. Zhang, H. Chen and C. Gao (2014). "Improving the performance of polyamide reverse osmosis membrane by incorporation of modified multi-walled carbon nanotubes." Journal of Membrane Science **450**: 249-256.

Zheng, Q.-Z., P. Wang, Y.-N. Yang and D.-J. Cui (2006). "The relationship between porosity and kinetics parameter of membrane formation in PSF ultrafiltration membrane." Journal of membrane science **286**(1): 7-11.

Zhu, Y., M. D. Stoller, W. Cai, A. Velamakanni, R. D. Piner, D. Chen and R. S. Ruoff (2010). "Exfoliation of graphite oxide in propylene carbonate and thermal reduction of the resulting graphene oxide platelets." Acs Nano **4**(2): 1227-1233.

Zodrow, K., L. Brunet, S. Mahendra, D. Li, A. Zhang, Q. Li and P. J. Alvarez (2009). "Polysulfone ultrafiltration membranes impregnated with silver nanoparticles show improved biofouling resistance and virus removal." Water research **43**(3): 715-723.

국문 초록

최근 심각해지고 있는 기후변화와 더불어 급증하는 인구로 인해 물부족 현상은 가속화되고 있다. 이처럼 날로 심각해지는 물부족 문제를 해결하기 위한 노력의 일환으로 하폐수의 재이용에서부터 해수담수화에 이르기까지 폭 넓은 논의와 연구가 진행돼 왔다. 상기 목적을 달성하기 위한 기술로서 막결합형 생물반응기와 역삼투 공정은 타 기술들에 비해 양질의 처리수 및 부지면적 최소화 등의 장점들을 가지고 있어 널리 이용되어 왔다. 하지만 두 기술 모두 기술 구현을 위한 핵심 요소에 내재해 있는 한계점으로 인한 문제점을 안고 있다. 예를 들어, 막결합형 생물반응기에서 사용되는 미생물들은 폐수 내 존재하는 유기물들을 효율적으로 제거해주는 역할을 하나, 다른 한 편으로 분리막 표면에 부착 및 성장을 함으로써 막오염을 유발시키는 원인을 제공한다. 역삼투 공정에 사용되는 역삼투막의 경우, 특유의 치밀한 구조로 인해 이온 제거능을 가지나 그로 인한 낮은 투수율 등의 에너지 효율 저하 문제를 유발한다는 단점이 있다. 본 연구에서는 친수성, 강한 기계적 강도 등으로 인해 최근 각광 받고 있는 나노 물질인 그래핀 옥사이드를 분리막에 첨가함으로써 앞서 언급한 한계점들을 극복하기 위한 전략을 제시하는 것을 목표로 한다. 구체적으로, 하폐수 처리에 이용되는 폴리술폰 한외여과막에 그래핀 옥사이드를 첨가함으로써 소수성 특성을 가진 분리막에 친수성을 부여할 수 있었고, 나아가 그래핀 옥사이드에 존재하는 기능기들로 인해 정전기적 반발력을 증가시킬 수 있게 됨에 따라 미생물에 대한 방오성 또한 향

상시킬 수 있었다. 또한, 본 연구에서는 지지층의 기공도가 극대화될 경우 활성층의 특성과 별개로 역삼투막의 성능이 향상될 수 있다는 사실을 발견하였고, 비파괴 검사를 통해 지지층의 구조적 특성과 역삼투막의 성능 간의 상관관계가 있다는 것을 실험적으로 규명하였다. 그 결과를 토대로 우수한 기계적 강도와 큰 종횡비로 인해 고분자 복합 물질의 기계적 강도를 효율적으로 증가시킬 수 있는 그래핀 옥사이드를 기공도가 극대화된 지지층의 기계적 강도를 증가시키기 위한 첨가제로서 사용하였다. 그렇게 준비된 그래핀 옥사이드 복합 다공성 지지층으로 제조한 역삼투막은 기공도가 극대화되더라도 상용막 수준의 기계적 강도를 가졌고, 그로 인해 안정적으로 역삼투 공정에 적용될 수 있었다. 더불어 기공도가 극대화된 지지층으로 인해 본 연구에서 제조한 역삼투막은 상용막을 능가하는 수준으로 성능이 크게 향상되었다.

주요어: 한외여과막, 역삼투 복합막, 그래핀 옥사이드, 방오성, 기계적 강도, 지지층 효과

학 번: 2009-21016